AN ABSTRACT OF THE THESIS OF

Michael S McCulla for the degree of Doctor of Philosophy in Geology presented on October 16, 1986

Title: Geology and Metallization of the White River Area, King and Pierce Counties, Washington

Redacted for Privacy

Abstract approved: Cyrus W. Field

Bedrock of the White River area is dominated by Miocene age volcanics of andesite to rhyolite composition, which may be in part coeval with plutonic phases of the nearby 26 - 14 m.y. Tatoosh batholith. These volcanic rocks host two spatially distinct and gold-bearing epithermal deposits of the acid-sulfate type that are structurally, temporally, and genetically related to the formation and resurgent magmatic activity at the margin of an early Miocene caldera (22.6 - 19.1 m.y.). The age of hydrothermal activity is 20.4 ± 0.1 m.y. based on 40Ar/39Ar analysis of hypogene alunite from the mineralized zone. Hydrothermal alteration and metallization of both deposits is chemically and mineralogically similar and consists of a central core of pervasive silicification that grades outward into zones of advanced argillic (alunite and quartz ± kaolinite, pyrite, enargite, and fluorite), argillic (kaolinite ± pyrite, other clays, and silica), and propylitic (chlorite, epidote, pyrite, and calcite) alteration.

The largest of the two target areas is defined by a silica capping that measures 3.5 miles in length, up to 1 mile in width, and

in places is at least 400 feet thick. Sulfur isotope analyses of cogenetic alunite-pyrite-enargite demonstrate a $\Delta(34)S$ of +28.8 o/oo for the alunite-pyrite mineral pair. This large fractionation corroborates other field and mineralogic evidence for the hypogene origin of the alunite, and provides a geologically reasonable isotopic temperature estimate of 190°C for this epithermal deposit. Gold was introduced in at least 3 distinct episodes of structural-hydrothermal activity that are represented by early stockwork veins of milky quartz, matrix-supported explosion breccias, and late pyrite-bearing veins. The highest concentration of gold is within a zone measuring 1,600 by 300 - 600 feet, and is localized in parts of the silica capping that contain outcrops of matrix-supported explosion breccias and veins having anomalous concentrations of up to 480 ppb Au, 13.7 ppm Ag, 1,900 ppm As, 213 ppm Sb, 7.5 ppm Hg, and 10 ppm Mo. Additionally, geobotanical samples of moss contain up to 510 ppb Au and 28 ppm Ag. Moderate to high concentrations of gold (up to 295 ppb Au) and other trace elements have also been detected within a second large target area, located a few miles to the southeast. Statistical analyses of 163 samples from the White River area show covarient groupings for Ag-Mo and As-Sb, and an antipathetic relationship between Au and Hg.

Geology and Metallization of the White River Area, King and Pierce Counties, Washington

by

Michael S. McCulla

A THESIS

submitted to

Oregon State University

in partial fulfullment of
the requirements for the
degree of

Doctor of Philosophy

Completed October 16, 1986

Commencement June 1987

APPROVED:

Redacted for Privacy

Professor of The Department of Geology in charge of major

Redacted for Privacy

Chairman of The Department of Geology

Redacted for Privacy

Dean of Graduate School

Date thesis is presented October 16, 1986

ACKNOWLEDGEMENTS

I would like to thank the Weyerhaeuser Corporation for its generous monetary support for this project. Moreover, thanks to the employees of the Weyerhaeuser Mineral Resources Division for their foresight as to the practicality and validity of the project. I would also like to thank Dr. Cyrus W. Field for his critical reviews of the manuscript and many helpful suggestions, and also for his knowledgeable guidance and friendship throughout my time at OSU. My sincere thanks to Dr. Allen F. Agnew for an endless supply of mining related publications, and also to Dr Larry W. Snee for the 40Ar/39Ar age determination of alunite from the project area, and to both for their friendship. I was deeply saddened by the passing away of one of my committee members, Dr. Harold E. Enlows. He will always be remembered by me as a knowledgeable scientist whoes kindness to other human beings was paramount. The pursuit of a lifestyle similar to his is an honorable goal.

Of the several friends I have made during my graduate program at OSU Jim McDougall and Bob Walker have made my stay especially enjoyable. I am deeply greatful to my parents, Lois and Robert, for their steadfast support and encouragement throughout my career as a geologist and to Margaret McHugh for her special friendship.

TABLE OF CONTENTS

	Page
INTRODUCTION	1
Methods of Study	3
Location and Access	4
Previous Work	6
REGIONAL GEOLOGY	10
Tertiary	10
General Magmatic Episodes	11
Plate Tectonics	13
Plate Tectonic-Magmatic Connection	14
Paleocene	15
Eocene	15
Oligocene to Miocene	22
Synopsis and Significance	24
LOCAL GEOLOGY	28
Huckleberry Mountain Formation	34
Alteration	41
Structure and Thickness	41
Age and Regional Correlation	42
Origin and Significance	43
Eagle Gorge Formation	44
Petrography and Chemistry	45
Structure, Thickness and Contact Relations	45
Age and Regional Correlation	47
Stevens Ridge Formation	47
Petrography and Chemistry	49
Thickness and Contact Relations	51
Age and Regional Correlation	51
Origin and Significance	52
Fifes Peak Formation	53
Petrography and Chemistry	54
Interflow Felsic Volcanics	54
Structure, Thickness, and Contact Relations	61
Age and Regional Correlation	63
Origin and Significance	64
Clear West Peak Complex	65
Petrography and Chemistry	66
Structure, Thickness, and Contact Relations	68
Age and Regional Correlation	70
Origin and Significance	71
Intrusions	72
Synopsis of Miocene Igneous Events	76
Structural Analysis	80
Structures Detected by Satellite Imagery	81
Faults	90
Folds	91

	Page
MODEL FOR VOLCANIC-HOSTED EPITHERMAL GOLD MINERALIZATION	95
MINERALIZATION IN THE WHITE RIVER AREA	101
Known Mineral Occurrences	102
Alunite	102
Silica	103
Others	104
Justification for Gold Exploration	105
West Area	108
Alteration	108
Geochemistry of Alteration	113
Mineralogy	127
Primary Target	141
Structure	141
Metallization	145
Geochemistry of Metallization	157
Breccias	163
East Area	168
Geology	169
Alteration	173
Metallization	174
STATISTICAL ANALYSIS	177
Basic Statistics	178
R-mode Factor Analysis	182
Q-mode Factor Analysis	184
SUMMARY AND CONCLUSIONS	192
REFERENCES	202
APPENDICES	206

LIST OF FIGURES

Figure		Page
1.	Location map of the White River area and reference maps used during the project.	5
2.	Tree thinning in section 9, T19N, R8E.	7
3.	Distribution of major mining districts, Tertiary plutons, and Tertiary to Recent stratavolcanoes in the Cascade Mountains of Washington and Oregon.	8
4.	Major Tertiary structural and igneous events in Pacific Northwest region.	12
5.	Location of exposed major Tertiary intrusive rocks in the central to north Cascade Range of Washington, the White River area, and Mount Rainier National Park.	25
6.	Location map of the White River area with selected geologic and tectonic features.	29
7.	General geologic map of the region surrounding the White River area.	31
8.	Major-element oxides from the Fifes Peak (19 samples) and Stevens Ridge (1 sample) Formations, from the Clear West Peak complex (2 samples), and from a rhyodacite intrusion (1 sample).	35
9.	AFM diagram with additional major-element oxide data from the same 23 samples plotted on Figure 8.	36
10.	Location map of the White River study area and outcrops of the Stevens Ridge and Huckleberry Mountain Formations.	37
11.	Hand specimen of volcanic breccia from the Huckleberry Mountain Formation.	39
12.	View to west of well-bedded carbonaceous volcaniclastic sedimentary rocks, striking N60-70°W and dipping 75°SW, within the Huckleberry Mountain Formation.	40

Figure		Page
13.	Hand specimen of pumice replaced by silica (NW1/4, NE1/4, sec. 1, T19N, R7E).	58
14.	Outcrop of felsic tuff replaced by silica (NW1/4, NE1/4, sec.12, T19N, R7E).	58
15.	Hand specimen of breccia replaced by silica (N1/2, SW1/4, sec. 6, T19N, R8E).	59
16.	Aggregate of spheroidal lapilli ranging in size from 0.5 to 4cm, collected from the SW1/4, SW1/4, sec. 1, T19N, R7E.	60
17.	View south across the White River of Fifes Peak andesites (approximately 2,000 feet thick) in in sec. 12, T19N, R8E.	62
18.	View northeast into the White River valley from the edifice of Fifes Peak andesites shown in Figure 17.	62
19.	Flow banding in Clear West Peak ash-flow tuffs from the NE1/4, SE1/4 sec. 34, T19N, R8E (along Milky Cr).	67
20.	Eutaxitic texture in the Clear West Peak ash-flow tuffs near the location of Figure 19.	67
21.	Fifes Peak andesite flows that are cut by late stage dikes of diorite porphyry (SW1/4, SW1/4, sec. 14, T19N, R8E) near the headwaters of Mineral Creek.	74
22.	Age determinations with error bars of: (1) Stevens Ridge ash-flow tuffs; (2) Fifes Peak andesite flows; (3) Clear West Peak ash-flow tuffs; and (4) Carbon river granodiorite stock.	77
23.	Diagramatic sketch of a model for the 24 - 20 m.y. emplacement of intrusions of the Tatoosh batholith and coeval volcanics.	78
24.	Digital composite of topographic relief from satellite imagery.	83
25.	Digital composite of topographic relief from satellite imagery that is an enlargement of Figure 24.	87
26.	Tectonic interpretation of Miocene fold patterns near the White River area.	92

Figure		Page
27.	Model of a Hot-spring gold deposit.	98
28.	Location map of the West and East areas and the approximate boundary of hydrothermal silicification within each.	107
29.	Diagrammatic sketch of the fossil hot-spring system in the West area that illustrates major alteration zones and structural features.	110
30.	Major areas of silicification within the West area.	114
31.	View of the 3.5 mile long area of silicification in the West area.	116
32.	Phase equilibria diagrams of alteration minerals in the White River area.	122
33.	Argillically altered Fifes Peak andesite along East Clay Creek.	126
34.	SEM photomicrographs of two microball-bearing hematite phases.	129
35.	Sample of enargite from the West area.	132
36.	Small silica quarry in the center of sec. 1, T19N, R7E.	134
37.	Hand specimens showing various types of quartz veining in the West area.	135
38.	Hand specimens of various pyrite-bearing rocks from the White River area.	138
39.	Location map of the Primary Target area and the Gold Zone, within the West area.	142
40.	Specimens of gold-bearing veins and breccias from the Primary Target area.	148
41.	Diagrammatic sketch of the surface and possible subsurface alteration and metallization within the Gold Zone.	152
42.	The White River gold prospect consisting of two adits driven in the 1890's.	155

Figure		Page
43.	pH verses -Log f02 diagram showing the stability relations of a gold bisulfide complex and minerals relevant to the fossil hot-spring systems of the White River area.	162
44.	Specimens of various types of breccia collected from the Primary Target area.	164
45.	Specimen WR-41 is a clast-supported fault breccia (NE1/4, SE1/4, sec. 31, T20N, R8E), and WR-136 is part of an extensive area of fault related veining in a felsic tuff and grades upward into breccias such as WR-41.	167
46.	Location map of the East area.	170
47.	Aerial veiws of the East area with sample locations plotted.	171
48.	Mean concentrations of Au, Ag, As, Sb, Hg, and Mo verses the central (C), middle (M), and outer (O) zones of the fossil hot-spring system.	179
49.	Histogram of unitized R-mode factor analysis of 163 samples.	183
50.	Trigram representation of the unitized results of R-mode factor analysis of 163 samples that illustrates the interrelationships between Au, Ag, As, Sb, Hg, and Mo.	185
51.	Plan map of the fossil hot-spring system in the West area showing major alteration patterns. R-mode and Q-mode factor analysis data are contoured and an area of potential subsurface gold mineralization is plotted.	187
52.	Summary diagram of hypogene metallization and alteration patterns in the White River fossil hot-spring systems.	190
53.	Schematic cross section of acid-sulfate epithermal gold mineralization in the White River area.	196

LIST OF TABLES

Table		Page
1.	Major-element oxide and normative analysis of propylitically altered pyroxene andesite from the Eagle Gorge Formation.	46
2.	Major-element oxide and normative analysis of light gray lapilli rich ash-flow tuff of the Stevens Ridge Formation.	50
3.	Major-element oxide and normative analysis of a typical andesite flow in the Fifes Peak Formation.	55
4.	Major-element oxide and normative analyses of ash-flows from the Clear West Peak complex.	69
5.	Data from major-element oxide XRF analyses and density (D) measurements of fresh volcanics and their silicified equivalents.	118
6.	Sulfur isotope analysis of cogenetic alunite-pyrite-enargite (NE1/4, sec. 7, T19N, R8E).	125
7.	The mean and range, and range of anomalous values for Au, Ag, Hg, Mo, As, and Sb in 163 samples collected throughout the White River area.	143
8.	Mean values, standard deviations, and ranges of Au, Ag, Hg, Mo, As, and Sb of the White River data set (163 samples) for the central, middle, and outer zones.	180
9.	The variances of six elements in the central, middle, and outer zones with data sets of 17, 17, and 129 samples, respectively.	181
10.	The F statistics of variances between the three geochemical zones.	181

LIST OF PLATES

Plate		Page
1A.	Geologic map of the White River area (scale, 1:24,000).	in pocket
1B.	Geologic map of the West Target area (scale, 1:12,000).	in pocket
2.	Alteration and Metallization Map of the West Target area.	in pocket
3A.	Sample location map of the White River area.	in pocket
3B.	Sample location and Gold Anomaly map of the West Target area.	in pocket

Geology and Metallization of the White River Area,

King and Pierce Counties, Washington

INTRODUCTION

Recent discoveries of precious metal deposits in surface outcrops, aggregating several billions of dollars in gross value, document decades of faulty and (or) unsuccessful exploration activity for gold and silver in the western U.S., and also point to a recent increase in the economic importance of bulk mineable near-surface mineral deposits. Factoring out improvements in technology and economic considerations, it is apparent in hindsight that the reasons for these deposits having been overlooked were largely attributable to the lack of modern models for precious metal ore genesis and derivative exploration techniques. Although some prospects are easy to evaluate in terms of economic potential, others are geologically and geochemically more subtle with respect to their surficial appearances. Evaluation of the latter requires a genetic model for the ore-forming process, to which the results of detailed geologic, mineralogic, and geochemical studies relating to host rocks and hydrothermal mineralization may be compared. Unfortunately, because of the competitive nature of the minerals industry, detailed genetic models for bulk mineable precious metal deposits at the inception of this project were not widely documented in the literature. Since that time a number of relevant articles dealing with the subject have been

published, which include: Berger (1985); Bonham (1985); Cunningham (1985); Strachan (1985); White (1985); Berger and Eimon (1982); Giles and Nelson (1982); Henley and Ellis (1984); Lewis (1982); and many others.

The purpose of this dissertation project was to conduct a detailed evaluation of the mineral resource potential, especially that relating to precious metals, in the White River area of western Washington. This included locating zones of precious metal mineralization and performing as detailed an evaluation of each as practicable. The work comprised an integrated study of the geology of this terrain including the structural, chemical, and mineralogical characteristics of host rocks and their mineralized equivalents. Areas of hydrothermal alteration were located, sampled, and studied in detail. A genetic model for the deposition of bulk mineable precious metals in volcanic host rocks had to be developed to determine the mineral resource potential of precious metals in the area. The model was based on published data that are available in the literature, on personal experience in the exploraton for such deposits, and geologic inferences derived from this study.

Evidence of precious metal mineralization in the White River area is subtle. Although hydrothermal alteration is extensive, provided the scattered outcrops are examined in detail, a cursory inspection would lead to rejection of the area because the discrete zones of metallization are difficult to locate and because vegetation is dense, soils are thick, topography is steep, and there is a lack of recorded mineral production. However, the presence of surface and subsurface

gold anomalies contained within a fossil hot-spring system and associated with a favorable trace element geochemistry documents the likely proximity of precious metals that warrant more careful and detailed investigation.

Methods of Study

Geologic mapping and sampling of the White River area was performed over two summer field seasons of three months each. Mapping was at a scale of 1:24,000, and more detailed mapping at a scale of 1:12,000 was initiated locally to better represent chemical, mineralogical, and structural complexities related to newly discovered mineralized zones. Since the volcanic stratigraphy in the area had been incorporated in several previous geological studies (Frizzell and others, 1984; Hammond, 1963 and 1980; Hartman, 1973; and Fischer, 1970) much of the basic geologic work entailed compilation of geologic maps and field checking of contacts and structures. Volcanic rocks are named in the following chapters primarily based on weight-percent silica of water-free normalized element analyses (Taylor, 1978).

basalt	48 - 53 weight-percent SiO_2
basaltic andesite	53 - 58 weight-percent SiO_2
andesite	58 - 63 weight-percent SiO_2
dacite	63 - 68 weight-percent SiO_2
rhyodacite	> 68 weight-percent SiO_2
rhyolite	> 73 weight-percent SiO_2
	and > 4 weight-percent K_2O

Numerous samples were collected for various chemical, mineralogic, and petrographic analyses. Geochemical analyses of 173 rock chip samples for Au, Ag, As, Sb, Hg, and Mo were by one of three

methods: fire assay (FA); atomic absorption (AA), or inductively coupled argon plasma (ICP). The ICP method of analysis also provided concentrations for an additional 24 elements. Five samples of moss growing on rock outcrops were also analyzed for gold and silver by AA, and an additional 6 rock chip samples were analyzed for Au, Ag, As, and Hg. Major-element oxide concentrations in 41 rock chip samples were determined using X-ray fluorescence (XRF) analysis performed by Professor P.R. Hooper, Washington State University. Total iron was obtained by XRF analysis and a ratio of 0.20 was used to assign the amounts of oxidized and reduced iron to each sample. This method is not applicable to altered and mineralized rock samples and for these the reported iron ratios are invalid. Calculations of normative mineralogy were performed by computer using a basic language program (PETCAL) written by Bingler and others (1976).

Location and Access

The dissertation project covers an area of approximately 58 mi2 along the White River in King and Pierce counties, in west-central Washington State as shown in Figure 1. It is close to the northern border of Mount Rainier State Park, with both the White River and U.S. highway 410 bisecting it in an east-west direction. Access to the property is via U.S. highway 410 east from Enumclaw, Washington for 4 - 17 miles. Although the highway itself is public, over 95 percent of the White River area is on private property owned by the Weyerhaeuser Company and permission must be obtained from them prior to entry.

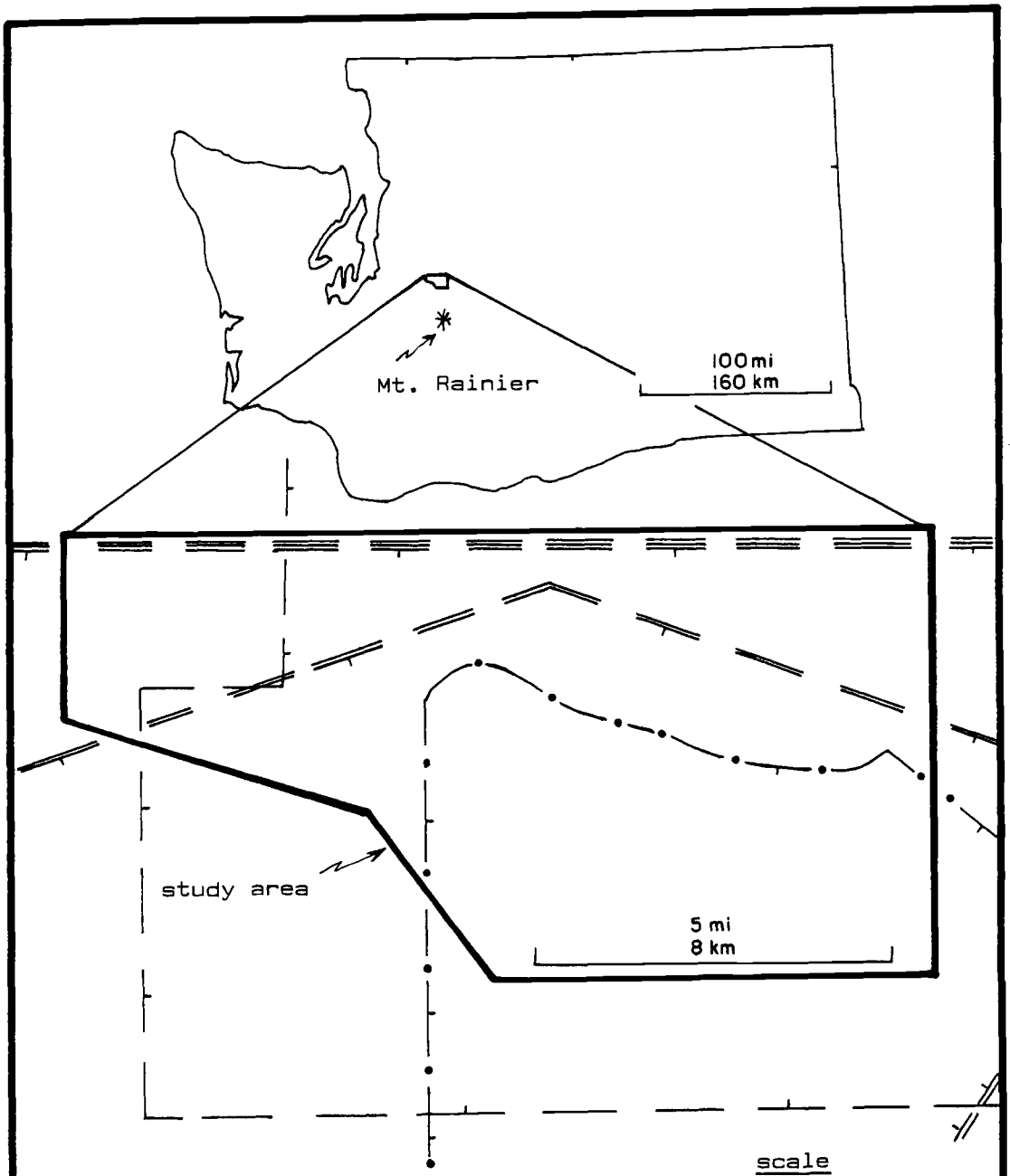

		scale
entire area	Frizzell and others, 1984	1:100,000
	Hammond, 1980	1:125,000
	_____, 1963	1: 62,500
	Hartman, 1973	1: 48,000
	Fischer, 1970	1: 62,500

Tick marks indicate the inside of a map area.

Figure 1. Location map of the White River area and reference maps used during the project.

This access, once obtained, provides a myraid of logging roads that permits entry throughout the area. The local topography is moderately rugged with altitudes ranging from 1,600 - 4,500 feet over a distance of less than two miles. Although vegetation is generally dense, the abundance of logging roads adds greatly to the amount of rock exposed in the area and provides important routes for mapping. Tree thinning is regularly performed in selected areas by Weyerhaeuser to increase the quality of the remaining trees. This practice is good for the timber growth, but it temporarily renders areas as shown in Figure 2 virtually impassable for periods of 10 to 15 years. These locations have been plotted on the 1:24,000 scale sample location map (Plate 3A) and represent areas where the acquisition of geologic information for this study was moderate to poor and an accurate geologic account remains speculative. Snow generally hampers access to altitudes above 2,000 feet for most of the winter (November - March). However, the Pacific Northwest is known for its temperate climate and periodic months of rain may greatly increase access to higher altitudes even during the winter.

Previous Work

The north - south allignment of major mining districts in the Cascade Mountains, and their distribution relative to Cenozoic age plutons, stratavolcanoes, and the White River basin are shown in Figure 3. The White River area has been partly to wholly included in a number of geologic investigations. Many of these have been

Figure 2. Tree thinning in section 9, T19N, R8E. Areas like this are virtually impassable for 10-15 year periods and make the acquisition of geologic and geochemical information limited to a few trails and roads. Thinned areas are plotted on Plate 3A.

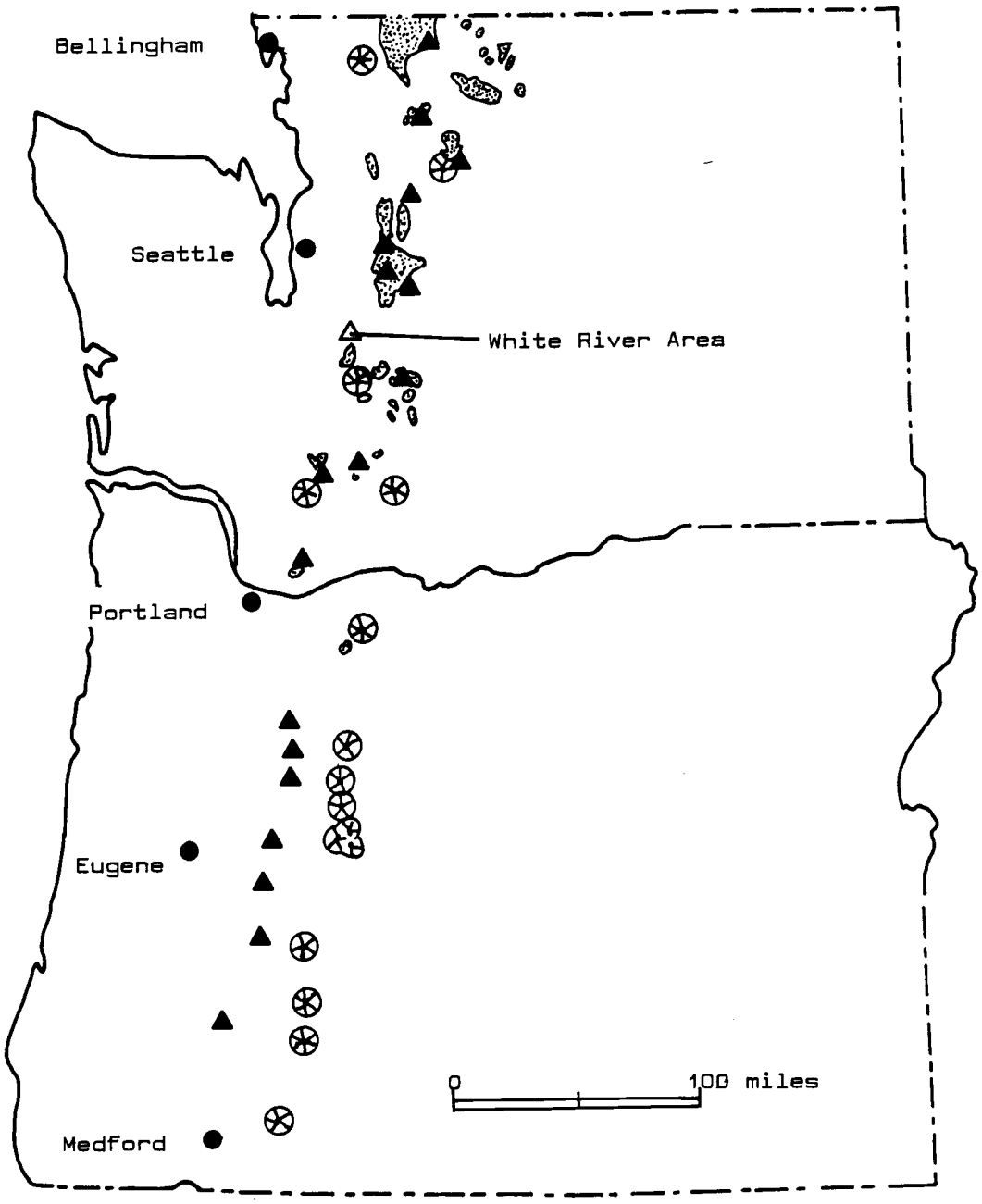

Figure 3. Distribution of major mining districts (closed triangles), Tertiary plutons (stipple pattern), and Tertiary to Quaternary stratavolcanoes (starred circles) in the Cascade Mountains of Washington and Oregon (modified from 1985 unpublished compilations of C.W. Field and S.G. Power).

concerned with glacial and mudflow deposits such as Bretz (1913), Anderson (1954), Crandell and Waldron (1956), and Crandell and Miller (1974). Others have dealt with the stratigraphy and structure of the Cascade volcanic and sedimentary rocks on a regional scale and these include Weaver (1916), Hammond (1963 and 1980), and Frizzell and others (1984). The local Tertiary volcanics have been mapped and described by Fischer (1970), Hartman (1973), and Frizzell and others (1984). The partial boundaries of five previous geological studies which were most helpful in determining the Tertiary volcanic stratigraphy and structure within the dissertation area are plotted on Figure 1. This area, from the perspective of economic geology, has been listed in publications of the Washington State Division of Mines and Geology Bulletins by Huntting (1955) for its gold occurrence and by Livingston (1971) for its alunite and silica potential. Several mining companies, since the early 1980's, have shown interest in the precious metal potential of the area. Recently, in the western portion of the White River area, minor oil exploration drilling has taken place and lithologic logs of the holes are on record with the Washington State Division of Mines and Geology.

REGIONAL GEOLOGY

Exploration geologists should have a comprehensive geologic knowledge of the terrane in which they work because the characteristic stratigraphic, magmatic, metamorphic, and tectonic features of the region may serve to define potential target areas that may host previously unknown mineral deposits. The following chapter outlines the regional geology of the Pacific Northwest throughout the Tertiary, and it has been added to the present study, in part for exploration geologists, as an aid to better understanding the geologic history and hence the origin of mineral deposits within this region. For information about the pre-Tertiary geologic history of the Pacific Northwest region major summaries are presented by Stewart, Stevens, and Fritsche (1977); and Howell and McDougall (1978).

Tertiary

Abundant igneous and sedimentary rocks of Tertiary age cover much of the land surface and constitute the most complete geologic record in the Pacific Northwest. Recent work by a number of authors, based mostly on previous geologic mapping and age dating by others, has added to a better understanding of the stratigraphic and tectonic evolution of this region. The synopsis of regional geologic events described as follows draws heavily from work by R.E. Wells, D.C. Engebretson, P.D. Snavely,Jr., R.S. Coe, R.W. Tabor, V.A.

Frizzell,Jr., J.A. Vance, T.E. Ewing, R.A. Duncan, as well as others.

General Magmatic Episodes

The early Tertiary igneous history of the Pacific Northwest region has been subdivided into three distinct episodes by Ewing (1980; p.623):

> "The first (65-53Ma) was an igneous arc extending northwest from northwestern Washington, with discontinuous magmatism in Montana and South Dakota. The second (53-42 Ma) was marked by a robust magmatic arc trending northwest-southeast from latitude 60° to latitude 40°, dominantly calc-alkaline but containing two alkaline provinces. This arc began about 53 Ma, reached its maximum intensity at 48 to 50 Ma, and decayed to 42 Ma. The third (42-30 Ma) was marked by the inception of the north-south Cascade arc south of 50° latitude and low intensity plutonism along the continental margin north of 49°.".

Magmatic activity in the Cascade arc of Oregon after this time produced voluminous silicic ash-flow tuff to about 18 m.y., followed by uplift marked by a regional unconformity and subsequent renewed volcanism of basaltic andesite to dacite composition with minor ash flows, from 17 - 9 m.y. (Wells and others, 1984). High Cascade volcanism after 9 m.y. took place in an extensional environment leading to eruptions of diktytaxitic olivine basalts as well as basaltic andesites and local silicic ash-flow tuffs (Wells and others, 1984). In northwestern Washington, the volcanics that erupted between 30 - 14 m.y. were composed primarily of dacite and pyroxene andesite flows and breccias punctuated by locally voluminous ash-flow tuffs. Subsequent High Cascade magmatic activity took place, mostly from the Pliocene to present, with mafic and intermediate extrusives in

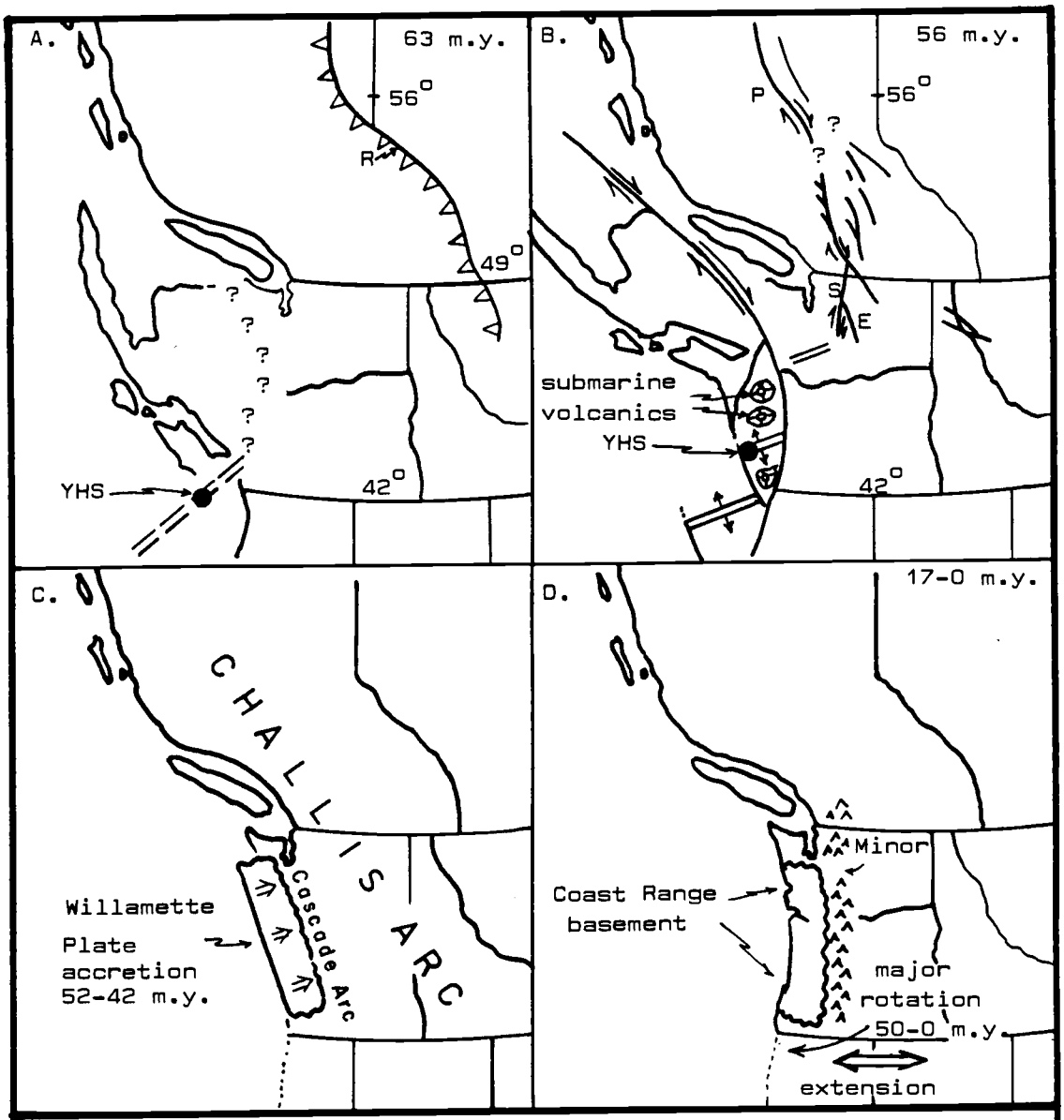

Figure 4. Major Tertiary structural and igneous events in the Pacific Northwest region (modified after Wells and others, 1984; Ewing, 1980; and Magill and others, 1982).

A). Relative position of the Yellowstone Hot Spot (YHS) at 63 m.y. and the Rocky Mt. thrust (R).

B). Rifting and northward translation of coastal rocks at 56 m.y. as the N.A. continent overrode the YHS. Inland rilght-lateral strike-slip megashearing along the Straight Creek (S) and Entiat (E) faults in Washington and others to the north.

C). Position of the Challis volcanic arc (55-43 m.y.), accretion of the Coat Range, and formation of the Cascade volcanic arc (post-42 m.y.).

D). Major clockwise rotation of the southern Cascade and Coast Range rocks and minor rotation of the N. Cascades (50-0 m.y.).

southern Washington and intermediate to silicic volcanism in central and northern Washington (Hammond, 1980).

Plate Tectonics

Wells and others (1984) have determined several major characteristics of plate motions in the northwest Pacific during the Tertiary on the basis of a relative motion study by D.C. Engebretson in 1982. These are defined by: (1) movement of both the Kula and Farallon plates northeast with respect to the North American plate throughout the entire Tertiary; (2) a major decrease in the relative convergence rate of the Farallon and North American plates, from 150 to less than 40 km/m.y., and which took place in several stages and particularly at 43 m.y. and 37 m.y.; and (3) several reorganizations of the Kula-Farallon spreading ridge between 61 and 34 m.y.

Off the west coast of North America, the Yellowstone hot spot was centered on the Kula-Farallon spreading ridge during the early Tertiary, and was overridden by the North American plate at about 63 m.y. (Wells and others, 1984; see Fig. 4A). This event created stresses that were sufficient to cause part of the North American plate to be rifted and transported northward towards proto-Alaska (Fig. 4B). Shear stresses, contemporaneous with these plate movements, produced by oblique subduction, hot spot rifting, and (or) an onshore transform fault caused intracratonic right-lateral megashearing and the formation of the Rocky Mountain-Tintina-Pasayten-Straight Creek fault systems (Ewing, 1980;

see Fig. 4B). This stress regime disappeared by late Eocene time and large strike slip displacements along these faults ceased (Ewing, 1980). For example, the Straight Creek fault in the southern portion of this megashear system was intruded by plutons and stocks of the Snoqualmie batholith at 25 m.y., and significant strike slip displacement along the fault has not been recorded in these intrusives (Tabor and Frizzell, 1979; Tabor and others, 1984). After the cessation of inland megashear faulting during the middle Eocene, dextral motion was taken up along the offshore Queen Charlotte transform system (Ewing, 1980). Throughout the Tertiary, relative plate motions and the presence of the Yellowstone hot spot have had a direct bearing on the location, chemistry, and abundance of magmaic acivity as well as the type and magnitude of tectonism in the Pacific Northwest (Wells and others, 1984; Ewing, 1980).

Plate Tectonic-Magmatic Connection

A major spatial change of Tertiary magmatic activity took place along the west coast of North America with the westward migration of volcanism from the northwest-trending Challis volcanic arc to the north-trending Cascade volcanic arc. This change was temporally coincident with accretion of the Coast Range basement rocks to the North American continent. Although the relocation of igneous activity westward may have been caused by this accretion event, Wells and others (1984) presented a good case for a cause-and-effect relationship between the changes in the absolute motions and rates of

movement of the Pacific, Kula, Farallon, and North American plates and the amounts, types, and location of igneous activity in the Pacific Northwest throughout the Tertiary. They noted that the decrease in convergence rates between the North American and Farallon plates from 150 to less than 40 km/m.y. between 43 and 28 m.y. ago is correlative with the westward step-wise migration of igneous activity from the Challis arc to the Cascade arc (42 m.y.), a flare-up of basaltic and alkalic volcanism in the Coast Range (44 to 30 m.y.), and increased ignimbrite activity in the Cascade arc (37 to 18 m.y.).

Paleocene

Convergence rates between the Kula and North American plates were about 133 km/m.y. in a northeast-southwest direction at 65 m.y. (Wells and others, 1984). A Paleocene compressional environment resulting from this convergence is evidenced by major inland thrust belts including the Rocky Mountain (Fig. 4A), Sevier, and Wind River thrusts. In British Columbia and north-central Washington, a belt of Paleocene intrusions marks the location of a northwest to southeast-trending magmatic arc from 48 to beyond 60° latitude, with discontinuous magmatic activity to the south and far inland (Ewing, 1980).

Eocene

Igneous and sedimentary rocks in the Cascade Mountains of

Washington record the presence of two significant volcanic arcs that were active during the Cenozoic. These are represented by the Challis volcanic arc of Eocene age and the younger Cascade volcanic arc (see Fig. 4C). The Challis volcanic arc was a major northwest-trending calc-alkaline volcanic provence that was active primarily between 53 and 42 m.y., with maximum volcanic activity from 51 to 48 m.y. according to Ewing (1980). He noted that its southern region, from 42 to 48° latitude, was a broad volcanic field 500 to 800 km wide. This volcanic arc narrowed in a northerly direction to 250 km between 48 and 56° latitiude and to 70 km in width north of 56° (Fig. 4C). Although the Challis arc was generally east of the younger Cascade arc and the two arcs had discretely different trends, they overlap in the northern Cascades of Washington with volcanic rocks of the Cascade arc superimposed on those of the Challis arc. Similarities in the calc-alkaline compositions of igneous rocks from both arcs makes it difficult to distinguish one suite from the other in the field, where they overlap (Ewing, 1980). It may be more correct to envision the northern Cascades of Washington as an area of long-lived periodic magmatic activity from the Eocene to present. As discussed in a previous section, Paleocene tectonism in the Pacific Northwest was compressional. A change in the stress regime may have taken place subsequent to termination of this compressional environment, as Vance (1982) reported that the abundant arkosic sedimentary and calc-alkaline volcanic rocks deposited in the Eocene Challis volcanic arc were formed in an extensional tectonic environment. However, right-lateral megashearing along the Rocky

Mountain-Tintina-Pasayten-Straight Creek fault systems is evidence of compressional stresses from late Paleocene to middle Eocene. Contemporaneous basin development throughout the Pacific Northwest also took place at this time, including: the nonmarine Tranquille, Merritt, Princeton, and White Lake Formations of British Columbia; the nonmarine Chuckanut, Swauk, and Roslyn Formations of Washington; as well as the deltaic to marine Raging River, Puget, Cowlitz, Roseburg, Flournoy, and Tyee Formations of Washington and Oregon (Ewing, 1980). The decline of volcanic activity in the Challis arc after 48 m.y. and its rapid demise after 42 m.y. (Ewing, 1980) was coincident with the accretion of the Coast Range basement complex onto the west coast of Washington and Oregon (Wells and others, 1984; see Fig. 4C). After emplacement of the Coast Range basement rocks, a dramatic westward shift in the regional magmaic activity took place from the northwest-striking Challis arc to the more north-trending Cascade arc (Figs. 4C and 4D). Whether or not this spatial change in the distribution of regional magmatic actvity resulted from the accretion event or from the changes in plate motions and subduction rates is speculative, although Wells and others (1984) presented reasonable evdence supporting the latter.

The Coast Range basement rocks of Washington and Oregon are composed of abundant tholeiitic marine pillow basalts, breccias, and flows of Paleocene to Eocene age (Duncan, 1981). Paleomagnetic evidence indicates that since their accretion onto the North American continent in the middle Eocene, these rocks have undergone considerable clockwise rotation of up to 77° (Magill and others,

1982). They believe that most of this allochthonous terrane has acted as a rigid block, the Willamette plate, with considerable rotation taking place in the southern end and much less rotation to the north (Fig. 4D). Wells and others (1984) agree with this interpretation and suggest that most of the rotation of the Willamette plate has taken place since it was accreted, which indicates that the rotation mechanism was primarily asymmetric back-arc spreading and superimposed right-lateral shearing. Magill and others (1982) have proposed that the clockwise rotation was caused by the northwestward termination of the Basin and Range extensional regime, which imposed dextral transform structures on continental rocks and the simultaneous rotation, rather than fracturing, of the rigid Willamette plate.

Wells and others (1984) have presented three models for the formation and emplacement of the Coast Range basement rocks. They are the Hot Spot model, the Leaky Transform model, and the Continental Rifting model. The Hot Spot model, proposed by Duncan (1981), calls for formation of the allochthonous Coast Range basement rocks from two linear oceanic island chains, which were produced by the superposition of the Yellowstone hot spot on the Kula-Farallon spreading ridge off the coast of North America. These oceanic islands and associated seamounts were then transported landward toward a subduction zone, eventually accreted to the west coast of Oregon and Washington, and subsequently rotated into their present position. Evidence in support of these events includes: (1) the typical oceanic island geochemistry of the Coast Range basement rocks (i.e. tholeiitic pillow basalts and breccias that grade locally into subaerially erupted alkali basalts);

(2) the anomalous (15 to 20 km) thickness of crust along the axis of the Coast Range; (3) the nearly symmetrically mirrored age distributions of these oceanic rocks from a younger central zone at about 46° latitude and increasingly older ages to the north and south; and (4) the Tertiary absolute motion studies of the Pacific, Kula, and Farallon plates together with the known proximity of the Yellowstone hot spot to the Pacific Northwest coast at that time (Duncan, 1981). The Leaky Transform model is a modification of the Hot Spot model by which Wells and others (1984) suggest that groups of seamounts periodically were generated along leaky transform faults as the Farallon and Kula ridge spreading centers reorganized at 61, 56, and 48 m.y. Many of these groups attained large size because of their close proximity to the Yellowstone hot spot. In this model the mirrored age distribution of the Coast Range basement rocks were formed as the sequentially younger events of ridge reorganization took place progressively closer to the continental landmass and subduction zone. Thus, islands that formed farther off the coast had more time to move larger distances north and south off the spreading ridge prior to their accretion onto the continent. A third model, that of Continental Rifting proposed by Wells and others (1984), appears to adequately explain formation of the Coast Range basement rocks and is temporally more consistent with the 1982 revised absolute motions of the Kula, Farallon, Pacific, and North American plates by D.C. Engebretson. This model includes the generation of submarine tholeiitic basalts in the wake of a rifted and tectonically transported continental margin (Figs. 4A and 4B). Wells and others

(1984) used both geologic and paleomagnetic evidence to determine the Late Cretaceous and early Tertiary positioning of a large landmass adjacent to, and possibly attached to, the west coast of Washington and Oregon. Included in this landmass are the Prince William and Chugach terranes of present day southeast Alaska. In the Continental Rifting model, Wells and others (1984) believe that rifting of this landmass from the continent took place as the North American plate overrode the Kula-Farallon ridge, with the Yellowstone hot spot centered beneath it, at 61 to 56 m.y. (Fig. 4B). Stress fields induced by this event caused large scale dextral shearing and the north-northwestward translocation of a large landmass toward proto-Alaska. A gulf, similar to the Gulf of California, opened up in the wake of the tectonically transported landmass with subsequent eruption of nearshore submarine volcanics. These volcanic rocks created an elongate section of oceanic crust near to and paralleling the newly formed coast line of North America. The presence of the Yellowstone hot spot was probably responsible for the eruption of prodigious quantities of submarine volcanics, which caused the formation of the anomalously thick oceanic crust presently under the Coast Range of Washington and Oregon. The formation of this thickened oceanic plate from a submarine spreading center might also explain the temporally symmetrical north-south arrangement of the Coast Range basement rocks. In this model, the thickened oceanic crust of the Coast Range basement rocks would have formed nearly in place without the necessity of long range tectonic transport. Forces that induced continental rifting and right-lateral strike-slip faulting near the

coast also may have caused the large right-lateral strike-slip fault systems up to several hundred miles inland (Wells and others, 1984; see Fig. 4B). Displacement models by Ewing (1980) show up to 310 miles of right-lateral movement along these faults. Continental sedimentary sequences and metamorphic basins of Eocene age, which are present in local and regional basins adjacent to major fault systems, indicate that pull-apart basins were a common result of the inland strike-slip movements (Ewing, 1980). An example is the Shuswap metamorphic terrane of northeastern Washington and southeastern British Columbia, which is bordered on the north by the central Rocky Mountain Trench and on the south by the Pasayten fault. A second example is seen in the continental sedimentary rocks of the Swauk basin of west-central Washington that were deposited in a graben formed by the Straight Creek fault on the west and the Entiat fault on the east. The formation of local basins (i.e. the Chuckanut basin of western Washington) was in part contemporaneous with formation of the Coast Range basement rocks. According to Wells and others (1984), final suturing of the Coast Range allochthon took place by 50 m.y. in southern Oregon and by 42 m.y. in northern Washington. The advantages of their Continental Rifting model over the others are twofold; first, it solves geometric problems associated with the Oceanic Island-Hot Spot model, and second, it is temporally more consistent with the moderate rates of age progression noted in basement rocks of the Coast Range. The one major drawback to this model relates to the explanation of compressional tectonics that are attributed to a strong deformational event recorded by basement rocks and the overlying

Eocene turbidites of the Coast Range in southwestern Oregon. This compressional event may be better explained using the accretion of oceanic island chains model (Hot Spot model) by Duncan (1981). However, Wells and others (1984) believe that an alternate cause of the compressional deformation could have been the closure of a marginal basin, accompanied by incipient subduction of the oceanic plate beneath the continental crust, as the Kula-Farallon ridge migrated northward. Radiometric age determinations of Coast Range basalts range from 62 to 49 m.y. (Wells and others, 1984). They also state that age constraints on the final emplacement of the Coast Range allochthon come from crosscutting dikes and plugs (initial Cascade arc intrusives) dated at 42 m.y. in the northern region, and the lower to middle Eocene Tyee Formation that covers the suture in the southern Coast Range.

Oligocene to Miocene

Igneous activity in the Challis arc reached a maximum about 51 to 48 m.y. ago, and decreased after 42 m.y. (Ewing, 1980). A general westward shift of igneous activity followed accretion of the Coast Range basement. Wells and others (1984) consider the 42 m.y. quartz diorite, andesite, and dacite plugs and dikes intruding the Coast Range basement rocks in northwestern Washington as marking the inception of the Cascade volcanic arc, with full robust volcanic activity by 35 m.y. This new volcanic arc was at a 30 to 40° angle (clockwise) to the Challis volcanic arc, and was situated east of and

parallel to the recently accreted Coast Range basement rocks (Ewing, 1980; see Figs. 4C and 4D). Vance (1982) states that the Challis arc was an important source of calc-alkaline volcanic and arkosic sedimentary rocks between 59 to 39(?) m.y., with Cascade arc volcanism beginning about 37 m.y. and continuing to present. Frizzell and Vance (1983) categorize the Eocene igneous and sedimentary rocks of Washington as related to or part of the Challis volcanic episode, with true Cascade arc volcanism beginning in the early Oligocene. However, Wells and others (1984) have noted that the Clarno Formation of eastern Oregon is both spatially and temporally (primarily 47 to 35 m.y.) between the Challis and Cascade volcanic arcs. Although the significance of the Clarno Formation is not well understood, they suggest that it may possibly represent the intermediate position of a volcanic arc during the westward migration of igneous activity. The end of the initial stage of igneous activity in the Cascade arc was marked by a widespread unconformity at about 38 to 35 m.y. (Wells and others, 1984). The off-shore subduction zone appears to have imparted a compressional tectonic regime to the Cascade volcanic arc during its initial stage of activity (Vance, 1982). However, after the initial magmatic pulse widespread extensional tectonics allowed the hypabyssal emplacement of major silicic batholiths, stocks, and plutons. Contemporaneous with these shallow intrusions was the Oligocene to early Miocene eruption of a thick sequence of silicic ash-flow tuffs and lavas throughout the Cascade arc which are temporally correlative with the 34 to 17 m.y. Basin and Range ignimbrite flare-up (Wells and others, 1984). They also report that in Oregon these felsic volcanics

include the Little Butte Formation and time-equivalent silicic ash-flow units of the John Day Formation, as well as other silicic ash-flow units of southern Oregon. In Washington this period of igneous activity is represented by the widespread Ohanapecosh and Stevens Ridge Formations as well as other time-equivalent formations. Because of differential uplift and erosion, the Oligocene and Miocene volcanic cover so prevalent in southern Washington and Oregon has been stripped away in northern Washington leaving excellent exposures of shallowly emplaced progenitor batholiths and plutons. In northern Washington these intrusions (north to south) include: the Chilliwack batholith (34, 30, and 24 m.y.) the Cloudy Pass batholith (22 m.y.); the Index batholith (34 m.y.); the Grotto batholith (25 m.y.); the Snoqualmie batholith (25, 20, and 18 m.y.); and the Tatoosh complex (24 to 13 m.y.) as summarized by Frizzell and Vance (1983). These ages are somewhat different than those summarized by Mattinson (1977) and depicted in Figure 5. Modern volcanoes of the Cascade Range, which are characterized by their rugged morphology and spectacular scenery, have been superimposed on this uplifted earlier magmatic-sedimentary arc, formed approximatey during the interval from 42 to 14 m.y.

Synopsis and Significance

The most complete record of geologic history in the Pacific Northwest region is found in rocks of Cenozoic age. Included in the record are two separate and distinct volcanic arcs, a major episode of

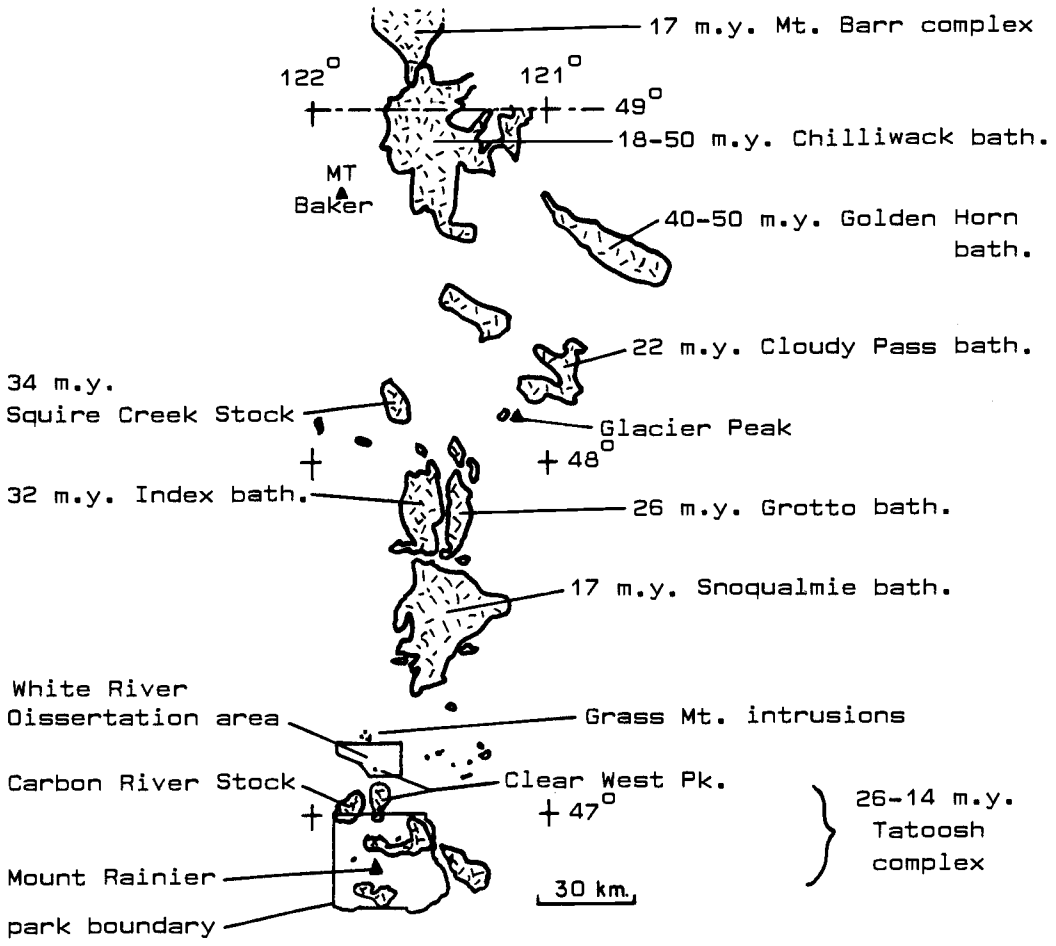

Figure 5. Location of exposed major Tertiary intrusive rocks in the central to north Cascade Range of Washington, the White River area, and Mount Rainier National Park (modified after Mattinson, 1977). The Bumping Lake pluton east of the park, the Carbon River stock in the northwestern part of the park, and the Clear West Peak igneous rocks north of the park are grouped with the Tatoosh complex.

strike-slip megashearing of the continental crust with possibly a contemporaneous continental rifting event, accretion of a large block of thickened oceanic crust onto the west coast and its subsequent clockwise rotation possibly caused by encroachment of the Basin and Range stress regime, and Pliocene to Recent volcanism of the High Cascades.

Accordingly, the Pacific Northwest contains a wide variety of rock types formed in geologically and geochemically diverse environments. Those in turn have given rise to an abundance and variety of associated types of mineral deposits. Although a detailed summary of all such mineral occurrences is beyond the scope of this study, the better known types within the region may be summarized as follows:

(1) sediment-hosted stratiform deposits of base and precious metals in the Belt Series (Spar Lake);

(2) sediment-hosted discordant silver-lead-zinc veins of the Coeur d'Alene type, possibly initially related to the stratiform ores but subsequently remobilized;

(3) magmatic deposits of chromite, magnetite, copper, nickel, gold, and platinum associated with ultramafic and mafic igneous rocks of largely oceanic origin, including those located in southwestern Oregon and northwestern California;

(4) igneous-related lead-zinc-silver replacement mantos, and base metal skarn deposits in miogeosynclinal carbonate host rocks, such as those in the Elkhorn Mts., Montana;

(5) porphyry copper or molybdenum stockwork intrusions with their

associated proximal and distal polymetallic base and precious metal vein systems, exemplified by the deposit at Glacier Peak, Washington; (6) igneous related epithermal precious metal veins and vein-stockwork systems, located in diverse geologic environments throuthout the Pacific Northwest region; and

(7) a large variety of industrial minerals and rocks that include silica, limestone, asbestos, talc, olivine, clays, and sand and gravel as well as a host of other commodities.

Metallization within the White River area is of the volcanic-hosted epithermal vein stockwork type. Polymetallic base and precious metal veins in mining and prospecting districts near the White River area are associated with granodioritic intrusions of Tertiary age. Alteration and metallization within the White River area is suspected to be genetically related to an unexposed granodiorite stock of Tertiary age.

LOCAL GEOLOGY

Local volcanic and sedimentary rocks are part of the north-south trending Cascade volcanic arc, as shown in Figure 6A, that formed in response to the emplacement of prodigious quantities of subduction related batholithic magmas. Regional structures imposed upon this volcanic arc, such as the Olympic-Wallowa lineament and the White River fault, are important factors controlling the local geology and these can be detected using satellite imagery (Fig. 6B). Volcanics, although initiated in a shallow submarine environment, became dominated by subaerial eruptions as the landmass increased by growth and coalescence of the earlier volcanic islands. After an initial stage that produced abundant subaqueous and subaerial andesitic volcanic breccias, magmatism became more felsic in composition. Extrusion of these magmas was commonly violent and formed large eruptions of siliceous ash-flow and airfall tuffs. Following and in part contemporaneous with this activity were voluminous flows of andesite and dacite erupted from shield and composite volcanic centers. The final stages of this magmatic event are defined by periodic compositional changes as the dominantly andesitic volcanics were intruded by and intercalated with rhyolitic rocks.

The U.S. Geological Survey (Frizzell and others, 1984) published a preliminary geologic map of the Snoqualmie Pass 1:100,000 quadrangle which includes the White River area. This map, along with previous geological studies within the district (Fig. 1), provide a good

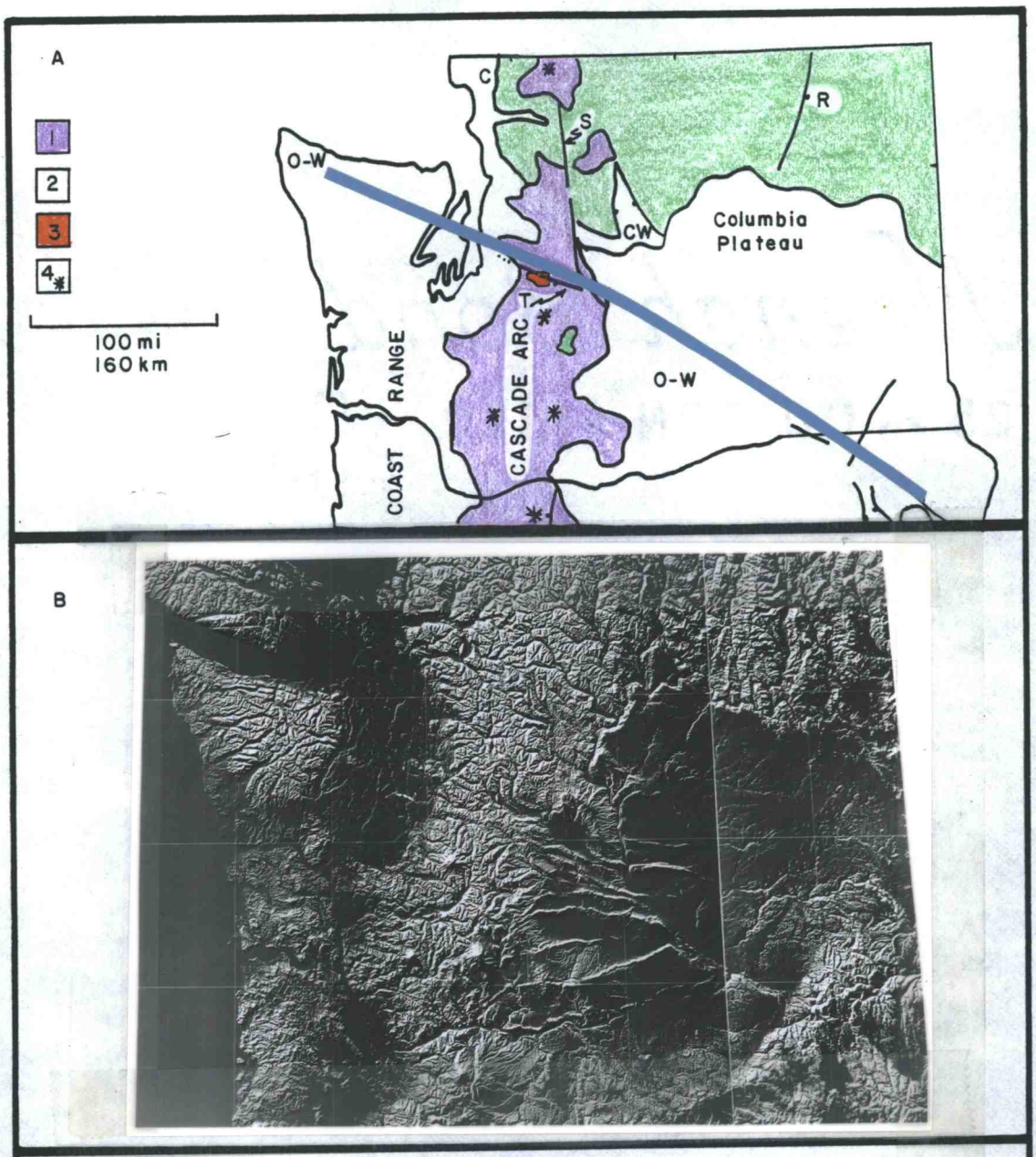

Figure 6. Location map of the White River area with selected geologic and tectonic features that include:

A). Tertiary and Quaternary volcanic rocks of the Cascade Range (1); Precambrian-Mesozoic rocks (2); White River area (3); Quaternary volcanoes (4); C, CW, and R are the Chuckanut, Chiwaikum, and Republic grabens; O-W, S, and T are the Olympic-Wallowa lineament, the Straight Creek and the Twin Creek faults; modified after Wells and others (1984).

B). Digital composite map showing topographic relief as determined by a satellite mounted laser rangefinder, with a data density of 3 arc seconds (approximately 30 meter spacings).

understanding of local volcanic stratigraphy, as well as the chemical evolution of the central Cascade volcanics through time. The geology of the White River area is not complex as depicted on Plate 1A at a scale of 1:24,000. It consists of two major structural blocks separated by the west to northwest-trending Twin Creek fault (the White River fault of Frizzell and others, 1984) as shown on the more detailed regional geologic map portrayed on Figure 7. The volcanic block north of the fault has been structurally uplifted and exposes the Huckleberry Mountain Formation, a thick accumulation of dacitic and andesitic volcanic breccias with subordinate volcaniclastic sedimentary rocks and tuffs. Andesite flows of the Eagle Gorge Formation in the White River area are exposed as two small erosional remnants overlying the Huckleberry Mountain Formation. Frizzell and others (1984) consider volcanics of the Huckleberry Mountain Formation to be lithologically and temporally similar, and probably equivalent, to those of the Ohanapecosh Formation, which forms the base of the volcanic sequence to the south. South of the Twin Creek fault is a volcanic sequence composed of subaqueous and voluminous subaerial eruptives and their derivative sedimentary rocks. The base of the sequence is composed of varicolored massive to well-bedded volcanic breccias, tuffs, and sedimentary rocks of the Ohanapecosh Formation. The dominant composition of the Ohanapecosh volcaniclastics ranges from andesite to basalt, with minor dacite and rhyolite (Frizzell and others, 1984). Interstratified with the volcaniclastics are subordinate flows of pyroxene andesite and minor basalt, rhyodacite, and rhyolite (Hammond, 1980). The pre-Pliocene volcanic rocks in

Figure 7. General geologic map of the region surrounding the White River area, modified after Frizzell and others (1984). The Stevens Ridge Formation is grouped with other Miocene volcanics outside of the White River area (according to Frizzell and others, 1984) and is plotted as separate unit within the area.

1. Pre-Oligocene interbedded nonmarine sedimentary and volcanic rocks of the Puget Group, Naches Formation, and volcanic rocks of Mount Persis (undifferentiated).

2. Oligocene andesite volcanic breccias, volcaniclastic sedimentary rocks, and dacite tuff of the Ohanapecosh Formation, the Huckleberry Mountain Formation, and volcanic rocks of Mount Daniel (undifferentiated).

3. Miocene andesite, dacite, and basalt of the Fifes Peak Formaiton, Cougar Mountain Formation and Eagle Gorge Formation; including rhyolite and rhyodacite ash-flow tuff and breccia of the Stevens Ridge Formaiton (undifferentiated except for the Stevens Ridge rocks which are subdivided within the White River area).

4. Miocene rhyolite and rhyodacite ash-flow tuffs and volcaniclastic sedimentary rocks of the Stevens Ridge Formation (outside of the White River area they are grouped with the Miocene andesites).

5. Miocene rhyolite and rhyodacite ash-flow tuffs, breccias, and minor intrusions of the Clear West Peak complex. The major outcrops, south of the White River area, appear to be part of a collapsed and possibly resurgent caldera system. The ash-flows (rheoignimbrite) within the area are their extracaldera equivalents.

6. Miocene intrusive rocks of intermediate composition (mostly granodiorite and tonalite) the Snoqualmie batholith, the Carbon River Stock (part of the Tatoosh batholith), and the Grass Mountain intrusions.

7. Quaternary volcanics (including the Canyon Creek olivine basalt).

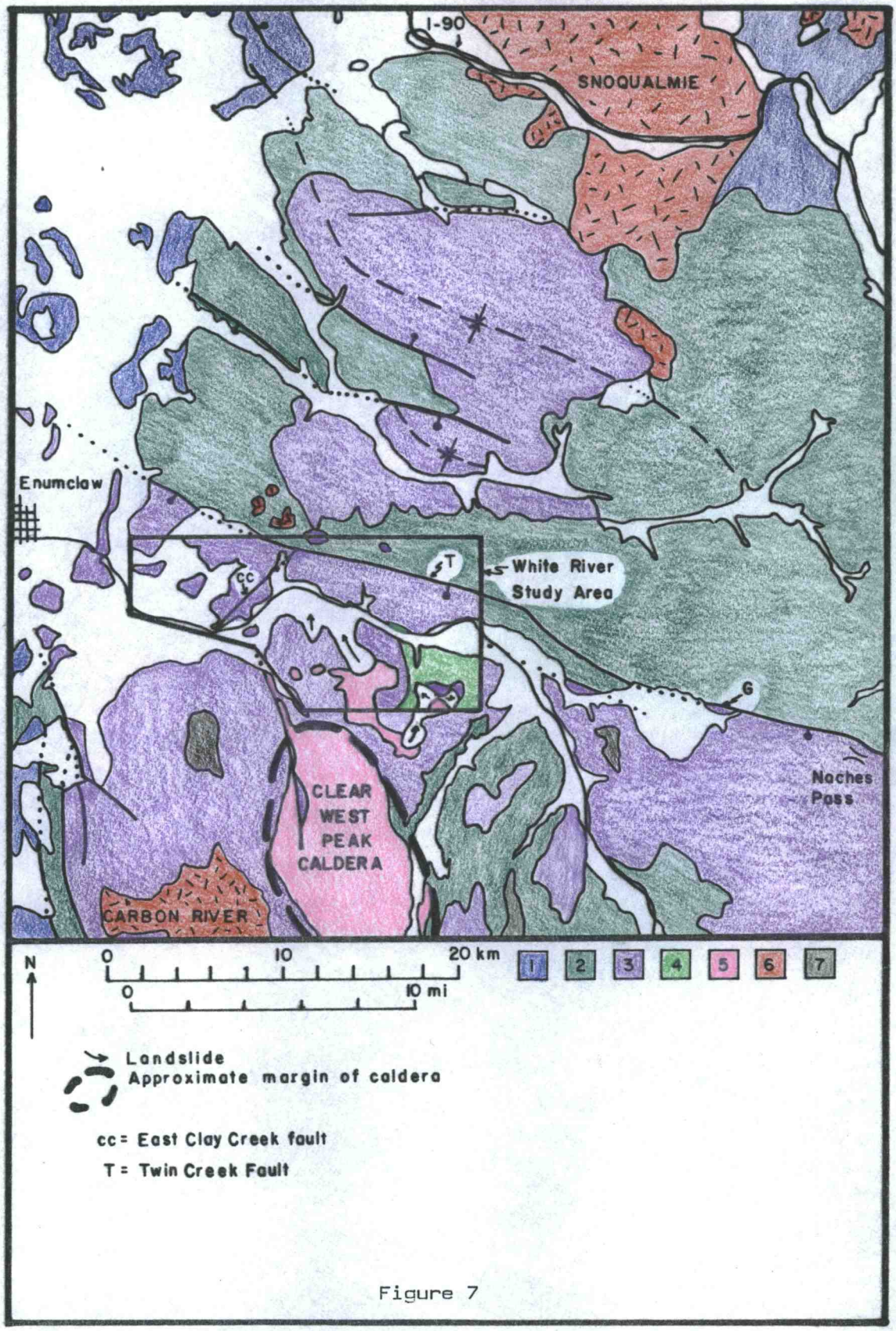
I-90
SNOQUALMIE
Enumclaw
cc
T
White River
Study Area
G
Naches
Pass
CLEAR
WEST
PEAK
CALDERA
CARBON RIVER
N
0
10
20 km
0
10 mi
1
2
3
4
5
6
7
Landslide
Approximate margin of caldera
cc = East Clay Creek fault
T = Twin Creek Fault

Figure 7

Mount Rainier National Park have been subdivided by Fiske and others (1963) into the Ohanapecosh, Stevens Ridge, and Fifes Peak Formations in order of decreasing age. Although the Ohanapecosh Formation does not crop out within the borders of the White river area, it forms the base of a tripartite volcanic sequence to the west, south, and east (Frizzell and others, 1984). These three rock units are in part contemporaneous and correlative with rock units within the White River area, to the north. Mapping by Fischer (1970) and Hartman (1973) indicates that most of the pre-Pliocene outcrops along the Clearwater River are part of the Ohanapecosh Formation. However, these rocks are assigned to the younger Fifes Peak Formation, in both the present study and that of Frizzell and others (1984). Fiske and others (1963) provide a comprehensive description of the Ohanapecosh Formation from outcrops within and near Mount Rainier National Park. The Stevens Ridge Formation unconformably overlies the Ohanapecosh Formation and is primarily composed of siliceous ash-flow tuffs and intercalated volcanic sediments, which were deposited on the deeply incised erosional surface of the Ohanapecosh Formation (Fiske and others, 1963). The Fifes Peak Formation, a thick accumulation of andesitic volcanic flows and breccias with subordinate felsic interflows, was deposited unconformably on the Stevens Ridge Formation. Capping the Fifes Peak andesites, and forming several ridge crests and peaks south of the White River, is the Clear West Peak ash-flow tuff. This unit exhibits both airfall and flow textures and may be a rheoignimbrite (Fischer, 1970; Frizzell and others, 1984).

Major-element oxide data from 41 samples of igneous rock units

within the White River basin are listed in appendix 3. Of this data, 23 samples representing the least altered of each rock unit are plotted on an alkali-lime variation diagram and also on an AFM ternary diagram, Figures 8 and 9 respectively. These igneous rocks formed over a short interval of time (about 24 - 20 m.y.) during emplacement of plutons of the Tatoosh batholith, as will be discussed in the section on Synopsis of Miocene Igneous Events. The close spatial and temporal association of Miocene age volcanic and intrusive rocks within the White River basin, which exhibit an alkali-lime crossover point of about 64% SiO2, indicates a local petrogenic suite of igneous rocks that is dominantly calcic in composition. Furthermore, Figure 9 indicates that this petrogenic suite of rocks did not undergo significant iron enrichment during magma differentiation and emplacement.

Huckleberry Mountain Formation

Outcrops of the Huckleberry Mountain Formation within the White River area are restricted to a tectonically elevated structural block north of the Twin Creek fault. Here, the multicolored andesitic lapilli breccias, tuff breccias, and volcanic sedimentary rocks that comprise this formation are exposed by rugged topography in the Slippery Creek drainage and westward, as shown in Figure 10. Hammond (1963) has subdivided the Huckleberry Mountain Formation into seven members, which from oldest to youngest are the McDonald Point Tuff, the Bear Creek Mudflows, the Rat Creek Tuff, the Champion Creek Tuff,

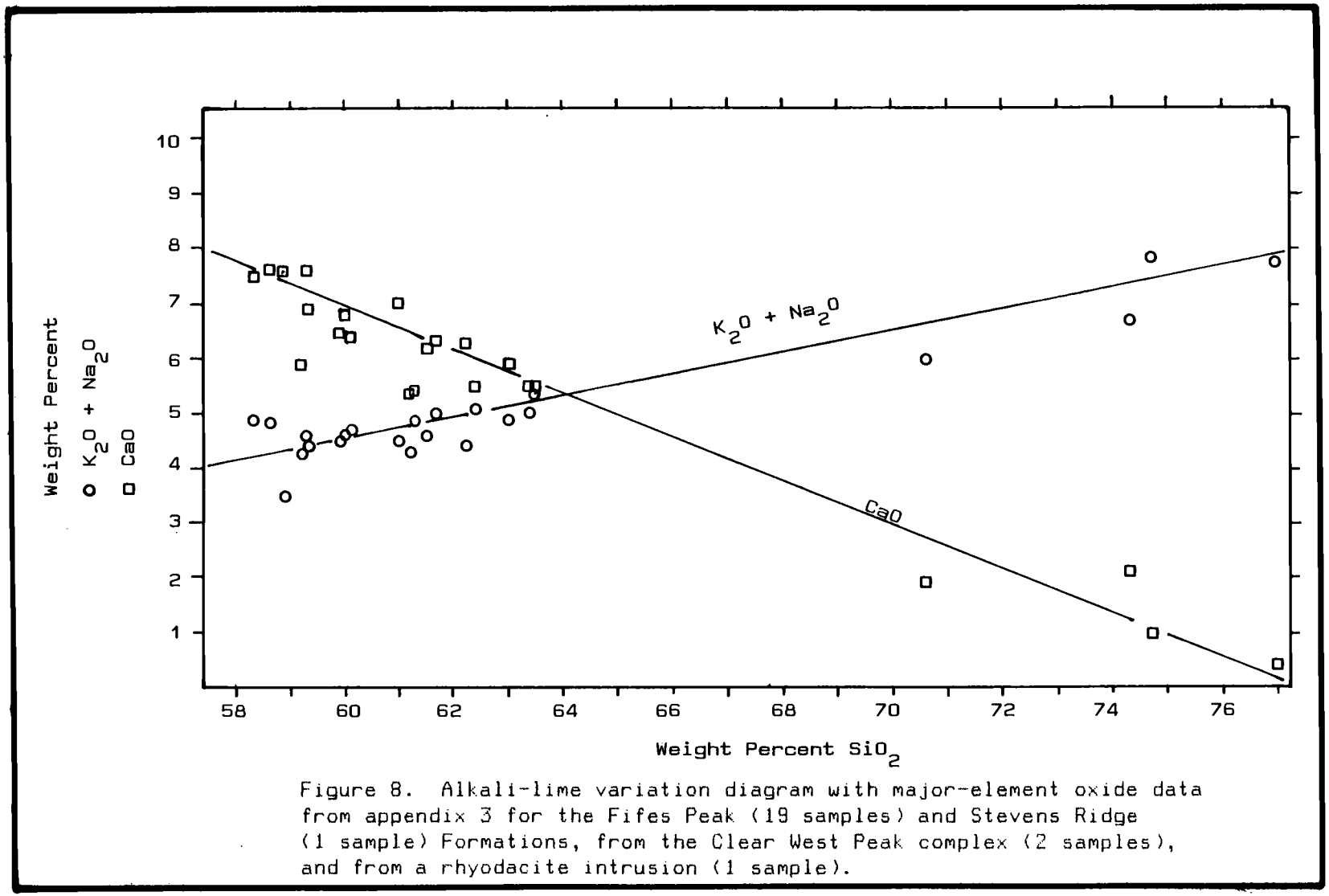

Figure 8. Alkali-lime variation diagram with major-element oxide data from appendix 3 for the Fifes Peak (19 samples) and Stevens Ridge (1 sample) Formations, from the Clear West Peak complex (2 samples), and from a rhyodacite intrusion (1 sample).

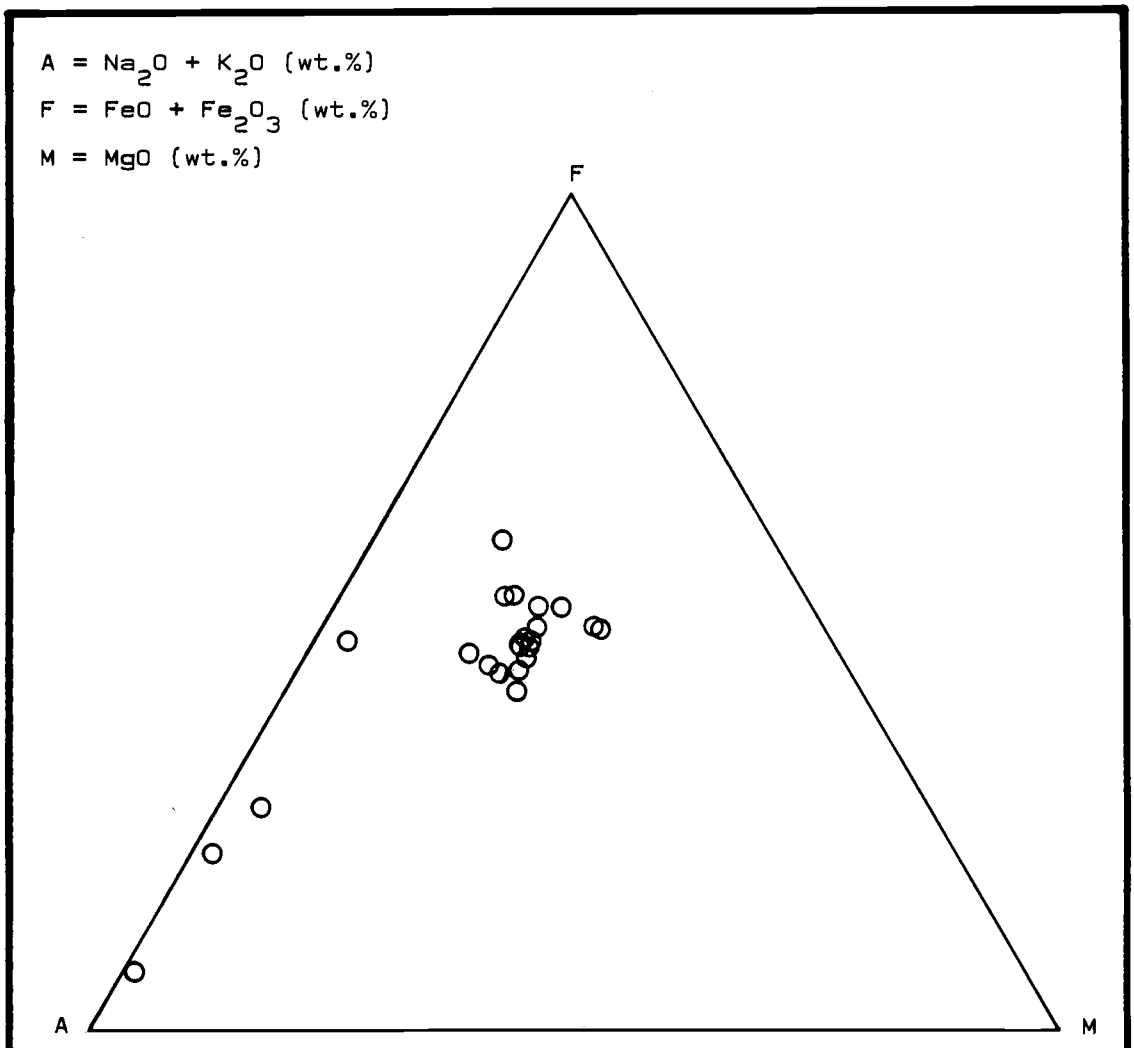

Figure 9. AFM diagram with 23 samples representing major igneous rock types present within the White River basin (major-element oxide data for these samples are listed in appendix 3).

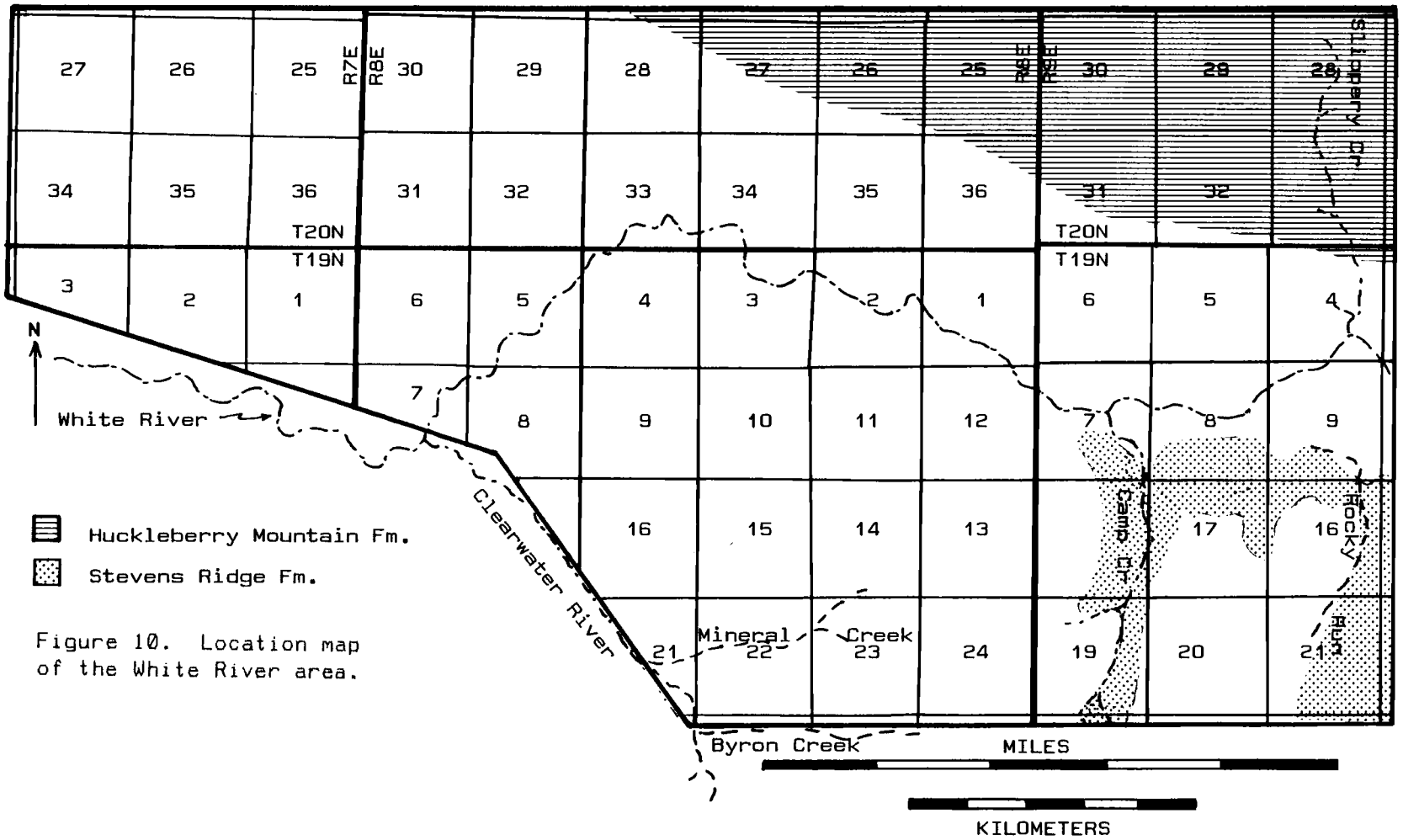

Figure 10. Location map of the White River area.

the Twin Camp Creek Flows, the Tacoma Creek Tuff, and the Snowshoe Butte Flow, and he has provided a detailed description of their genesis. The Huckleberry Mountain Formation has been described by Frizzell and others (1984) as being composed primarily of well-bedded andesite and basalt volcanic breccias, tuffs, and flows with minor dacite and rhyolite tuffs, volcanic breccias, and derivative volcanic sedimentary rocks. They note that volcanic flows become more abundant near the base of the formation and near its eastern and western margins. According to Hammond (1980), this formation consists of interstratified pyroxene andesite porphyry flows, breccias, and tuffs. Within the White River area, rocks of the Huckleberry Mountain Formation are predominantly massive to well-bedded volcanic breccias consisting of lapilli-size clasts of altered andesite and basalt(?), which grade locally into beds rich in either block size clasts or ash. The lapilli breccias are predominantly clast-supported with a variable amount of tuffaceous matrix, but which locally grade into matrix-supported breccias or tuffs. The volcanic breccias are interstratified with subordinate amounts of well-bedded volcaniclastic sedimentary rocks composed mostly of sandstones and siltstones with local accumulations of carbonaceous material (Figs. 11 and 12). Numerous dikes and sills of andesite intrude the Huckleberry Mountain Formation, and they are particularly well exposed along Slippery Creek.

Figure 11. Hand specimen of volcanic breccia from the Huckleberry Mountain Formation (sec. 36, T20N, R8E).

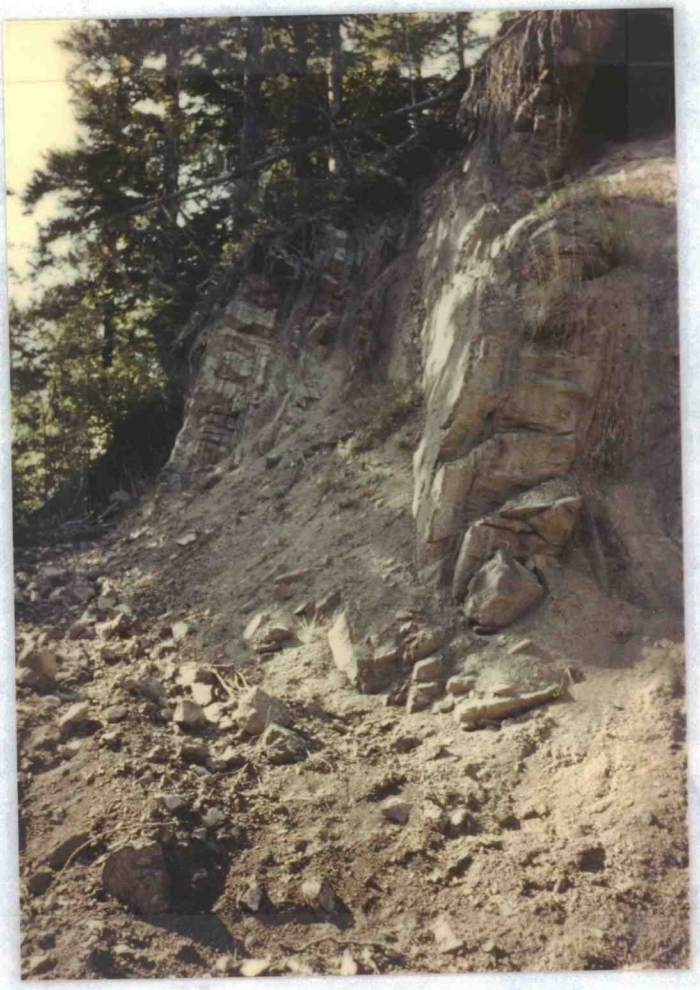

Figure 12. View to west of well-bedded carbonaceous volcaniclastic sedimentary rocks, striking N60 - 70°W and dipping 75°SW, within the Huckleberry Mountain Formation (sec. 33, T20N, R9E).

Alteration

The Huckleberry Mountain Formation exhibits pervasive low grade alteration caused by burial beneath a thick volcanic pile, intrusions of locally abundant dikes and sills, and by the presence of highly permeable breccias. Hand lens identification of minerals contained in these alteration assemblages include chalcedonic and opaline silica, pyrite, epidote, calcite, various clays, chlorite, and fibrous zeolite. The zeolite, identified as laumontite through X-ray diffraction analysis, commonly forms white 1 - 2 in. radiating crystal masses within fault zones.

Structure and Thickness

Frizzell and others (1984) show the Huckleberry Mountain Formation as having been folded into a series of anticlines and synclines with west to northwest-trending fold axes. These folds are commonly associated with faults which strike in a similar direction. The entire series of west-northwest trending folds and faults is an expression of the Olympic-Wallowa lineament that passes between the White River and the Snoqualmie River 20 miles to the north (Figs. 6A, 6B, and 7). Within the area of study the Twin Creek fault bounds the Huckleberry Mountain Formation on the south and has folded it into a high angle asymmetric anticline. Dips of many beds adjacent to the fault are nearly vertical (Fig. 12) and some are locally overturned. Farther to the north of this fault the dips become increasingly

shallow. Rocks of the Huckleberry Mountain Formaton are in contact with the younger two-pyroxene andesite flows of the Fifes Peak Formation along the Twin Creek fault. The contrasting lithology of these two formations makes them distinctive and the fault zone easy to map. Hammond (1963 and 1980) has mapped a series of north-northwest trending folds that pass from the structural block south of the Twin Creek fault into the Huckleberry Mountain Formation to the north, whereas Frizzell and others (1984) do not indicate a continuation of these north-south folds across the fault zone.

Hammond (1980) has estimated the Huckleberry Mountain Formation to have a thickness of between 2,300 and 9,800 ft., and its probable equivalent (the Ohanapecosh formaiton) as attaining a maximum thickness of about 16,000 ft. in southern Washington. Within the White River area the Huckleberry Mountain Formation is exposed for over 2,200 ft. of topographic relief. The base of this formation is not exposed here and its true thickness is probably much greater.

Age and Regional Correlation

Hammond (1980), using the 1977 age determinations by J.A. Vance and C.W. Naeser, reinterpreted the stratigraphic position of the Huckleberry Mountain Formation to be below that of the Stevens Ridge Formation, its age to be Oligocene, and its contact with the Fifes Peak Formation to be structural. Frizzell and others (1984) list nine fission-track and potassium-argon age determinations of rocks from the Huckleberry Mountain Formation and dikes intruding it. These indicate

a range of ages from 35.2 to 24.7 m.y. (Oligocene), which make it an approximate temporal equivalent of the 36 to 28 m.y. age Ohanapecosh Formation. Rocks of the Huckleberry Mountain Formation are lithologically and temporally similar, and probably equivalent, to those of the Ohanapecosh Formation (Frizzell and others, 1984). The Ohanapecosh Formation has an extensive linear north-south trending distribution in western Washington and Oregon. Mapping by Hammond (1980) has shown the boundaries to extend from at least as far north as the central Cascades of Washington (north of 47° latitude) and southward over 100 miles into at least the northern part of Oregon. Frizzell and others (1984) have mapped the Huckleberry Mountain Formation, the probable equivalent of the Ohanapecosh Formation, as extending at least 18 miles north of the Twin Creek fault.

Origin and Significance

The Huckleberry Mountain Formation can be envisioned as a northward extension of the same type of subaerial and subaqueous explosive arc-related volcanism that produced the volcaniclastics of the Ohanapecosh Formation. Fiske and others (1963) provide a detailed description of the Ohanapecosh Formation from outcrops within and near Mount Rainier National Park. They have demonstrated that much of this unit formed in a shallow subaqueous environment, possibly similar to a shallow sea or large inland lake. Fischer (1970) has corroborated the underwater depositional environment for the majority of tuffs and tuff breccias that compose the bulk of the Ohanapecosh Formation. The tuff

breccias were deposited from either subaqueous eruptions, or as subaerial pyroclastic eruptions that flowed into the water from nearby volcanic sources on land. Hartman (1973) has envisioned the depositional environment as having been a broad floodplain that underwent semi-continuous subsidence as pyroclastics and epiclastic mudflows issued from nearby volcanic centers. Rock units of the Ohanapecosh and Huckleberry Mountain Formations were probably formed in a shallow submarine volcanic arc environment where both subaqueous and subaerial eruptions were common, as volcanic islands were constructed, coalesced, or subsided. Volcanic eruptions from a nearby landmass added to the volume of pyroclastic rocks which eventually underwent uplift to form an elevated terrane. This landmass was subjected to further uplift and subsequently to deep erosion prior to the initial eruptions of the next protracted volcanic episode (Fiske and others, 1963).

Eagle Gorge Formation

The Eagle Gorge Formation crops out in the north-central portion of the White River area as two small erosional remnants of dark-grey pyroxene andesite flows capping the Huckleberry Mountain Formation (Fig. 7). North of and bordering the White River area, a thick accumulation of predominantly andesite and basalt flows, monolithic breccias, and minor tuffs and volcanic sedimentary rocks comprise the Eagle Gorge Formation (Frizzell and others, 1984). Although most of these volcanics appear to have been extruded subaerially, Hammond

(1980) has suggested that some breccias may have formed in a subaqueous environment.

Petrography and Chemistry

A single thin-section examination and major-element oxide analysis were made from a sample of this formation (see Table 1). Petrographic analysis determined the sample to be a propylitically altered pyroxene andesite. Although Frizzell and others (1984) indicate that this formation contains both augite and hypersthene, only one pyroxene (augite) was detected in this sample. The pervasive alteration of mafic phenocrysts to chlorite and pyrite throughout this thin-section may have obliterated evidence of the former presence of hypersthene. Concentrations of major-element oxides in this sample are within the range of those found in fresh andesites of the Fifes Peak Formation, with the exception of a higher TiO_2 content in the Eagle Gorge andesite.

Structure, Thickness, and Contact Relations

The Eagle Gorge Formation crops out predominantly within a 10 by 12 mile area on the northern border of the White River area. Here, the formation attains a thickness of at least 3,900 ft. and rests unconformably on the Huckleberry Mountain Formation, as indicated by cross sections from Frizzell and others (1984). The two small outcrops of Eagle Gorge Formation present within the White River area

Table 1. Major-element oxide and normative analysis of propylitically altered pyroxene andesite porphyry from the Eagle Gorge Formation (sample R27-1; NW1/4, sec. 27, T20N, R8E).

Table 1

Major Oxide	Percent
SiO2	60.43
TiO2	1.20
Al2O3	15.63
Fe2O3	3.99
FeO	4.57
MgO	2.76
CaO	6.36
Na2O	3.15
K2O	1.57
P2O5	0.21
MnO	0.14

Sum of oxide values = 100.01

A:F:M ratio = 30.2 : 52.2 : 17.6

Normative Minerals	Percent
Quartz	17.9
Orthoclase	9.3
Albite	26.7
Anorthite	23.9
Diopside	5.1
Hypersthene	7.8
Magnetite	5.8
Ilmenite	2.3
Apatite	0.5

Normative Plagioclase = AN 47.2

Normative Color Index = 20.9

attain a maximum thickness of 250 feet. North of the White River area rocks of this formation are folded into a series of northwest-trending anticlines and synclines and are cut by a series of normal faults that strike in the same general direction.

Age and Regional Correlation

Zircons from a rhyodacite crystal-lithic ash-flow tuff member of the Eagle Gorge Formation north of the White River area were analyzed and yielded a fission-track age determination of 20.8 m.y. (Frizzell and others, 1984). They note that this member is an extensive rhyodacite ash-flow tuff about 1,000 feet above the base of the Eagle Gorge Formation and is probably a northern equivalent of the Stevens Ridge Formation. The age, lithology, and chemical composition of the Eagle Gorge Formation are similar to those of the Stevens Ridge and Fifes Peak Formations, cropping out to the south, and all appear to have been produced from composite or shield volcanoes during an intense and widespread period of volcanism in the Cascade Arc.

Stevens Ridge Formation

The Stevens Ridge Formation was named by Fiske and others (1963) for outcrops along Stevens Ridge in the south-central portion of Mount Rainier National Park. Rocks within this formation crop out in the southeastern part of the White River area as plotted on Figure 10. The formation is primarily composed of massive rhyolite and rhyodacite

vitric, crystal, and lithic-rich ash-flow tuffs with subordinate airfall tuffs and volcaniclastic sedimentary rocks that become increasingly abundant in the upper part of the formation. Welding of the ash-flow sheets is poorly developed and is generally restricted to the lower half of the formation. Exposures near the mouth of Rocky Run Creek are moderately welded and exhibit crude columnar jointing. The ash-flow tuffs are light gray to tan with some beds locally bright green in color. The green color of some beds is predominantly caused by discoloration of the pumice and lithic clasts with alteration. The presence of abundant phenocrysts of quartz and biotite makes this formation mineralogically distinctive in comparison with other formations of the White River area. Hartman (1973) has subdivided the Stevens Ridge Formation into three members. These consist of a basal member that is a composite ash-flow sheet having three densely welded lithic-rich cooling units, a middle member containing massive pumice-rich ash-flows with minor amounts of interbedded volcaniclastic sedimentary rocks, and an upper member rich in epiclastic and volcaniclastic sedimentary rocks with subordinate ash-flow tuffs. Fischer (1970) has mapped the Stevens Ridge Formation as two assemblages. They are defined as (1) a western assemblage composed of abundant volcanic breccias and blocks of andesite in a matirx of lapilli-tuff that crops out along South Prairie Creek, approximately 6 miles southewst of the White River area, and (2) an eastern assemblage composed predominantly of lithic-rich ash-flow tuffs and interbedded volcaniclastic sediments that crops out along Camp Creek.

Petrography and Chemistry

The size of lithic fragments as well as the ratios of lithic to crystal, glass, and ash components varies considerably over intervals of 10 ft. or less throughout the Stevens Ridge Formation. Petrographic examination of four thin-sections detected the presence of phenocrysts of quartz, plagioclase feldspar, biotite, hornblende, and opaques. In addition to these minerals, Frizzell and others (1984) have also recorded the presence of phenocrysts of clinopyroxene and hypersthene. Lithic fragments are composed of felsic volcanic clasts including pumice fragments, and mafic volcanic clasts. Fischer (1970) reported the presence of the following alteration minerals: chlorite, prehnite, epidote, and albite as determined by thin-section analysis and low albite, quartz, potassium feldspar, wairakite, and clinoptilolite as determined by X-ray diffraction analysis.

Chemical and normative mineralogical data for a single sample of lapilli-rich ash-flow tuff from the Stevens Ridge Formation are given in Table 2. This sample, as it contains 74.26 percent SiO2 and 3.89 percent K2O, is a rhyodacite. Major oxide analyses have previously been reported by Fischer (1970) for two rock samples from the Stevens Ridge Formation. One sample containing 71.9 percent SiO2 and 5.05 percent K2O is a rhyolite, and the other containing 65.4 percent SiO2 and 2.75 percent K2O is a dacite. The large variability in potassium content of these three analyses may be in part a function of the volume of mafic clasts contained within each sample.

Table 2. Major-element oxide and normative analysis of light gray lapilli-rich ash-flow tuff of the Stevens Ridge Formation (sample RA8-1; NW1/4, NW1/4, sec. 8, T19N, R9E).

Table 2

Major Oxide	Percent
SiO2	74.26
TiO2	0.38
Al2O3	13.03
Fe2O3	1.31
FeO	1.50
MgO	0.52
CaO	2.11
Na2O	2.88
K2O	3.89
P2O5	0.09
MnO	0.03

Sum of oxide values = 100.00

A:F:M ratio = 67.9 : 26.9 : 5.2

Normative Minerals	Percent
Quartz	36.8
Corundum	0.5
Orthoclase	23.0
Albite	24.4
Anorthite	9.9
Hypersthene	2.4
Magnetite	1.9
Ilmentie	0.7
Apatite	0.2

Normative Plagioclase = AN 28.8

Normative Color Index = 5.0

Thickness and Contact Relations

Based on their work within Mount Rainier National Park, Fiske and others (1963) determined that a rugged topography with at least 1,500 ft. of relief was cut into the Ohanapecosh Formation prior to deposition of the Stevens Ridge Formation. They note that the unconformity between these two formations was later preferentially intruded by numerous sills of the Tatoosh pluton. The upper contact of the Stevens Ridge Formation with rocks of the Fifes Peak Formation is conformable, or nearly-conformable, within the White River area. The basal contact of the Stevens Ridge Formation does not crop out within the White River area and its true thickness here is speculative. However, rocks within this unit are deeply dissected by Camp Creek providing excellent exposures for over 1,800 feet of topographic relief. It also crops out in a landslide scar on the north side of the White River for over 250 feet of topographic relief. Within Mount Rainier National Park this formation attains a thickness in outcrop of about 3,000 feet (Fiske and others, 1963).

Age and Regional Correlation

Fossils in stratigraphically correlative rocks to the east of Mount Rainier National Park led Fiske and others (1963) to tentatively date the Stevens Ridge Formation as middle Oligocene to early Miocene. Frizzell and others (1984) list eight age determinations for the Stevens Ridge Formation. Of these, seven range from 23.3 to 19.5 m.y.

(Miocene) and the other (34.0 m.y.) is probably inaccurate. Fiske and others (1963) document the extensive intrusive nature of the Tatoosh complex into the Stevens Ridge and Fifes Peak Formations. Not only is the Stevens Ridge Formation widely distributed throughout Mount Rainier National Park and northward, but Frizzell and Vance (1983) have noted that it is regionally extensive and is sporadically exposed from the park southward to at least as far as the Columbia River.

Origin and Significance

The composite ash-flow sheets of the Stevens Ridge Formation mark a widespread and extremely violent period of felsic volcanism in the Cascade volcanic arc. This period is suggestive of an extensional tectonic regime that permitted the shallow emplacement and differentiation of batholithic magmas throughout the arc system, and probably is related to large scale oceanic-continental plate interactions. Local units of the Stevens Ridge Formation are suspected to be outflow caldera deposits genetically related to one or more of the stocks that comprise the Tatoosh batholith. Although Fiske and others (1963) document the extensive intrusive nature of the Tatoosh complex into the Stevens Ridge and Fifes Peak Formations, their spatial proximity and overlapping ages of formation suggest a genetic relationship between the three. The Stevens Ridge Formation, Fifes Peak Formation, and the intrusive and extrusive rhyolite phases of Clear West Peak may represent separate, but interrelated, events

genetically associated with the protracted episodic igneous activity of the Tatoosh pluton and its outlying stocks. These apparent cogenetic relationships are thus compatible with proposals by J.A. Vance and V.A. Frizzell and colleagues to equate the Stevens Ridge and Fifes Peak Formations and the Clear West Peak Complex and the Fifes Peak Formation, respectively, as cited by Frizzell and others (1984).

Fifes Peak Formation

The Fifes Peak Formation is a thick series of andesite lava flows and breccias, their derivative mudflows and sedimentary rocks, minor felsic tuffs, flows, and intrusives(?), and minor flows of basalt. It is widespread and comprises the majority of outcrops within the White River area (Fig. 7). The Fifes Peak Formation includes the Enumclaw Formation of Hammond (1963 and 1980), and of Fischer (1970). Frizzell and others (1984) include the Clear West Peak rhyolite as an upper member of the Fifes Peak Formation. However, for the present study the Clear West Peak rhyolite was mapped as a separate unit. The Fifes Peak Formation within the White River area consists of a thick volcanic pile composed primarily of andesite flows and breccias and that locally is interspersed with minor felsic flows, domes(?), airfall lapilli-tuff, and carbonaceous volcaniclastic sedimentary rocks. The andesites are gray to dark gray, porphyritic, and contain macroscopic phenocrysts of plagioclase feldspar, hypersthene, and augite. Andesite flows within the Clearwater River drainage are cut by numerous late stage dikes and sills of greenish-gray

phenocryst-poor diorite porphyry.

Petrography and Chemistry

Several tens of thin sections and 26 major-element oxide analyses were made of fresh rocks from the Fifes Peak Formation and their altered equivalents. These results indicate that the chemical and mineralogical composition of andesites throughout the Fifes Peak volcanic pile are largely homogeneous. Andesite flows consistently contain 20 - 30 percent fine to coarsely crystalline phenocrysts of plagioclase feldspar and 5 - 15 percent fine to medium size phenocrysts of pyroxene (augite and hypersthene). Phenocrysts of plagioclase feldspar up to 1 cm in length are common in many andesite flows and lengths up to 2 cm are present within a few flows. Volcanic breccias within the Fifes Peak Formation are generally monolithologic and contain clasts that are mineralogically similar to the andesite flows. Major-element oxide analyses were performed on 16 samples of fresh rock from the Fifes Peak Formation. Of these samples, 14 are andesites and 2 are dacites. A typical andesite from the Fifes Peak Formation contains 61 - 62 percent SiO_2, 0.90 - 0.95 percent TiO_2, and phenocrysts of plagioclase feldspar with an anorthite component of about An 48 as shown in Table 3.

Interflow Felsic Volcanics

Felsic rocks within the Fifes Peak Formation are present as

Table 3. Major-element oxide and normative analysis of a typical andesite flow in the Fifes Peak Formation (sample M-5; SW1/4, NW1/4, Sec. 36, T20N, R7E) and the compositional range of all 16 samples.

Table 3

Analysis number M-5		Range of Sixteen analyses	
Major Oxide	Percent	Percent	Percent
SiO2	61.53	58.27	64.61
Al2O3	16.30	15.73	17.50
Fe2O3	3.37	2.75	3.94
FeO	3.86	3.15	4.51
MgO	3.45	2.42	4.04
CaO	5.40	3.48	7.61
Na2O	3.16	2.68	3.42
K2O	1.69	1.10	2.06
TiO2	0.97	0.78	1.13
P2O5	0.18	0.15	0.22
MnO	0.10	0.08	0.17

Sum of oxide values = 100.01

A : F : M ratio = 31.9 : 45.4 : 22.7

Normative Minerals	Percent
Quartz	18.5
Orthoclase	10.0
Albite	26.7
Anorthite	25.3
Diopside	0.3
Hypersthene	11.4
Magnetite	4.9
Ilmenite	1.8
Apatite	0.4

Normative Plagioclase = AN 48.6

Normative Color Index = 18.3

interflow units of airfall tuffs, flows, and breccias of rhyolitic(?) composition. The Fifes Peak volcanics also host intrusions of rhyolite dikes, sills, and small plugs. An excellent exposure of unaltered interflow rhyolite(?) and associated airfall tuff crops out along U.S. highway 410 in the SW1/4, sec. 34, T20N, R8E. Here, a cliff face provides over 300 feet of vertical exposure of the rhyolite(?) flow, which is similar in appearance to both the Clear West Peak rhyolite, and rhyolitic intrusions along the Twin Creek fault (in secs. 3 and 4, T19N, R9E).

Intraformational airfall tuffs are moderately well exposed for about one mile along a roadcut in secs. 3 and 4, T19N, R8E. A zone of well-bedded pumice-rich carbonaceous sediments crops out for over 100 feet in the eastern part of this road cut. Numerous exposures of volcanic sediments, interbedded with Fifes Peak andesite flows, crop out in the Mineral Creek drainage. Carbonaceous sediments and pyroclastic flows are intruded and baked by a rhyolite plug of post-Fifes Peak Formation age, cropping out in the SW1/4, sec. 14, T19N, R8E.

A rhyolitic flow or ash-flow, its associated airfall tuff, and intrusion(?) breccias crop out in the nortwestern part of the White River area (in secs. 1 and 12, T19N, R7E; secs. 5, 6, and 7, T19N, R8E; and sec. 36, T20N, R7E). The age of this unit is unclear. It overlies some andesite flows of the Fifes Peak Formation and is topographically below others. However, direct evidence could not be found to establish its origin as an intraflow member of that formation. It is discussed here because its close spatial proximity

suggests a genetic tie to the Fifes Peak andesites. Intense hydrothermal alteration has obliterated many of the primary volcanic features of this rhyolitic unit, and pervasive silicification has changed its chemistry dramatically. A typical sample of the unmineralized silica cap contains 98 percent SiO2, <1 percent TiO2, and minor iron. Evidence indicating the presence of a flow or ash-flow of rhyolitic composition is provided by sparse remnant morphologic features such as flow banding, shard and pumice textures, ghosts, molds, and casts of crystals, and also breccias that may be intrusive in nature (see Figs. 13, 14, and 15). The overall morphology of the hill at VABM Taugow is suggestive of a dome-plug complex, but unequivocal proof is lacking. Evidence of an airfall lapilli-tuff within this part of the White River area is sparce but spectacular. An aggregation of spheroidal volcanic lapilli (up to 1.5 inches in diameter) was located in the SW1/4, sec. 1, T19N, R7E. These lapilli are similar in outward appearance to, but generally larger than, accretionary lapilli. However, their environment of formation differs from accretionary lapilli in that accretion appears to have taken place under high temperature conditions. The inside of each lapilli sphereoid contains a pumice fragment that is surrounded by accreted layers of volcanic glass, ash, and crystals, which appear to have been welded on in a semi-molten or state as shown in Figures 16A and 16B. Although the mode of formation of these spheroidal volcanic lapilli is unclear, the following two intrpretations are among the most likely of several possible explanations. In the first interpretation it is suggested that the spheroidal lapilli formed

Figure 13. Hand specimen of pumice replaced by silica (NW1/4, NE1/4, sec. 1, T19N, T7E). Less silicified fragments were weathered out leaving a porous silica framework.

Figure 14. Outcrop of felsic tuff replaced by silica (NW1/4, NE1/4, sec. 12, T19N, R7E). Note the remnant flow banding.

Figure 15. Hand specimen of breccia replaced by silica (N1/2, SW1/4, sec. 6, T19N, R8E). Possible origin of the breccia includes: (1) intrusion breccia; (2) volcanic flow breccia; and (3) explosion breccia.

A

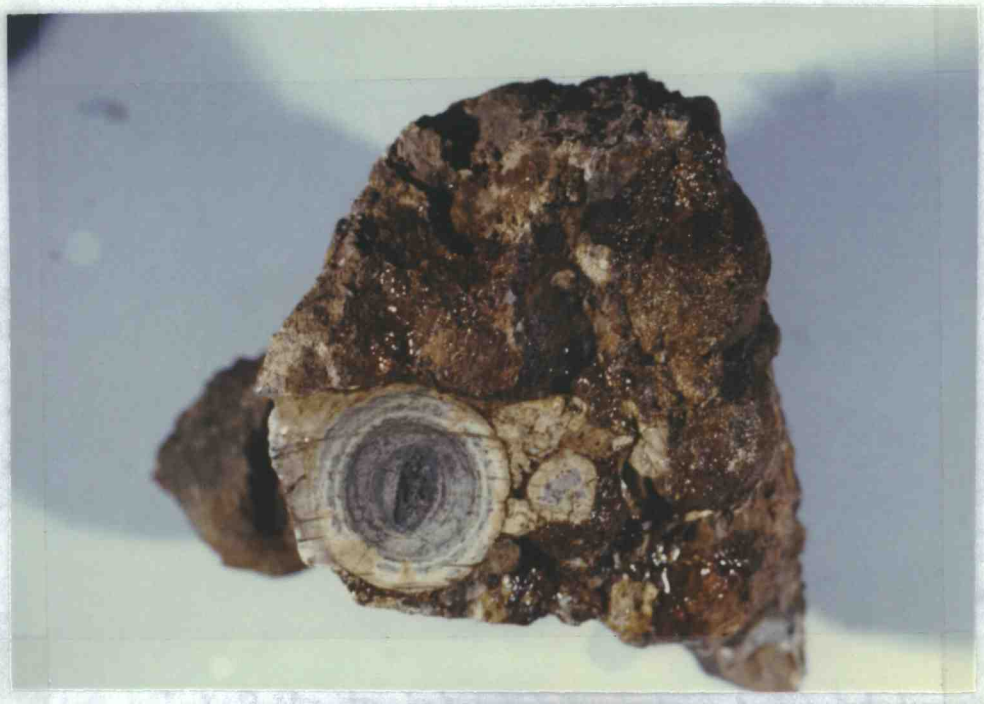

B

Figure 16. Spheroidal lapilli (volcanic hail) from the SW1/4, SW1/4, sec. 1, T19N, R7E.

A). An aggregate of spheroidal lapilli that range in size from 0.5 to 4 cm. One has been cut open revealing a central core of pumice.

B). An individual spheroidal lapilli (about 3 cm in diameter). The central core is a pumice fragment surrounded by what appear to be welded fragments of volcanic ash, dust, and crystals. The dark gray is fine grained pyrite filling open spaces.

during a pyroclastic eruption from a small felsic vent. Here, pumice fragments were suspended in a fireball of hot gases issuing from the throat of the vent or directly above it. Within the vent, twirling tumbling pumice fragments were nuclei for accreting incandescent volcanic glass, dust, and crystal fragments that welded onto their surfaces. The eccentric accretionary banding exhibited by the spheroidal lapilli in Figure 16B is suggestive of accretion during flight. A second possible mode of formation for these spheroidal volcanic lapilli is under cooler conditions, such as those under which true accretionary lapilli form. In this model, post-depositional silicification of the lapilli by hot-spring waters results in a concretionary texture giving the appearance of having been welded during flight. Of these two models the accretionary-welding process is favored for the formation of the spheroidal volcanic lapilli, and the term volcanic hail is suggested to characterize their mode of formation.

Structure, Thickness, and Contact Relations

Mapping by Hammond (1980) and Frizzell and others (1984) shows that the Fifes Peak Formation is at least 8,100 feet thick. The formation crops out for over 2,800 feet of topographic relief along Mineral Creek, within the White River area, and forms a prominent cliff face and ediface for over 2,000 feet of topographic relief along the White River, in sec. 12, T19N, R8E (see Figs. 17 and 18). Numerous faults and fractures cut exposures of the Fifes Peak

Figure 17. View south across the White River of Fifes Peak andesites (approximately 2,000 feet thick) in sec. 12, T19N, R8E.

Figure 18. Veiw northeast into the White River valley from the edifice of Fifes Peak andesites shown in Figure 17.

Formation. The largest of these is the northeast-trending Twin Creek fault. The Twin Creek fault is a normal fault that juxtaposes rocks of the Fifes Peak Formation (Miocene age) with those of the Huckleberry Mountain Formation, as depicted in Figure 7. The East Clay Creek fault is another large structure cutting the Fifes Peak Formation. This fault zone is over 4.5 miles long and was the main center of felsic igneous activity and hydrothermal mineralization along the White River (see plates 1A and 2).

Mapping by Fiske and others (1963) shows that the basal flows of the Fifes Peak Formation are concordant with stratigraphic units of the Stevens Ridge Formation within Mount Rainier National Park, and probably overlie them conformably. In contrast, mapping by Hartman (1973) has shown the contact between these two formations to be unconformable within and near the White River area. Fischer (1973) also has reported an erosional surface between these two formations within the White River area. Exposures of the contact between the Fifes Peak and Stevens Ridge Formations were examined along Camp Creek and north of the White River (in sec. 8, T19N, R9E). Here, the two formations exhibit an overall concordant relationship, although small-scale surfaces of erosion are apparent.

Age and Regional Correlation

Fiske and others (1963) placed the probable age of the Fifes Peak Formation as early Miocene, based on its stratigraphic position and regional stratigraphic relationships to other formations. Age

determinations of rocks from four flows of Fifes Peak andesite are between 24.0 and 17.1 m.y. (Frizzell and others, 1984). The early Miocene age of these lavas overlaps the age determinations for the Stevens Ridge Formation and the Clear West Peak complex, as reported in Frizzell and others (1984). The Fifes Peak Formation is widespread, cropping out sporadically throughout the central and southern Cascade Range of Washington. It is similar in age, chemistry, and petrology and is possibly correlative to the Eagle Gorge Formation, which crops out to the north.

Origin and Significance

Volcanics of the Fifes Peak Formation represent a radical change in the style and chemistry of volcanism within the Cascade arc, from the previous violent eruptions of rhyolite and rhyodacite ash-flow tuffs that formed the Stevens Ridge Formation, to a more quiescent period of andesitic lava flow eruptions from shield volcanoes. However, the partly contemporaneous eruption of both andesite and rhyolite differentiates in close spatial proximity to each other suggests that regional tectonics played only a minor role in the difference in chemistry between the Fifes Peak andesites and the Stevens Ridge and Clear West Peak ash-flow tuffs. This modification in type and chemistry of local magmas probably relates more to differences in the crustal residence time of batholithic differentiates than to arc-wide changes in tectonic regimes. The Fifes Peak and Stevens Ridge Formations and the Clear West Peak

complex all appear to be genetically related to the protracted intrusive activity of the Tatoosh batholith.

Clear West Peak Complex

The Clear West Peak complex includes a large body of finely crystalline welded ash-flow tuffs that were deposited inside the rim of a collapsed caldera, dikes and sills of rhyolite that intrude country rocks perpheral to the rim of the caldera, and a distal ash-flow tuff or rheoignimbrite. The main body of caldera-fill crops out over a 30 square mile area bordering, and south of, the White River area (Figure 7). Dikes, sills, and other small apophyses of Clear West Peak rhyolite intrude the Fifes Peak Formation peripheral to the rim of the caldera, along Mineral and Byron Creeks. A thin rhyolitic ash-flow tuff or rheoignimbrite caps many of the hills and ridges in the south-central portion of the White River area and is suspected to have originated as an outflow from the caldera eruptions. Fischer (1970) has provided a detailed description of the Clear West Peak complex, its contact relationships, morphology of its flow and eutaxitic banding, petrology, chemistry, and age.

Fiske and others (1963) describe the main Clear West Peak body as a "huge plug of flow-banded vitrophyre and contemporaneous welded tuff". The hypothesis that this large mass of rhyolitic ash-flows formed as a caldera infilling was first proposed by Fischer (1970), as one of three possible explanations for its great thickness and monolithologic nature along the Clearwater River. The other two

hypotheses he proposed for the formation of the Clear West Peak complex are based on the multiple injections of large sills. The Clear West Peak intracaldera ash-flows exhibit pervasive fluidal and eutaxitic banding as shown in Figues 19 and 20, over an extensive area. These textures are due to flowage and the partial to complete welding of portions of ash-flow tuffs.

Petrography and Chemistry

Ash-flow tuffs compose the bulk of the Clear West Peak complex. They are composed of rhyolite and rhyodacite vitroclastic flows with a consistently low percentage of crystals. A detailed comparative analysis of the lithology, mineralogy, and chemistry of the Clear West Peak intracaldera ash-flow tuffs and their extracaldera equivalents, which extend to the north, is provided by Fischer (1970). Varying degrees of fluidal and eutaxitic structure and vitroclastic texture are exhibited by both intra- and extracaldera ash-flows of the Clear West Peak complex. Modal counts of phenocrysts in vitrophyric rocks from both the intra- and extracaldera ash-flows are nearly identical, and contain similar amounts of plagioclase feldspar (5 - 7 percent) and less than 1 percent augite and hypersthene (Fischer, 1970). Petrographic examination of the intra- and extracaldera ash-flows by Hartman (1973) established the presence of minor amounts of biotite and hornblende in each.

Major-element oxide and normative mineral analyses were performed on two samples from the Clear West Peak complex during the present

Figure 19. Flow banding in Clear West Peak ash-flow tuffs from the NE1/4, SE1/4 sec. 34, T19N, R8E (along Milky Creek).

Figure 20. Eutaxitic texture in the Clear Weat Peak ash-flow tuffs near the location of Figure 19. Pumice lapilli exhibit various stages of collapse.

study and are listed in Table 4. A sample of intracaldera ash-flow tuff contains 74.70 percent SiO2 and 4.73 percent K2O (rhyolite), and a sample of extracaldera ash-flow tuff contains 76.96 percent SiO2 and 4.98 percent K2O (rhyolite). Fischer (1970) also has provided major-element oxide analyses for five samples of the Clear West Peak intra- and extracaldera ash-flows. Of these, two are rhyolites and three are rhyodacites and their SiO2 contents range from 70.6 to 73.8 percent and those of K2O from 2.07 to 4.61 percent (see Table 4).

Structure, Thickness, and Contact Relations

The Clear West Peak complex consists of a collapsed caldera system infilled by thousands of feet of ash-flow tuffs bordering and south of the White River area, extracaldera ash-flows within the White River area, and numerous dikes, sills, and plugs of rhyolite intruding Fifes Peak andesite near the caldera margin. The steeply dipping contact of the Clear West Peak caldera with flows of the Fifes Peak andesite is apparent in the deeply incised Clearwater River drainage. Hartman (1973) has described the Clear West Peak rhyolite as intrusive with sharp steeply dipping contacts often bordered by a reddish oxidized zone. Several caldera-related rhyolite intrusions are also exposed within the Clearwater River drainage, especially along Mineral Creek and Byron Creek. The abundance of rhyolite intrusions increases to the south, near the caldera margin. The caldera-fill ash-flow tuffs are exposed for over 4,000 feet of topographic relief from the mouth of Milky Creek southeast 6.5 mi. to the summit of Clear West

Table 4. Major-element oxide and normative analyses of ash-flows from the Clear West Peak complex (sample M-2, NW1/4, sec. 32, T19N, R9E; and sample R59D, NW1/4, sec. 13, T19N, R8E).

Table 4

Analysis M-2		R59D	Range of Five analyses (Fischer, 1970)*	
Oxide	Percent	Percent	*Percent	*Percent
SiO2	74.70	76.96	70.6	73.8
Al2O3	13.46	13.73	11.4	12.8
TiO2	0.39	0.35	0.38	0.46
Fe2O3	1.06	0.34	1.39	1.68
FeO	1.12	0.39	0.80	2.45
CaO	0.96	0.43	0.96	2.15
MgO	0.24	0.00	0.15	0.58
K2O	4.73	4.98	2.07	4.61
Na2O	3.16	2.79	2.89	4.61
P2O5	0.05	0.03	0.03	0.06
MnO	0.03	0.00	0.02	0.04
			H2O- 0.0	2.6
			H2O+ 0.8	4.2

	Analysis M-2	R59D
A:F:M Ratio	77 : 21 : 2	92 : 8 : 0
Normative Minerals		
quartz	35.3	40.5
corundum	1.5	3.0
orthoclase	28.0	29.4
albite	26.7	23.6
anorthite	4.4	1.9
hypersthene	1.4	---
magnetite	1.5	0.2
ilmenite	0.7	0.7
apatite	0.1	0.1
Normative plagioclase An	14.2	7.6
Normative Color Index	3.7	1.1

Peak, exemplifying their considerable thickness. Local steep to vertical flow banding in rhyolite near Clear West Peak indicates the presence of a volcanic dome or intrusive plug, a common feature in caldera systems. Eutaxitic banding and flow banding do not exhibit consistent orientation throughout the main body of ash-flow tuffs. This apparent multiplicity of primary attitudes may be the result of multiple vent sources within the caldera and (or) structural complexities due to post-caldera resurgence.

To the north, within the south-central part of the White River area, Clear West Peak extracaldera ash-flow tuffs cap hilltops and ridges stratigraphically above the Fifes Peak Formation. Here, the ash-flow tuffs are relatively thin with accumulations measuring in the hundreds of feet, unlike the thick caldera-fill to the south. In the SW1/4 sec. 14, T19N, R8E Frizzell and others (1984) have mapped a small outcrop of Fifes Peak andesite overlying the Clear West Peak ash-flow tuff, and advocate reducing the Clear West Peak complex to a member within the Fifes Peak Formation. However, recognition of the Clear West Peak ash-flows as part of a caldera complex may confirm their individuality as a separate mapable unit.

Age and Regional Correlation

Near the rim of the Clear West Peak caldera, dikes and sills of Clear West Peak rhyolite intrude andesite flows of the Fifes Peak Formation and thus cannot be older than early Miocene. Hartman (1973) has reported one whole-rock potassium-argon age determination for a

sample collected near the base of Clear West Peak, within the main body of intracaldera ash-flows. Frizzell and others (1984) recalculated his data using 1976 IUGS decay and abundance constants and list a corrected age of 19.1 m.y. Uranium-lead age determinations on two samples of zircons collected from the Clear West Peak intracaldera ash-flow tuffs are reported by Mattinson (1977) to have yielded ages of 22.6 and 21.8 m.y. (early Miocene), of which the younger was interpreted to be probably the more accurate.

The pulse of magmatism that produced the Clear West Peak ash-flow tuffs is younger than the Huckleberry Mountain Formation (Oligocene) and the tuffs are stratigraphically above the Stevens Ridge Formation and most, if not all, of the Fifes Peak Formation. However, Frizzell and others (1984) have mapped Clear West Peak ash-flow tuffs interbedded with andesite flows of the upper Fifes Peak Formation in the SW1/4, sec. 14, T19N, R8E. It may be best to consider the Stevens Ridge, Fifes Peak, and Clear West Peak volcanism as largely contemporaneous igneous events that overlap in age and stratigraphy. This magmatic activity was the result of one or more intrusive pulses of the Tatoosh batholith.

Origin and Significance

The Clear West Peak caldera is just one in a series of igneous events that created shallowly emplaced highly differentiated magma chambers locally. The Stevens Ridge Formation is the oldest local example of highly differentiated magmas, and may also represent

eruption from a caldera system. Subsequent to collapse and infilling of the Clear West Peak caldera a resurgent pulse of magma emplaced the Carbon River stock. This stock is composed of biotite-pyroxene granodiorite, has an exposed area of about 15 square miles, and borders the Clear West Peak caldera margin on the west-southwest as depicted in Figure 7. As is the case with the Clear West Peak ash-flow tuffs, the Carbon River stock is a local phase of the Tatoosh batholith, and its 19.4 to 17.1 m.y. age (Frizzell and others, 1984) probably overlaps or is slightly younger than the Clear West Peak complex. Bordering the caldera on the north is the White River area. Here, several square miles of intense hydrothrmal alteration contain a precious metal, base metal, and trace element geochemistry compatible with the presence of a large shallowly emplaced intrusion. It is suspected that this intrusive-related hydrothermal activity represents an even younger pulse of local magmatism from the Tatoosh batholith. Although the mode of formation of the Clear West Peak complex was not an initial focal point of the present investigation, its recognition as a resurgent caldera system is important to a more accurate interpretation of the genesis of precious metal, base metal, and trace element anomalies located within the White River drainage basin.

Intrusions

Many dikes, sills, and small intrusions are located within the White River area. These small bodies are subdivided compositionally into diorite porphyry, rhyolite, and other miscellaneous intrusions.

The first group, consisting of diorite porphyry intrusions, crop out as numerous dikes and sills in the Clearwater River drainage. The crosscutting relationship of diorite porphyry dikes through Fifes Peak andesite flows is very apparent in sec. 14, T19N, R8E as shown in Figure 21. Dikes of a similar composition cut rocks of both the Huckleberry Mountain and Fifes Peak Formations in the eastern part of the White River area and are especially abundant within the Slippery Creek drainage. In contrast to flows of Fifes Peak andesite, the diorite porphyry is finely crystalline and phenocryst poor.

The second group of intrusions consists of dikes, sills, and small intrusive plugs of rhyolite that are compositionally similar to, and spatially associated with, magmatic activity of the Clear West Peak complex. These intrusions cut Fifes Peak andesites in the southern part of the White River area and increase in abundance near the margin of the Clear West Peak caldera, between Mineral and Milky Creeks. The rhyolites generally contain 5 percent disseminated pyrite within the main intrusive body, and 2 - 5 percent pyrite within the glassy matrix of their associated intrusion breccias.

Miscellaneous intrusions vary in composition from rhyolite(?) to quartz diorite(?). Small intrusions of rhyodacite are exposed along and near the Twin Creek fault (secs. 3 and 4, T19N, R9E; and sec. 31, T20N, R9E). These intrusions were preferentially emplaced along the Twin Creek fault but have been sheared in sec. 4, and sheared and cut by andesite dikes in sec. 31. Therefore, at least some magmatic and structural activity along the Twin Creek fault has taken place since emplacement of the rhyodacite intrusions. A small intrusive plug of

Figure 21. Fifes Peak andesite flows that are cut by late stage dikes of diorite porphyry (SW1/4, SW1/4, sec. 14, T19N, R8E) near the headwaters of Mineral Creek.

intermediate composition cuts Fifes Peak andesites and crops out in east-central sec. 1, T19N, R8E. This intrusion is propylitically altered (abundant calcite, epidote, chlorite, and pyrite) and has a TiO2 content of 0.75 percent, which is much lower than any of the surrounding andesites and diorites (generally between 0.85 - 0.95 percent TiO2). The lower percentage of TiO2 in the intrusion indicates that its original composition was probably quartz diorite. A broad zone of argillic and propylitic hydrothermal alteration surrounds the intrusion. Numerous veinlets of quartz, tourmaline, pyrite, and calcite cut both the quartz diorite and the surrounding andesite flows.

Lastly, it is proposed that an epizonal stock of moderate size underlies the southwest part of the White River area. This would explain the presence of many square miles of hydrothermal alteration within the White River basin. Intrusion(?) breccia that crops out in the SW1/4, sec. 6, T19N, R8E and is shown in Figure 15 may be genetically related to this epizonal stock. Precious metal, base metal, and trace element geochemistry of the altered zones indicate that the composition of this unexposed stock is probably intermediate to felsic; similar to that of the Carbon River granodiorite, that crops out over a 15 square mile area about 8 miles south of the White River, or that of the Grass Mountain intrusive tonalite, that crops out north of and bordering the White River area as depicted in Figure 7.

Synopsis of Miocene Igneous Events

Post-Oligocene (post-Huckleberry Formation) igneous and sedimentary rocks within the White River basin are largely a product of early Miocene magmatic activity that accompanied emplacement of the Tatoosh batholith and its associated intrusive stocks, shield and composite volcanoes, and calderas. Enormous quantities of magma were erupted throughout the 26 - 14 m.y. lifespan of the Tatoosh batholith, with the most productive period being 24 - 20 m.y. Age determinations of 16 samples that represent the four major Miocene rock units within and around the White River basin are plotted on Figure 22 (data from Frizzell and others, 1984); and also plotted is the age of metallization, as determined by 40Ar/39Ar analysis. The overlapping ages of these four extensive volcanic units attest to the rapidity with which voluminous amounts of magma were erupted during emplacement of Tatoosh plutons. Both age and stratigraphic relationships indicate that the Stevens Ridge, Fifes Peak, and Clear West Peak volcanics are in part contemporaneous. A model for the emplacement of the Tatoosh batholith and formation of three local volcanic units within a 24 - 20 m.y. period in the White River basin is illustrated in Figures 23A and 23B.

In this model, the first stage of emplacement of stocks and plutons of the Tatoosh batholith is recorded by minor amounts of andesite and basalt flows that formed local shield volcanoes on pre-Miocene basement rocks. These flows of andesite and basalt form the basal portion of the Fifes Peak Formation, which explains why its

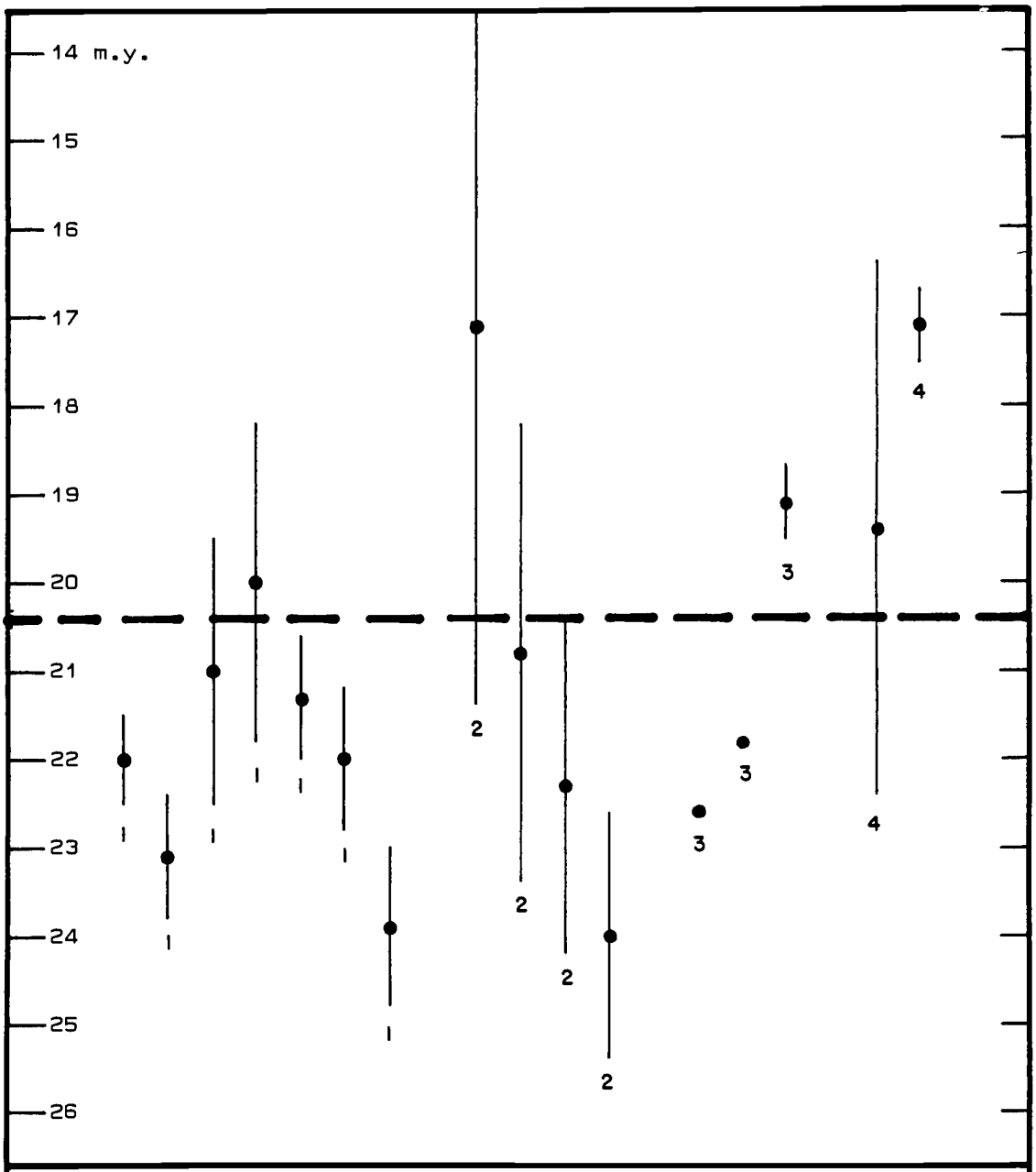

Figure 22. Age determinations with error bars of: (1) Stevens Ridge ash-flow tuffs; (2) Fifes Peak andesite flows; (3) Clear West Peak ash-flow tuffs; and (4) Carbon River granodiorite stock (data from Frizzell and others, 1984). Analyses were by various methods including K-Ar mineral, K-Ar wholerock, U-Pb of zircons, and Fission Tracks in zircons. Note that errors for two U-Pb analyses of zircons from Clear West Peak rocks were not reported. Dashed horizontal line represents the 20.4 $\pm$ 0.1 age of metallization in the White River area, as determined by 40Ar/39Ar analysis of hypogene alunite (Snee, 1986; see appendix 1).

Figure 23. Diagrammatic sketch of a model for the 24 - 20 m.y. emplacement of intrusions of the Tatoosh batholith and their cogenetic volcanics. This model includes: (1) initial eruption of minor andesite and basalt flows of the Fifes Peak Formation as depicted in Fig. 23A; (2) eruption of a thick sequence of Stevens Ridge ash-flow tuffs and subsequent caldera collapse, during which minor volcanism of Fifes Peak andesites continued (see Fig. 23A); (3) major eruption of Fifes Peak andesites and the formation of shield and composite volcanoes concealing the Stevens Ridge caldera as shown in Figure 23B; and (4) eruption of Clear West Peak pyroclastics and the generation of a second collapsed caldera, and an extracaldera ash-flow breaching the north rim (see Fig. 23B). Pre-Miocene basement rocks are the Ohanapecosh and Huckleberry Mountain volcanics and the underlying Puget Group sediments.

FP = Fifes Peak Formation - Mostly andesite volcanic flows with some dacite, basalt, and rhyolite interflow units.

SR = Stevens Ridge Formation - Composite rhyolite and rhyodacite ash-flow sheets with abundant volcaniclastic sedimentary rocks in the upper half of the formation.

CWP = Clear West Peak complex - A thick sequence of rhyolite and rhyodacite ash-flow tuffs within the margins of a collapsed caldera and their less abundant extracaldera equivalents.

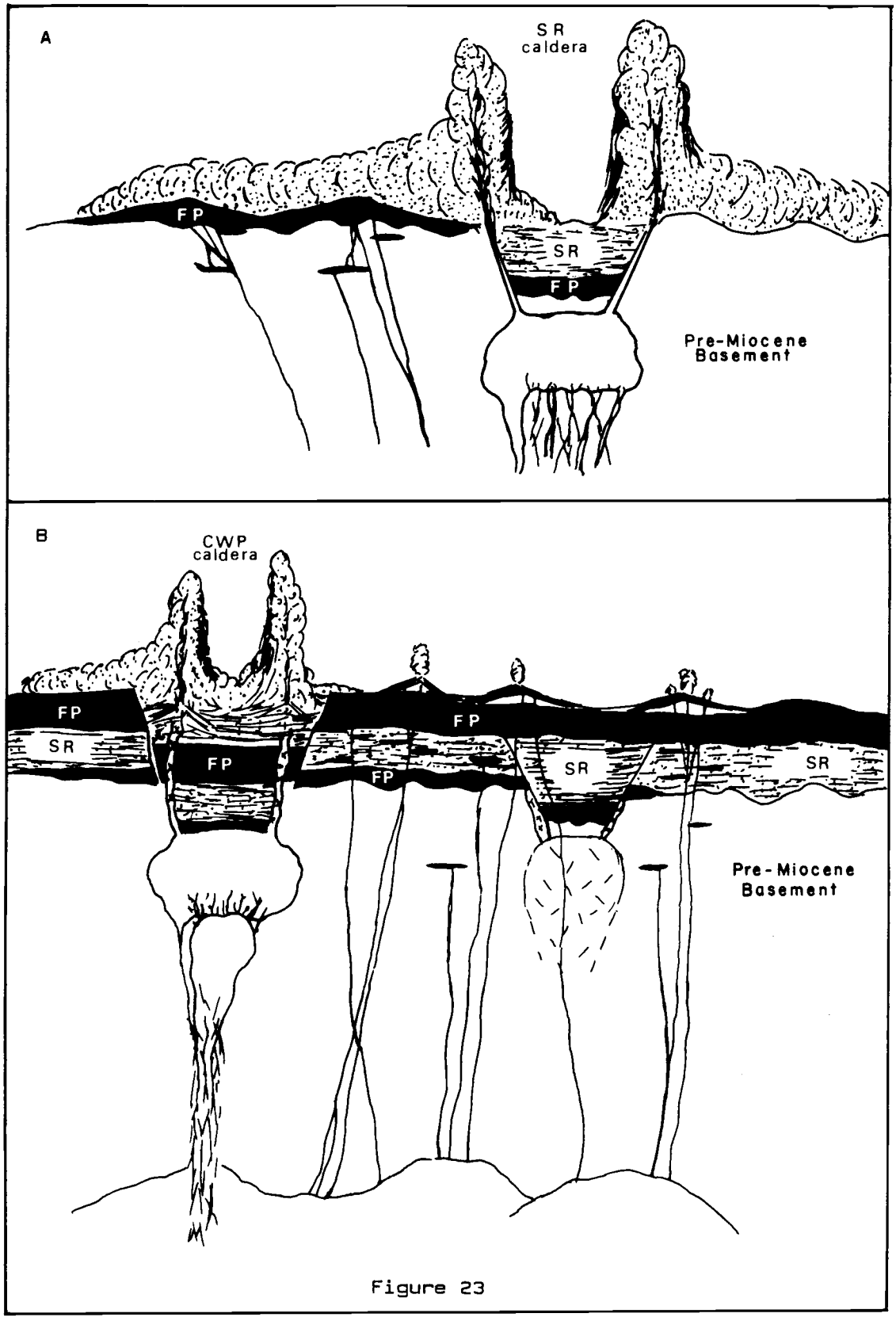
A
SR
caldera
FP
SR
FP
Pre-Miocene
Basement
B
CWP
caldera
FP
SR
FP
FP
FP
SR
SR
Pre-Miocene
Basement

Figure 23

type section is older than that of the Stevens Ridge ash-flows. Subsequent to the initial igneous activity, voluminous felsic differentiates erupted from high level magma chambers and formed ash-flow deposits of the Stevens Ridge Formation. This major venting of pyroclastics probably resulted in the collapse of a caldera (as depicted in Fig. 23A) that is now concealed beneath a thick cover of younger volcanic rocks.

A thick sequence of volcanics was rapidly constructed with continued emplacement of Tatoosh plutons. This volcanism was the main extrusive phase of the Fifes Peak Formation, which primarily consisted of andesite and dacite shield and composite volcanoes (see Fig. 23B). Andesite flows of the Eagle Gorge Formation probably represent a northward extension of the Fifes Peak Formation.

During the waning stages of Fifes Peak volcanism, large amounts of highly differentiated felsic magma breached the surface and caused a second major pyroclastic eruption, ensuing caldera collapse, and subsequent infilling by ash-flow tuffs. This volcanaic event formed the Clear West Peak complex, a series of intra- and extracaldera rhyolitic ash-flows as depicted in Figure 23B. Resurgent magmatic activity emplaced the Carbon River granodiorite on the border of the Clear West Peak caldera and possibly a hypabyssal intrusion of similar composition near the White River.

Structural Analysis

Post-Oligocene structural deformation in the White River area and

surrounding region is a complex overprint of local stresses that were produced during emplacement of the Tatoosh batholith and its associated stocks and calderas and regional tectonism. The intersection of several large scale tectonic features takes place in the White River area and includes: (1) a 35 mile long fault that is the southernmost expression of the Olympic-Wallowa lineament; (2) two large (10 - 12 mile diameter) circular features that are probably structural domes and form the southeast and southwest borders of the White River area; and (3) the Clear West Peak caldera, a resurgent caldera complex bordering the White River area on the south. Satellite imagery proved an important source of structural information not previously recognized by surface mapping programs.

Structures Detected by Satellite Imagery

Local and regional topographic and related geomorphic features have been examined by satellite imagery that produced a digital composite of topographic relief, as determined by a satellite mounted laser rangefinder with a data density of 3 arc seconds (approximately 30 meter spacings between data points). Topographic relief, depicted on the resultant black and white images, serves to enhance or highlight many geomorphic features that are related to regional structures. The Olympic-Wallowa lineament imparts an important structural fabric to the local terrane that shows up exceedingly well on satellite imagery (see Figs. 6A and 6B). Moreover, this structure appears to control the strike of the Twin Creek fault zone, other

faults and folds to the north, and a possible fault concealed beneath alluvium of the White River valley (see Fig. 7). However, naming the fault postulated to exist below alluvium of the White River valley represents a problem in terminology. Frizzell and others (1984) refer to the normal fault that juxtaposes the Huckleberry Mountain and Fifes Peak Formations, north of the White River valley, as the White River fault. This structure was originally named the Twin Creek fault by Hammond (1963), and the term is retained in the present study. Accordingly, the strike-slip fault, which is postulated to be present beneath alluvium of the White River valley, is termed the White River fault.

Other important geomorphic features that have been detected from the satellite imagery include two large circular structures. These structures are each approximately 10 to 12 miles in diameter and are located north-northwest and north-northeast of Mount Rainier, as depicted by the numbers 1 and 2 on Figure 24. Both features are topographic highs that probably represent structurally uplifted blocks or domes, and not calderas. Moreover, the Clear West Peak caldera occupies the terrane between these circular features and its margins extend into both. These circular features are of relevance to the present study because one hosts a mining district, the other hosts a mining/prospecting area, and collectively they both account for the only significant local production of precious and base metals. The production in each case came from areas near the margins of these structures. The Summit mining district is located along the southern margin of feature 2. This district was a producer of gold and silver

Figure 24. Digital composite of topographic relief from satellite imagery (refer to Fig. 6B for the regional locations). Plotted are: Mount Rainier (R); the Carbon River stock (CR); approximate margins of the Clear West Peak caldera (CWP); the White River area; circular features (1) and (2); the trace of the proposed White River left-lateral strike-slip fault (WR). Note the extension of the Olympic-Wallowa lineament into the Greenwater River and White River valleys. For scale, the White River area is approximately 12 miles wide.

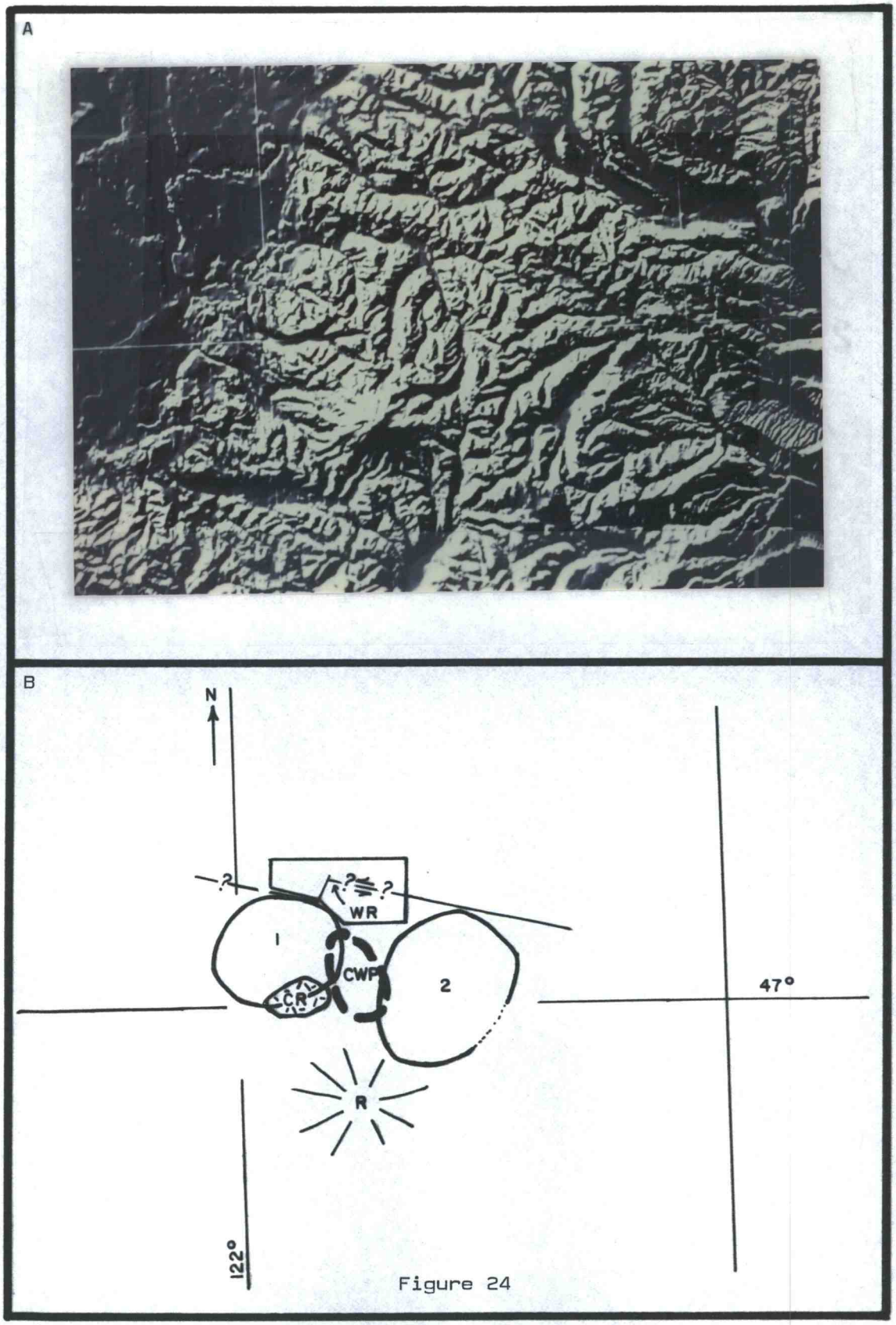

Figure 24

from high grade precious and base metal veins hosted mostly in Fifes Peak andesite. Granodiorite intrusions crop out sporadically near the mineralized andesites, but their relationship to metallization is unclear. The Carbon Ridge - Cayada Creek mining/prospect area is along the southeastern margin of feature 1. Fischer (1970) reports the presence of at least 10 adits in this area, the longest having over 1,000 feet of workings. Production came from copper and gold-bearing veins in the Carbon River granodiorite. The focal point of the present study is an area of extensive hydrothermal alteration and mineralization that is exposed along the White River at the north-northeast margin of feature 1. The circular features are topographic highs, as previously noted, which may represent arches or domes of district-wide scale. Because of their large size, classic domes with quaquaversal dips are not expected to be present. Circular features such as these in the southwestern U.S. are commonly associated with mining districts. Areas of uplift, arches, and domes are present in Nevada at various scales, ranging in size from that of an individual ore deposit to that of an entire mining district. The deformation may occur prior to, during, or after metallization. Classic domes with quaquaversal dips are present in the Talapoosa mining district, Lyon county, Nevada, whereas similar topographically uplifted circular regions hosting the Austin and Ely mining districts of Nevada do not exhibit such dips. The circular feature northwest of Mount Rainier (feature 1) is younger than the local early to middle Miocene igneous rocks. This structure cuts across the western margin of the 22-19 m.y. Clear West Peak caldera and the southern part of the

19-17 m.y. Carbon River stock (Fig. 24). The sequence of geologic events leading to the formation of this structure may have been as follows: (1) emplacement of a stock or pluton of the Tatoosh batholith and composite phases at an intermediate depth; (2) eruptions of felsic differentiates from a related but higher level magma chamber to form the Clear West Peak caldera complex; (3) collapse of the caldera followed by resurgent magmatism at its southwest margin,to form the Carbon River granodiorite stock; and (4) long-term district-wide uplift and the generation of circular feature 1, without obvious doming of the overlying country rocks. The presence of precious and base metal mineralization near the margins of these circular structures may be circumstantial or may be genetically linked to underlying plutons. Moreover, the location of mineralized areas along the White River may also be controlled by a major fault zone, the White River fault, that lies hidden beneath alluvium of the valley.

Possibly the most important local geomorphic feature shown by satellite imagery is the pronounced northeasterly change in direction of the White River valley along the northern margin of circular feature 1 as shown in Figure 25. The northeasterly trend along this part of the river parallels the East Clay Creek fault and a zone of pervasive silicification 3.5 miles in length. This abrupt change in the direction of the White River valley may indicate the influence of regional, rather than local, tectonics in the formation of the East Clay Creek fault as part of the larger White River strike-slip fault. Raisz (1945) has noted that the Olympic-Wallowa lineament "offsets the

Figure 25. Digital composite of topographic relief from satellite imagery that is an enlargement of Figure 24. Plotted on it are: Mount Rainier (R); circular features (1) and (2); the Carbon River stock (CR); approximate margins of the Clear Weat Peak caldera (CWP); the White River area; approximate location of the Greenwater River valley (G); the Twin Creek fault (TC) with a bar and ball on the downdropped side; the proposed White River fault (WR) and its probable offset the east Clay Creek (CC). For scale, the White River area is approximately 12 miles wide.

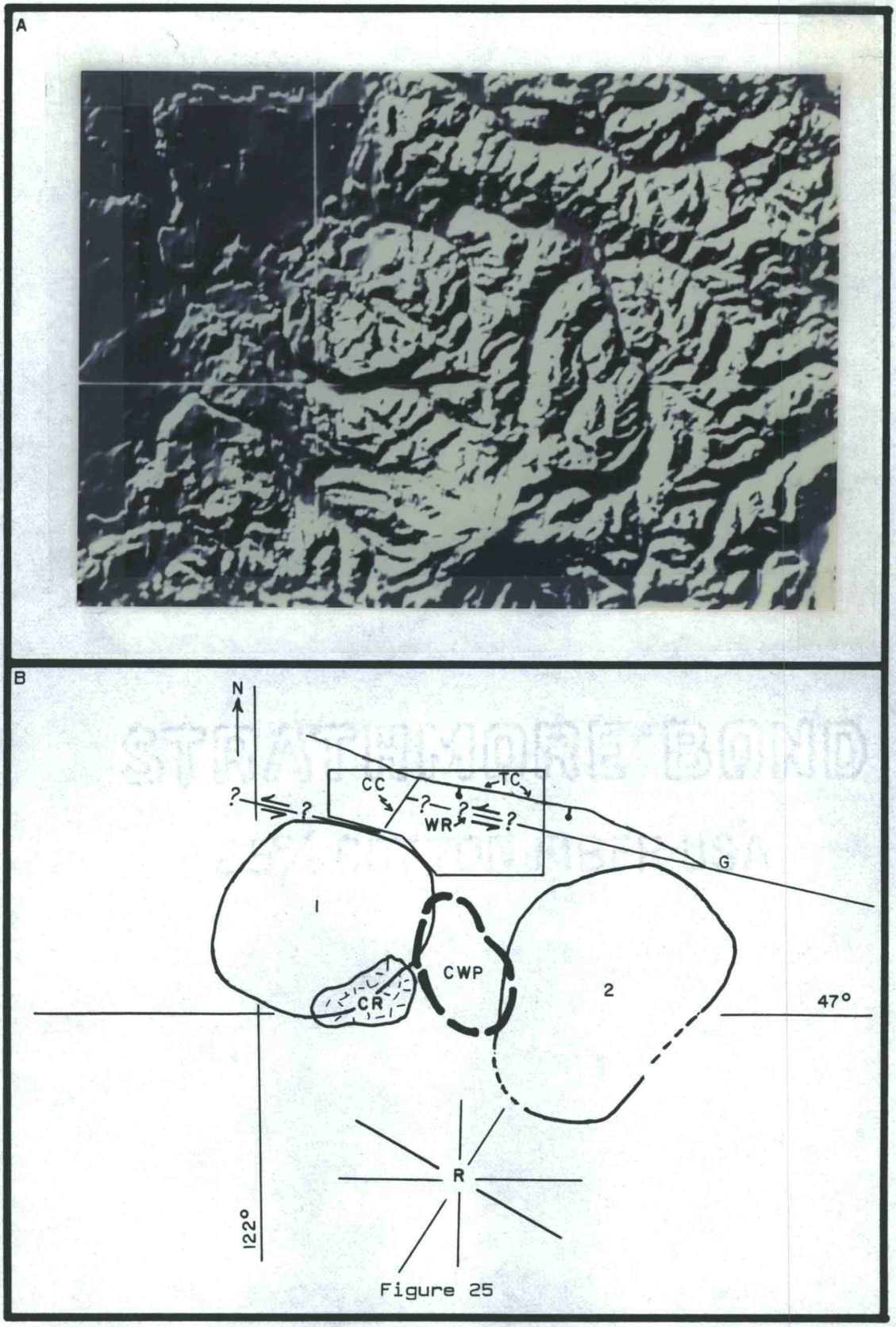

Figure 25

main crest of the Cascade Mountains about six miles to the northwest on its northern side, and the crest of the Blue Mountains by roughly the same amount and in the same direction", indicating left lateral displacement. The abrupt change in direction of the White River valley may indicate an offset in a left-lateral strike-slip fault system, which controls the course of the White River from Mud Mountain dam to the town of Greenwater and much of the course of the Greenwater river to the east (see Figs. 24, and 25).

Evidence of a major structure (the White River fault) concealed beneath alluvial gravels is based on the following data: (1) satellite imagery that indicates the White River valley to be a major structural continuation of the Olympic-Wallowa lineament (see Figs. 6B and 24); (2) the East Clay Creek fault that is located between two major strands of the proposed White River fault and possibly connects the two; (3) contamination of local wells by acid-sulfate rich groundwaters; and (4) structural analysis of local and regional fold patterns that indicate the presence of a stress regime capable of inducing left-lateral strike-slip fault displacement during Miocene time. This last point will be discussed in the section on Folds. Water wells drilled into bedrock of the White River valley, for at least 0.5 miles west-southwest of the town of Greenwater, often encounter acid-sulfate rich groundwaters. In contrast, andesite volcanic flows surrounding this part of the valley are largely unaltered and water within these aquifers is fresh. The presence of a fault system with locally abundant sulfide mineralization (probably pyrite) underlying the White River valley is suggested by this

contamination. Extensive pyrite-bearing zones of argillic alteration are common along major faults within the area (i.e. the East Clay Creek fault) and acid-sulfate waters have been observed to originate from some of these.

Faults

Several of the creek drainages and erosional patterns within the White River area are fault controlled (see Plates 1A and 1B). Structurally initiated drainages are especially evident in silicified rocks, as present in sec. 6, T19N, R8E and secs. 31 and 32, T20N, R8E. The morphology of the White and Greenwater River valleys also indicate that they may be fault controlled drainages.

The Twin Creek fault (the White River fault of Frizzell and others, 1984) is a major normal fault within the area. The Olympic-Wallowa lineament controls the west-northwest strike of this fault and others to the north as depicted in Figure 7. Mapping by Frizzell and others (1984) shows the Twin Creek fault extending for at least 35 miles with a dip slip displacement of >6,500 feet. A dip slip offset of at least 2,500 feet can be documented within the White River area and the actual displacement is probably greater. The Twin Creek fault juxtaposed rocks of the Fifes Peak Formation (Miocene) with those of the Huckleberry Mountain Formation (Oligocene) to the north (see Fig. 7).

Another major structure within the White River area is the East Clay Creek fault (see Plates 1A and 1B). It extends for at least 4.5

miles in a northeast-southwest direction and intersects the Twin Creek fault, but apparently does not displace it. The East Clay Creek fault and several smaller faults, shears, and fractures around it served as principal conduits for the hydrothermal fluids. The country rocks surrounding these channelways were intensely altered by base leaching and silicification. The East Clay Creek fault may be part of a larger strike-slip fault (the White River fault) postulated to exist beneath alluvium in the White River valley.

Several episodes of faulting appear to have taken place within and around the White River area. However, faults within the area are of less pratical use in defining paleo-stress directions than are folds, because the vectors of displacement for the individual faults and the age relationships between faults are poorly defined.

Folds

Regional fold patterns are well documented by Fiske and others (1963) in Mount Rainier National Park south of the White River area, by Hammond (1963 and 1980) south of and including part of the White River area, and by Frizzell and others (1984) within the Snoqualmie Pass 1:100,000 quadrangle inclusive of the entire White River area. Structures mapped by these workers show that stratigraphic rock units within the region are folded into a series of broad en echelon anticlines and synclines with north to northwest-trending fold axes (see Fig. 26A). According to Hammond (1963; 1980), the trend of these fold axes becomes more westerly by a few tens of degrees as the White

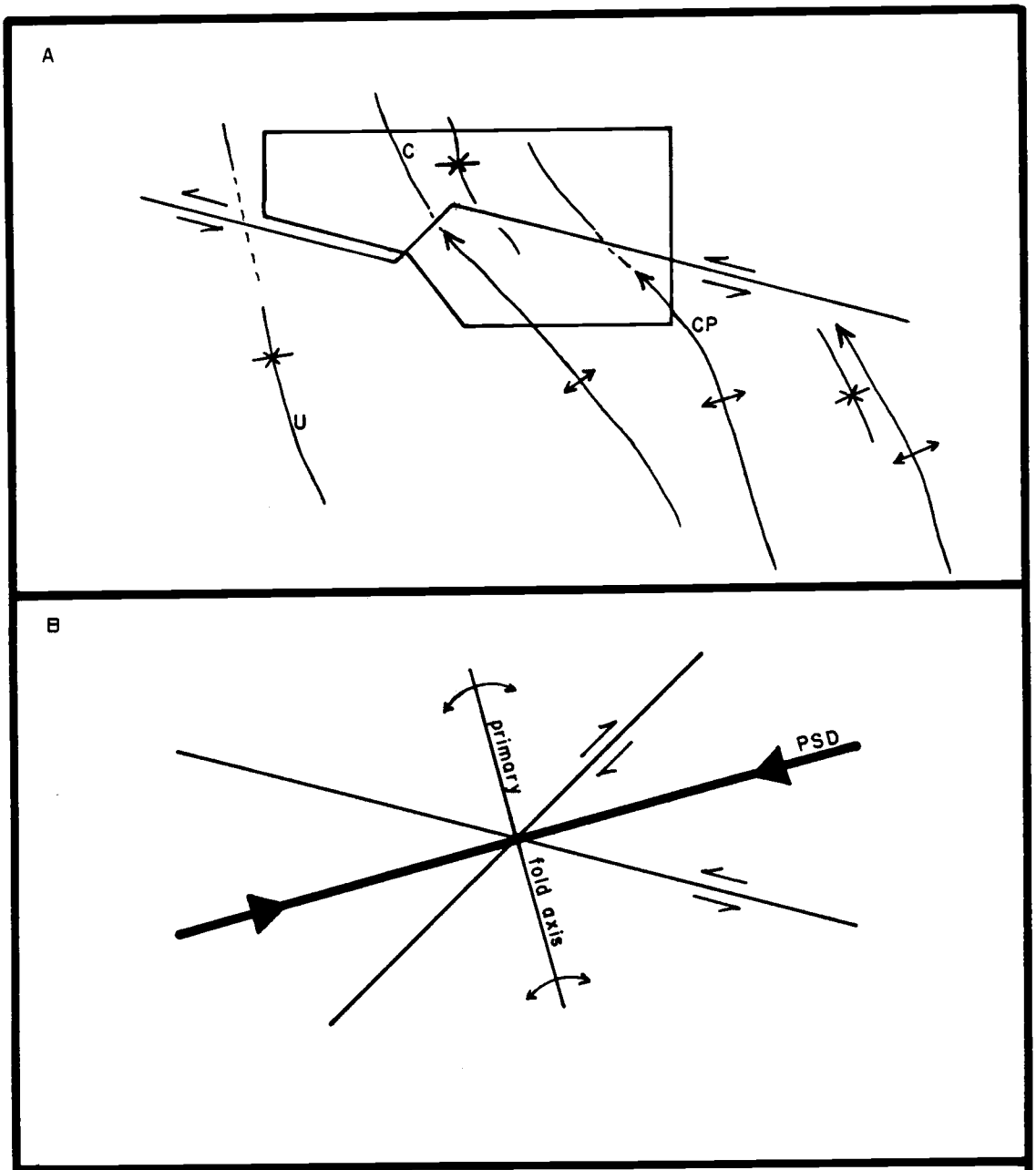

Figure 26. A tectonic interpretation of Miocene fold patterns near the White River area.

A). Location map showing the White River area, the proposed White River fault, and the trend of early Miocene fold axes: Unicorn Peak syncline (U), Coal Creek anticline (C), Chinook Pass anticline (CP), and others (after Hammond, 1980).

B). Diagrammatic representation of the stress regime (primary stress direction = PSD), which could account for early Miocene folding and left-lateral strike-slip displacement along the proposed White River fault.

River area is approached from the south. Geologic mapping of the White River area during the present study has corroborated the local fold pattern as mapped by Fiske and others (1963), Hammond (1963 and 1980), and Frizzell and others (1984). The north to northwest-trending fold axis of the Chinook Pass anticline is expressed in sedimentary rocks cropping out near the headwaters of Mineral Creek. Sedimentary rocks exposed along Canyon Creek are also folded into a north-trending anticline and may be part of the Chinook Pass anticline. Sedimentary rocks along Lyle Creek (about one mile west of the study area) are folded into a north to northwest trending syncline.

Fiske and others (1963) determined the age of north-northwest en echelon folding as postdating deposition of the Ohanapecosh Formation (Oligocene) and predating emplacement of the Tatoosh pluton. Given the present knowledge of the protracted emplacement history of the Tatoosh batholith (at least 12 m.y.), it is more time restrictive to note that rocks as young as the Fifes Peak Formation (early Miocene) were folded. The fold axes of Miocene deformation are depicted in Figure 26A and indicates a northeast-southwest compressional primary stress direction as shown in Figure 26B. The stress regime responsible for this folding is also oriented properly to produce a left-lateral strike-slip fault, having a trend similar to that of the proposed White River fault and with conjugate shearing in the same general direction as that of the East Clay Creek fault. The increased westerly trend of the en echelon folds near the proposed White River fault is also consistent with left lateral strike slip displacement,

as produced from experiments in wrench tectonics by Wilcox and others (1973).

The regional fold pattern suggests that early Miocene deformation was in response to a compressional regime having a northeast-southwest trending principal stress direction (Fig. 26B) that produced a series of north to northwest-trending folds, a major west to northwest-trending strike-slip fault, and subsidiary folds and conjugate shears within the White River area. Thereafter, the regional stress regime changed and normal fault displacements took place along several of the major structures associated with the Olympic-Wallowa lineament. The Twin Creek fault, with its large normal fault displacement, probably formed at this time.

MODEL FOR VOLCANIC-HOSTED EPITHERMAL GOLD MINERALIZATION

Classifications of epithermal precious metal deposits have been based on criteria such as host rocks, metals, mineralogy, and morphology. Although none are perfect, that recently proposed by Hayba and others (1986) subdivides volcanic-hosted epithermal deposits of the precious metals into acid-sulfate and adularia-sericite types on the basis of distinctive contrasts in alteration mineralogy. The mineralogical differences between these two types relate to variations in the chemistry of the hydrothermal fluids from which they were deposited. Acid-sulfate type deposits formed by fluids having higher hydrogen ion to potassium ion ratios and oxygen fugacities than the adularia-sericite type. In contrast, classification of these deposits based on morphology, such as distinctions between vein, manto, and hot-spring occurrences, conveys little information about the chemistry of the associated hydrothermal fluid, but may provide to engineers a superficial indication of the geometry of the deposit. The two-fold classification utilizing alteration mineralogy is preferred because it is both genetic and readily identified in the field. The adularia-sericite type of precious metal deposit is defined by an alteration assemblage composed of adularia-sericite-pyrite-quartz-chlorite that occupies an intermediate position between zones of propylitic alteration at depth or laterally adjacent and silicificaion immediately above (Hayba and others, 1986). It is markedly different from the acid-sulfate type of epithermal

deposit that has the following general characteristics according to Hayba and others (1986, p.134-135).

> "The association of these deposits with intrusive centers, particularly ring-fracture volcanic domes on the margins of calderas, appears to be a critical genetic factor (Heald et al., 1986) in contrast to the Adularia-Sericite type deposit where the role of calderas is one of ground preparation for later younger hydrothermal fluids (Lipman et al., 1976; Steven and Lipman, 1976).
>
> * * * * * * *
>
> Acid-Sulfate type deposits are typified by the occurrence of the vein mineral assemblage enargite+pyrite ± covellite. Adularia and chlorite are absent or rarely present. Ore occurs primarily as native gold, silver and electrum with sulfides, sulfosalts, and tellurides.
>
> * * * * * * *
>
> A definitive characteristic of Acid-Sulfate type deposits is the association of advanced argillic alteration with the ore. Kaolinite, usually accompanied by alunite, occurs close to the vein and is often coextensive with silicification. Farther from the vein, argillic alteration, sometimes intermixed with sericitc alteration, surrounds the zone of advanced argillic alteration. The argillic alteration zone is often mineralogically zoned itself, with kaolinite nearer the vein and smectite farther from the vein. The outer-most alteration zone consists of propylitic alteration.

Hot-spring type gold deposits are a classification of ore deposit types based primarily on several distinctive characteristics that include the surface venting of large quantities of hydrothermal fluids, the surface deposition of metals dispersed throughout sinter deposits, and the near-surface deposition of gold and other elements in a myriad of stockwork veins at a relatively shallow depth (less than about 500 feet). A hot-spring type gold deposit can form in either an acid-sulfate type or an adularia-sericite type of hydrothrmal system. Moreover, they often exhibit characteristics common to both, with adularia-sericite alteration occurring at depth

and acid-sulfate alteration in the near-surface environment, as shown in a diagrammatic sketch of a hot-spring type gold deposit by Berger and Eimon (1983) and illustrated here in Figure 27.

In general, three criteria are important to the formation of major hot-spring systems: (1) a heat source capable of driving a large hydrothermal convection system over a long period of time; (2) a groundwater regime sufficient to continuously replenish ascending hydrothermal solutions throughout the life of the system; and (3) a structural setting that permits convective circulation of the hydrothermal fluids from deep to shallow parts of the system. In addition to these criteria, several geochemical parameters control the capacity of hydrothermal fluids to transport precious metals.

Geology and Age -- Hot-spring gold deposits form in a wide variety of geologic environments and are hosted by diverse rock types. These deposits are especially abundant in subduction-related volcanic arcs of the Circum-Pacific belt and are often located along basin and range faults or proximal to transform faults that cut continental crust. The age of hot-spring gold deposits present in the western U.S. is generally young because of their close genetic tie to igneous activity that was abundant during the Cretaceous and Tertiary (White, 1985), and their susceptibility to erosion.

Structure -- Local structures are important to the development of a hot-spring system and the focusing of hydrothermal fluids. Ring and radial faults related to calderas, en-echelon splays along range-front faults, and rhombochasms (pull-apart basins) that may accompany strike-slip faults are all structural features associated with

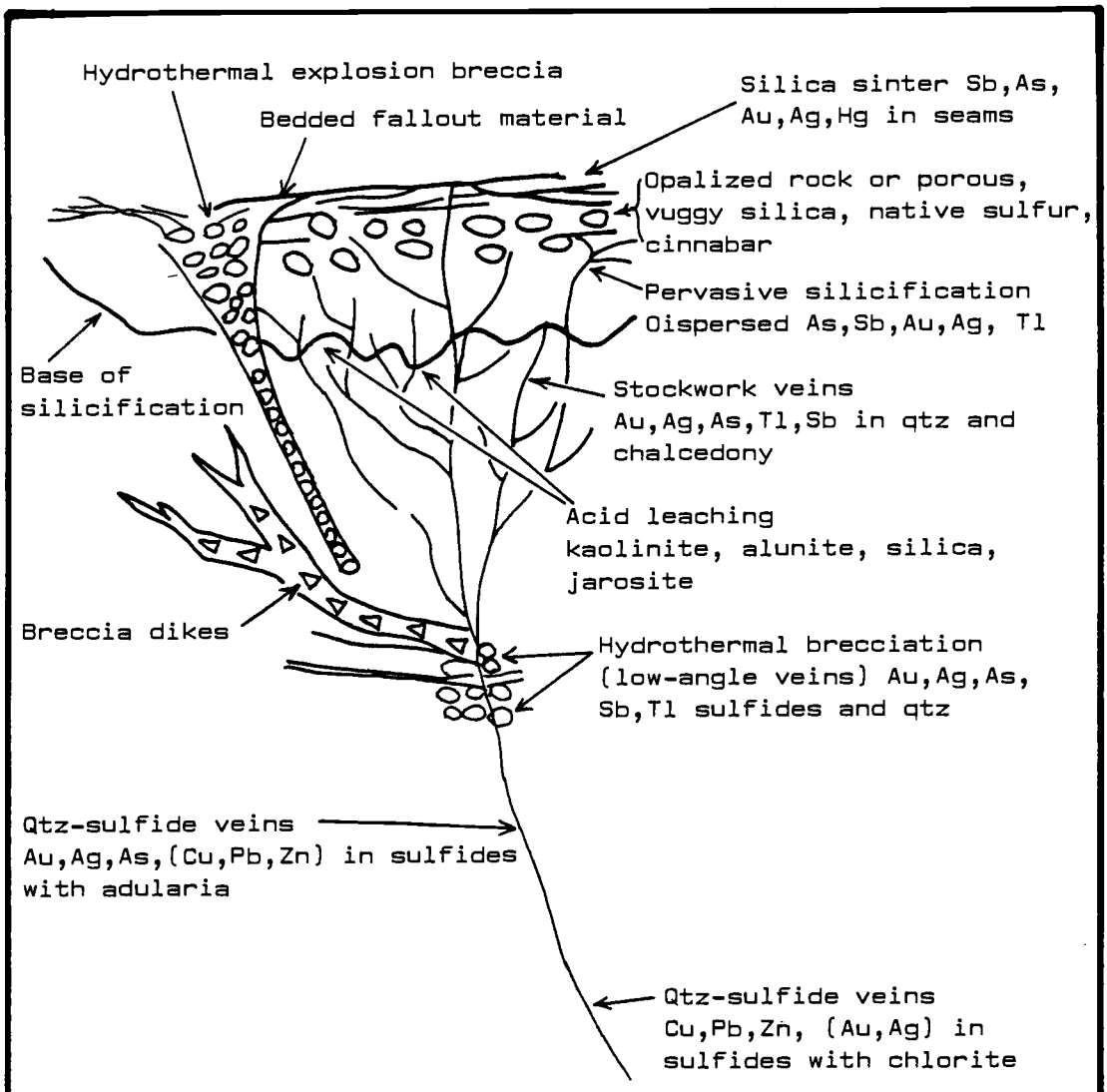

Figure 27. Hot-spring gold model (from Berger and Eimon, 1983).

hot-spring systems.

Mineralogy -- Surface metallization in large precious metal deposits is often polymetallic near major hydrothermal conduits. The surface sinter above hot-spring gold deposits is generally rhythmically banded and contains discrete (thin) layers of precious metals, base metals, and other trace elements that increase in concentration near the hydrothermal vents. There is often a horizontal and vertical zonation of base metals, precious metals, and other trace elements in hot-spring deposits, as is present at Pueblo Viejo in the Dominican Republic (Kesler and others, 1981). Large geochemically anomalous concentrations of Au, Ag, Sb, As, Hg, and Tl are often present in the surface and near-surface environment of hot-spring gold deposits. These generally decrease with depth, whereas concentrations of the base metals (Cu, Pb, and Zn) and other elements may increase with depth (Berger and Silberman, 1986; and Smith, 1943).

Alteration -- The types of alteration mineral assemblages present in hot-spring deposits vary locally with differences in the chemistry of the hydrothermal fluids. However, an extensive zone of silicification invariably dominates the surface and near-surface environment of hot-spring deposits and locally may extend downward along hydrothermal conduits. Below this silica capping is a blanket of argillic alteration (kaolinite and other clays) that grades outward and downward into propylitic alteration (chlorite, calcite, and epidote). Provided the hydrothermal fluids responsible for alteration are extremely acid, then an advanced argillic mineral assemblage (alunite $\pm$ kaolinite, pyrite, and enargite) is likely to be

formed in country rocks next to hydrothermal conduits, and the surrounding envelope of argillic alteration may be extensive. In contrast, hydrothrmal fluids within a few pH units of neutrality that contain abundant potassium are likely to form an adularia-sericite alteration mineral assemblage instead of the kaolin group minerals and alunite of the assemblages that are characteristic of acid-sulfate systems.

Large acid-sulfate type hot-spring deposits are generally localized in highly conspicuous geologic features. The silica capping forms ridges and hills that are surrounded by widespread argillic alteration, both of which may be the site of locally brilliant red to yellow color anomalies as a result of the presence of hematite, jarosite and other iron oxides (limonite). Exploration geologists often use the presence of industrial minerals (i.e. clays, sulfur, silica, fluorspar, and pyrophyllite) as indicators for the possible nearby presence of fossil hot-spring systems.

MINERALIZATION IN THE WHITE RIVER AREA

Precious metal mineralization within the Central and Northern Cascade Range of Washington is largely spatially and genetically related to Tertiary intrusions of intermediate to felsic composition. Mineralization is commonly hosted by veins within the intrusions, and to a lesser extent with their coeval volcanic and sedimentary country rocks, where present. A review of the deposits and literature of precious and base metal mineralization within Washington State can be found in the State of Washington, Department of Natural Resources, Division of Geology and Earth Resources (WDGER) publications, that include: WDGER Bulletins 42, 58, 61, 63, and 69; and Information Circular 57. It is evident from these reports that base metals are present in important quantities within many precious metal veins. Base metals were historically the primary economic consideration in several mining districts within the Cascade Mountains, with precious metals recovered only as byproducts. These base metals also dominate the precious metal veins at mining districts near the White River area. In the Carbon Ridge - Cayada Creek mining district, southwest of the White River area, the principal ore was copper $\pm$ gold in vein systems hosted by the Carbon River granodiorite. Gold - silver veins containing base metals are present in Fifes Peak andesite within the Summit mining district, southeast of the White River area.

Known Mineral Occurrences

Several nonmetallic mineral occurrences that are also common to acid-sulfate type hot-spring gold deposits are present within the White River area. These minerals include alunite, quartz, clays, and native sulfur and a brief description of their distribution and occurrence follows.

Alunite

A history of the discovery of alunite within the White River basin in the early 1930's and its subsequent exploration and evaluation through the 1950's has been recorded in detail by Livingston (1971). On the basis of this work, alunite is known to be present in at least 12 sections of the White River basin. Exploration work by Kalunite, the U.S. Geological Survey, and the Washington State Division of Mines and Mining has identified more than one million tons of low grade alunite-bearing rock (about 20 - 30% alunite) in 4 of these 12 sections. The alunite is located below a silica capping, especially in cross cutting zones of breccia and near large veins of quartz. The alunite is present as aggregates of finely crystalline micaceous-like plates, and its color is often salmon pink or various shades of cream and white. X-ray diffraction analysis of one sample indicates an atomic ratio of 75:25 percent potassium to sodium in the mineral.

Silica

Large deposits of nearly pure silica probably represent the greatest potential for exploitable industrial minerals within the White River basin. A hot-spring deposited silica capping 3.5 miles in length, up to 1 mile in width, and in places at least 400 feet thick is present within the western part of the study area. This silicified host rock exhibits a textural range from massive (dense silica) to open-porous framework (silica sponge) with numerous vugs. The capping is composed primarily of individual quartz crystals 30 - 500 microns in size, which upon crushing take on a fine sucrosic texture. The silica capping formed during base leaching and replacement of the volcanic host rocks and grades outward into zones of advanced argillic and argillic alteration. The amount of silica present is on the order of at least several hundred million tons. However, a considerable amount of this estimated reserve is contaminated by clays, sulfates (alunite), and sulfides (pyrite). The greatest contamination probably is caused by pyrite that initially flooded much of the capping. However, large zones of nearly pure silica are present within the western part of the White River area. Several samples of the porous silica capping collected and examined during this study contain more than 95 percent SiO_2, 1 - 5 percent Fe_2O_3, about 1 percent TiO_2, and less than 0.5 percent combined CaO, K_2O, and Na_2O. The silica capping forms ridges and hills 200 to 400 feet in height and in which widespread oxidation and supergene leaching have removed much of the pyrite to depths of a few hundred feet. These ridges contain

extensive zones of nearly pure silica and they provide the best exploration targets for this industrial mineral. Moreover, the ridges also make ideal locations for quarrying operations because they afford easy access from the valley below and topographically elevated working faces for gravity-aided extraction.

Others

Small quantities of native sulfur are present in several outcrops within the western part of the White River area. Weyerhaeuser Company reports state that one of Kalunite's exploration drill holes encountered a zone of sulfur-saturated rock (averaging 16.5 percent sulfur for 48 feet) in sec. 32, T20N, R8E. Another report indicates that large boulders of native sulfur, although discontinuous in distribution, were encountered in landslide rubble from a small (50 foot) exploration adit driven in the SW1/4, sec. 33, T20N, R8E for sulfur. The native sulfur in both reported occurrences is present in areas of argillic and advanced argillic alteration.

An extensive outcrop of fuller's earth is reported to be present in sec. 29, T20N, R8E (Weyerhaeuser Company report). Fuller's earth consists of attapulgite and montmorillonite clays; it is nonplastic, generally high in magnesia, and has a wide variety of uses as an absorbent and as a thickening agent (Ampian and Polk, 1980). They list 1980 prices for fuller's earth at about $32 - $57 per ton (depending on clay type). None of the clay deposits in the study area were mapped or examined for their economic potential. However, most

outcrops of clay are contaminated with disseminated pyrite, which renders them unsatisfactory for industrial purposes.

Justification for Exploration in the White River Area

My interest in the mineral potential of the White River basin was established during a literature search of WDGER publications. The presence of extensive areas of silicification, alunitization, argillic alteration (clays), and moderate amounts of native sulfur indicated the likely presence of at least one large fossil hot-spring system within the White River basin. In addition to this information, Moen and Huntting (1975) have reported the presence of a minor gold occurrence and the existence of two adits in silicified and argillically altered volcanic rocks within the White River area. The adits were driven during the 1890's, and for a short time a small stamp mill was present to process gold ore (Huntting, 1955). The results of samples collected from adits by WDGER personnel in the 1920's revealed gold abundances of $0.54 - $1.40 per ton (0.02 - 0.07 oz/ton), at the prevailing gold price of $20 per ounce (Moen and Huntting, 1975). My exploration interest was additionally encouraged by the presence of a small copper - gold mining/prospecting district and a small to medium size gold - silver mining district south and southeast of the White River, respectively.

From this review of the literature it was surmised that: (1) a large-scale hydrothermal system had been superimposed on a thick andesitic volcanic pile in the White River basin; (2) the morphology

of alteration, suggestive of a thick silica capping underlain by extensive argillic and advanced argillic alteration, was similar to that commonly associated with acid-sulfate hot-spring systems; and (3) the presence of variable concentrations of gold (up to ore grade) in two short adits within this large system afforded the logical conclusion that volcanic rocks of the White River area might host significant gold mineralization.

Results of the present investigation suggest the presence of at least two major and distinctly separate gold-bearing zones within the White River basin. They were recognized on the basis of several favorable geologic, mineralogic, and geochemical features, as described in the sections that follow, and are believed to be representative of the acid-sulfate hot-spring type of volcanic-hosted epithermal gold deposit. These two zones are herein defined as the West and East areas, respectively, and their locations and associated silicified host rocks are shown in Figure 28. The age of hydrothermal alteration and metallization in the White River area is 20.4 $\pm$ 0.1 m.y. (see appendix 1), based on the 40Ar/39Ar analysis of hypogene alunite from a mineralized zone (NE1/4, NE1/4, sec. 12, T19N, R7E). This hydrothermal activity is interpreted as being genetically related to the formation of the Clear West Peak caldera (22.6 - 19.1 m.y.) and (or) resurgent magmatic activity along its margin.

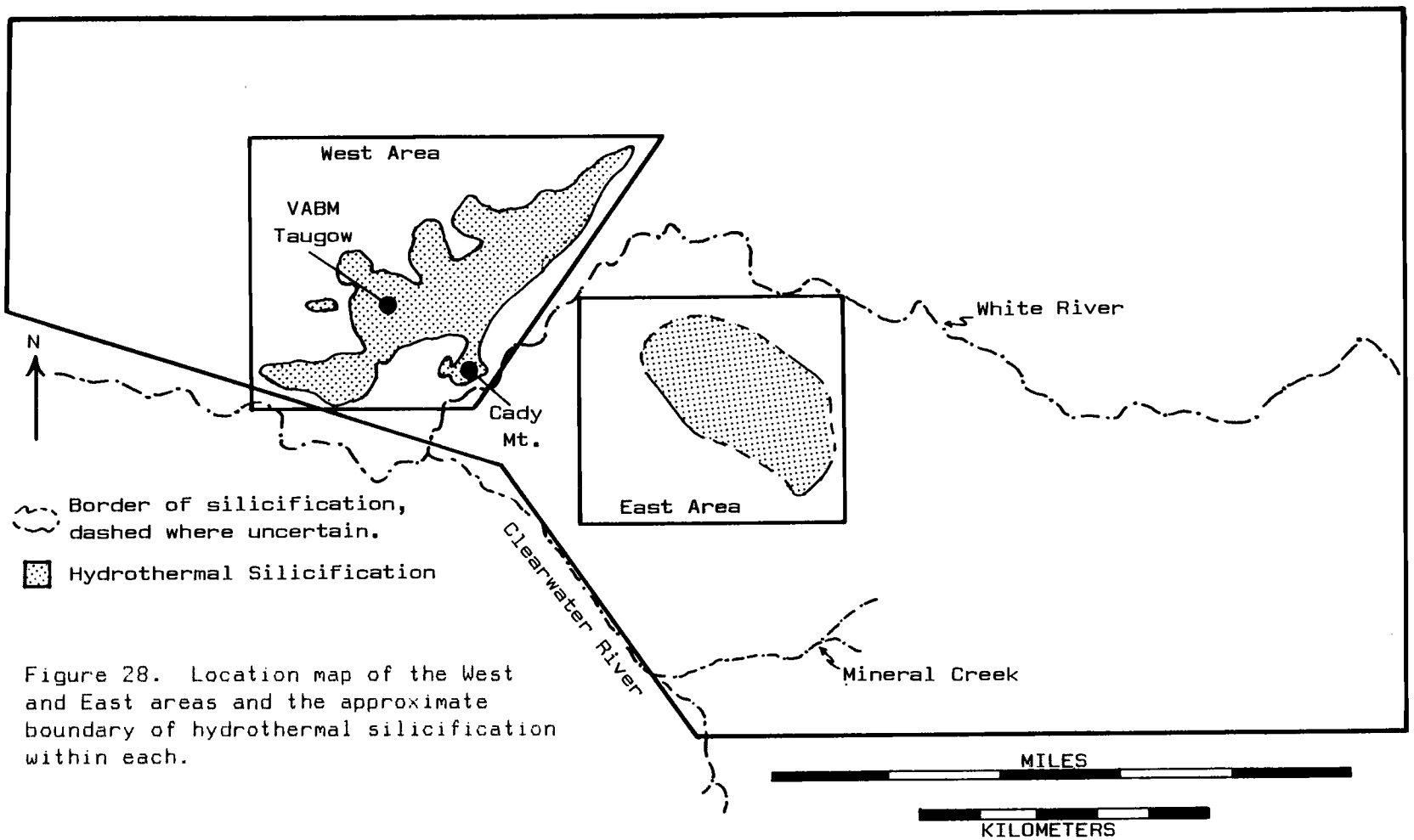

Figure 28. Location map of the West and East areas and the approximate boundary of hydrothermal silicification within each.

West Area

Country rocks of the West area consist of two major types; andesite and rhyolite. The most abundant are andesites of the Fifes Peak Formation that are present as volcanic flows and breccias that contain phenocrysts of plagioclase feldspar, augite, and hypersthene. Rhyolitic volcanics of the Fifes Peak Formation(?) constitute a significant, but not fully mapped, unit and overlie Fifes Peak andesite flows in the West area. A major hydrothermal system was superimposed on this central part of the rhyolitic unit and replaced most of it with pervasive silicification. The original rhyolitic composition of these volcanics was determined from remnant textural evidence (see Figs. 13 through 16B). The East Clay Creek fault is the principal structure in the West area. It strikes N40 - 50°E and is terminated at the intersection with the Twin Creek fault and thus appears to be the older structure.

Alteration

Evidence that a very large and dynamic hot-spring system was present within the West area includes: (1) argillic and advanced argillic alteration over several square miles; (2) a silica capping that is 3.5 miles in length, locally up to 1 mile in width, and in places at least 400 feet thick; and (3) several zones showing multiple events of hydrofracturing and explosive brecciation. A diagrammatic

sketch of the principal alteration zones created by the hot-spring system within the West area is illustrated in Figure 29 and includes the general shape of the silica capping and possible structural orientations. The following is a generalized description of this mineralogy and its zonation, as the West area is traversed from fresh country rocks (andesite lava flows) inward to the core of the fossil hot-spring system.

Fresh andesite volcanics host numerous small fault and fracture controlled veins for several miles surrounding the hot-spring system. These veins generally lack gold, and may or may not contain significant anomalies of arsenic, antimony, mercury, copper, molybdenum, lead, and zinc. They are often narrow structures in the outer and distal parts of the fossil hot-spring system, and contain quartz, calcite, and pyrite between alteration envelopes of clays, chlorite, epidote, calcite, pyrite, and zeolites present in the adjacent wall rocks.

A broad zone of propylitic alteration surrounds the fossil hot-spring system in the West area. The alteration mineral assemblage in the propylitic zone is primarily composed of pyrite, epidote, quartz, chlorite, montmorillonite (and other clays), calcite, and zeolites. Pyrite is present as disseminations throughout the country rock and formed at the expense of ferromagnesian minerals. The propylitic alteration mineral assemblage is indicative of a low temperature near-neutral to moderately-alkaline environment. This propylitic assemblage grades outward into fresh unaltered volcanic host rocks, and inward to a zone of argillic alteration.

Figure 29. Diagramatic sketch of the fossil hot-spring system in the West Target area that illustrates major alteration zones and structural features.

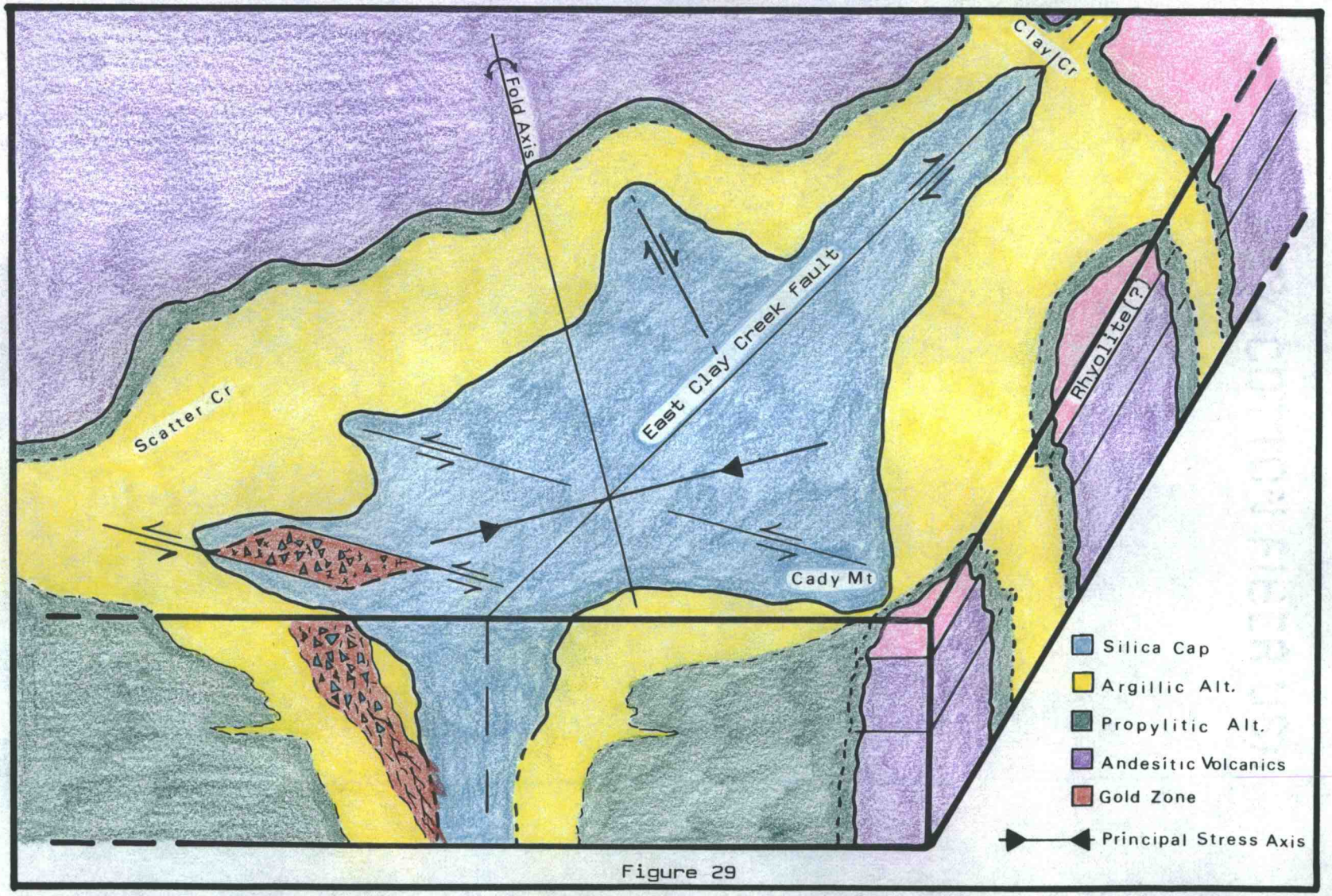
Fold Axis
Clay Cr
East Clay Creek fault
Scatter Cr
Rhyolite(?)
Cady Mt
Silica Cap
Argillic Alt.
Propylitic Alt.
Andesitic Volcanics
Gold Zone
Principal Stress Axis

Figure 29

Argillic alteration is best developed in igneous rocks and is principally a product of hydrogen metasomatism of intermediate to calcic plagioclase feldspars, according to Meyer and Hemley (1967). Argillic alteration in the West area is well-developed in andesitic volcanic rocks that have been subjected to intense hydrogen metasomatism. This highly acid environment resulted in extensive base leaching and produced kaolinite, other clays (especially the montmorillonite group), pyrite, and minor quartz. Much of the kaolinite is of hypogene origin, as is indicated by the association with abundant, disseminated, and unoxidixed finely crystalline pyrite. Argillic alteration is distributed around and beneath a surface and near-surface cap of silica and is present as matrix material in veins and breccia zones that cut the silica capping. Abundances of precious and base metals and other trace elements are unevenly distributed within the argillic alteration zone. Gold-bearing breccias and stockwork veins, within major hydrohermal conduits, may extend vertically through the silica capping and into or below underlying argillic alteration. The precious and base metals may also be present in significant concentrations within argillically altered host rocks that border major breccia and vein networks. The central core of the West area has been subjected to pervasive silicification as is illustrated by Figures 28 and 29. A zone of advanced argillic alteration is situated between the silica core and argillic alteration. Advanced argillic alteration in the West area is characterized by the total destruction of feldspar and the presence of alunite, pyrite, and quartz $\pm$ kaolinite, other clays, fluorite, and

barite. Alunite is present as a hypogene mineral in irregular pods and masses within and below the silica capping, as a matrix mineral in breccia zones and veins that cut massive silicification, and as discrete replacements of plagioclase feldspar phenocrysts in local volcanic units.

The silica capping is composed primarily of finely crystalline quartz with individual crystals on the order of 20 - 500 microns in size. These quartz crystals interlock loosely to form a highly porous and permeable framework. Identification of feldspar ghost crystals and volcanic textures is possible in some outcrops. However, most primary minerals and textural features of the original host rocks have been hydrothermally obliterated within the silica capping. Areas of massive silicification are present within the porous silica capping and commonly form erosion-resistant knobs and surface outcrops of dense silica or silica breccia. In fact, the entire silica capping is more resistant to erosion than the surrounding zones of argillic or propylitic alteration and it forms prominent hills and ridges such as those shown in Figures 30A, 30B, and 31.

Geochemistry of Alteration

Several constraints upon the geochemistry of hydrothermal fluids can be deduced from a study of alteration and vein mineralogy and their respective spatial patterns of distribution. Near-surface hypogene minerals are commonly out of equilibrium with one another and caution must be taken when using them to interpret the geochemistry of

Figure 30. Major areas of silicification within the West area.
A). Aerial view of the silica capping in the West area of the White River basin. The view is to the north and extends about 2.5 miles east-west. The silica ridge formed along the East Clay Creek fault and is exposed for about 600 feet of topographic relief from the ridge-top to U.S. highway 410.
B). Line drawing depicting the approximate boundary of silicified outcrops. Sample WR-114 was collected for geochemical analysis and sulfur isotope analysis of cogenetic alunite-pyrite-enargite.

Note: The name "Cady Mountain" is an informal name found in Weyerhaeuser Company reports and is not present on state or federal maps.

A

B

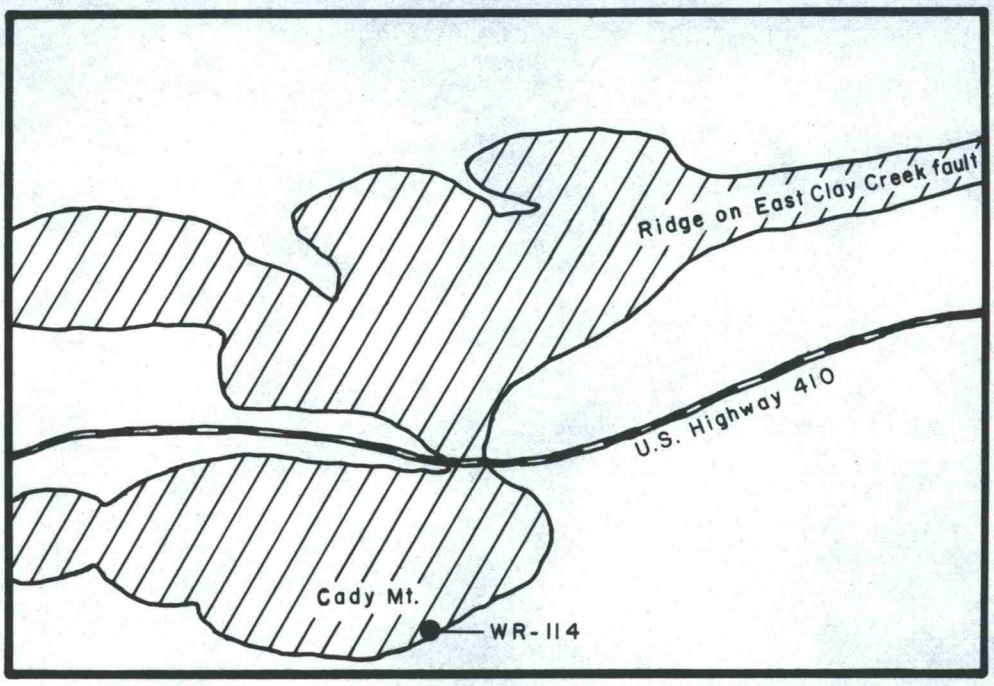

Figure 30

Figure 31. Silicified zone of the West area approximately 3.5 miles in length. View is to the east-northeast and includes the White River in the foreground, the silica ridge in the midground, hills of Fifes Peak andesite in the background, and in the far-background are the Puget Lowlands and Enumclaw, Washington; for reference, s = ridges and hills of silica and includes Cady Mountain (C) and VABM Taugow (T).

hydrothermal solutions. Reliable information about the composition of hydrothermal fluids can generally be deciphered from vertical patterns of mineral deposition within major hydrothermal conduits. The mineralogy of the fossil hot-spring system in the West area includes abundant microcrystalline quartz, hematite, enargite, pyrite, alunite, fluorite, kaolinite as well and other clays, and also minor amounts of chlorite, epidote, calcite, and zeolites. The vertical zonation of hypogene mineralogy in the West area grades from alunite $\pm$ pyrite, enargite, and kaolinite at depth to quartz (pervasive silicification) and local zones of hematite near the surface. Roots of silica also extend downward along major hydrothermal conduits.

A very large silica capping was created in the West area by extensive base leaching, including the mobilization of alumina, and the introduction of SiO2. Hydrothermal fluids responsible for formation of the silica capping contained moderate to high concentrations of fluoride and sulfur and were probably acidic (within a few pH units of neutrality). This silica capping represents a very extensive and thorough replacement by quartz of nearly all major-element oxide components locally within the andesite and rhyolitic volcanics. The compositions of four samples from the silica capping range from 97 - 99 weight-percent SiO2 and 0.65 - 2.84 weight-percent TiO2, whereas most other elements are present at trace to undetectable concentrations, as listed in Table 5. The porosity of this capping varies from extremely low (less than 1% by volume) in local zones of massive silicification to high (about 20% by volume) in areas of loosely packed microcrystalline quartz. The highly porous

Table 5. Data from major-element oxide XRF analyses and density (D) measurements of fresh volcanics and their silicified equivalents.

Table 5

Sample	D	SiO2	Al2O3	TiO2	Fe	MnO	CaO	K2O	Na2O
Fresh Andesite:									
4 Wt.%		62.36	16.45	0.80	6.44	3.08	5.51	1.87	3.23
g/cc	2.68	1.67	0.44	0.02	0.17	0.08	0.15	0.05	0.09
5 Wt.%		61.53	16.30	0.97	7.23	3.45	5.40	1.69	3.16
g/cc	2.62	1.61	0.43	0.03	0.19	0.09	0.14	0.04	0.08
7 Wt.%		61.23	16.70	0.96	6.16	3.10	7.00	1.73	2.80
g/cc	2.67	1.63	0.45	0.03	0.16	0.08	0.19	0.05	0.07
12 Wt.%		63.47	15.73	0.89	6.33	2.42	5.51	2.06	3.30
g/cc	2.66	1.69	0.42	0.02	0.17	0.06	0.15	0.05	0.09
14 Wt.%		62.99	15.90	0.78	5.90	3.35	5.94	1.58	3.30
g/cc	2.66	1.68	0.42	0.02	0.16	0.09	0.16	0.04	0.09
Average Rhyolite & Rhyodacite:									
2 Wt.%		74.70	13.46	0.39	2.28	0.24	0.96	4.73	3.16
g/cc	2.44	1.82	0.33	0.01	0.06	0.01	0.02	0.12	0.08
6 Wt.%		70.61	13.86	0.88	5.97	0.46	1.86	2.96	3.05
g/cc	2.54	1.79	0.35	0.02	0.15	0.01	0.05	0.08	0.08
16 Wt.%		76.96	13.73	0.35	0.73	----	0.43	4.98	2.79
g/cc	2.31	1.78	0.32	0.01	0.02	----	0.01	0.12	0.06
Silica Cap:									
26 Wt.%		98.82	----	1.07	----	----	----	----	0.10
g/cc	2.47	2.44	----	0.03	----	----	----	----	tr
27 Wt.%		98.20	0.73	0.65	----	----	----	0.08	0.33
g/cc	2.53	2.48	0.02	0.02	----	----	----	tr	0.01
28 Wt.%		97.08	----	2.84	----	----	----	----	0.05
g/cc	2.22	2.16	----	0.06	----	----	----	----	tr
29 Wt.%		98.88	----	0.97	----	----	----	----	0.13
g/cc	2.42	2.39	----	0.02	----	----	----	----	tr

rock is commonly termed "silica-sponge" and generally contains numerous vugs, which were occupied by phenocrysts or lithic fragments prior to alteration. Silica enrichment in the surface and near-surface environment of the West area took place by at least two mechanisms: (1) silica was introduced by ascending hydrothermal solutions and deposited primarily due to a reduction in temperature; and (2) a residual accumulation of silica formed as extreme base-leaching removed most other elements from the host rock. Data from whole-rock major-element oxide analyses and density measurements indicate that host rocks underwent an increase in SiO2 content of about 35 to 50 percent during formation of the silica capping in the West area. This conclusion is based on data from five samples of fresh andesite that contain an average of 1.66 g/cc SiO2, three samples of fresh rhyolite and rhyodacite that contain an average of 1.80 g/cc SiO2, and three samples of the porous to massive silica capping that contain an average of 2.44 g/cc SiO2. Therefore, much of the silica capping in the West area is composed of SiO2 transported and deposited by the ascending hydrothermal fluids. Formation of a silica capping over an area as extensive as that in the West area requires an uncommon fluid chemistry. Nearly all of the major-element oxides have been removed from country rock, totaling a least a few hundreds of millions of tons, and replaced by silica. The pH range necessary to create such extensive base leaching may be considerably higher than is generally believed to be the case among exploration geologists, provided the hydrothrmal fluids contain greater than 1 or 2 ppm fluoride. Experiments by J.D. Hem (reported in the Handbook of

Geochemistry, 1978) demonstrate that the solubility of aluminum at STP increases dramatically with the addition of minor to moderate amounts of fluoride. His results are most spectacular over the near neutral pH ranges, where aluminum is generally considered to be insoluble in pure water. Hem (1978; p.13H-4) stated:

> "A concentration of 0.0001 molar, equivalent to 1.9 ppm (mg/l), of F is capable of increasing the equilibrium dissolved aluminum concentration by a factor of ten at pH5 and nearly a hundred at pH6, as compared with lower solubilities for conditions in the absence of fluoride.".

High fluoride concentrations are present in samples of massive silicification from both the West and East areas. Concentrations of fluoride in samples from these areas at hundreds of ppm are common, a few thousamd ppm are not unusual, and one sample contains over 6,000 ppm. Fluorite crystals are present within the silica capping exposed in a small quarry in the NW1/4, NW1/4, sec. 7, T19N, R8E, and have also been reported from other localities within the West area (Weyerhaeuser Company reports). It is proposed that hydrothermal fluids at moderate temperature (200°C), which contain abundant fluoride and are within a few pH units below neutrality, could effectively promote disolution of aluminum silicate minerals. The addition of fluoride to hydrothrmal fluids should dramatically enhance the effects of base leaching and alumina mobility and promote the formation of an extensive near-surface zone of silicification, such as the silica capping in the West area.

The presence of large quantities of alunite below and locally within the silica capping is representative of advanced argillic

alteration. Much of the alunite in the West area is hypogene in origin and is present as highly crystalline salmon-pink aggregates of micaceous-like plates, up to 1 mm in length. Minor amounts of pyrite, enargite, and fluorite are locally intergrown with and presumably cogenetic with this alunite. The formation of alunite by hydrothermal processes is restricted to environments that are both oxidizing and low in pH. The presence of hypogene alunite brackets the chemistry of fossil hydrothermal fluids, with respect to pH and fO2, and gives a qualitative indication of sulfur and potassium content. Pyrite and enargite, as minerals associated with alunite, restrict the chemistry of these fluids even further. The narrow field of stability for the codeposition of pyrite and alunite at 250°C is shown in Figure 32A, as modified from Kesler and others (1981). Hematite is locally present with alunite in the West area, and although the genetic relationship between the two minerals is not fully understood, a high oxygen fugacity and low pH is indicated by their association. High activities of sulfate, potassium, and hydrogen ions within the hydrothermal fluids increase the stability of alunite, rather than kaolinite, as depicted in Figure 32B (after Hemley and others, 1969). A high total sulfur content is also necessary to form alunite (Knight, 1977). The stability field of alunite is shown in Figure 32A for hydrothermal fluids that contain a total sulfur concentration of 0.01 moles/liter and are at a temperature of 250°C. Alunite is stable at a pH of less than about 2.8 under these conditions. The stability field of alunite expands to a pH of approximately 3.7 if the total concentration of sulfur is increased to 0.1 mole/liter, but shrinks to

Figure 32. Phase equilibria diagrams for alteration minerals in the White River area.
A). pH verses -Log f02 diagram; alu, hm, kao, mag, musc, po, and py represent alunite, hematite, kaolinite, magnetite, muscovite, pyrrhotite, and pyrite respectively; at a temperature of 250°C with 0.01 molar total sulfur and 0.01 molar total potassium. The stipple pattern indicates the overlapping stability fields of pyrite and alunite. Modified from Kesler and others (1981).
B). Mineral stability diagram showing the general relationships between fields of alunite, kaolinite, and muscovite as a function of the individual activities of potassium, hydrogen, and sulfate ions; with quartz present and at a constant temperature and pressure (after Hemley and others, 1969).

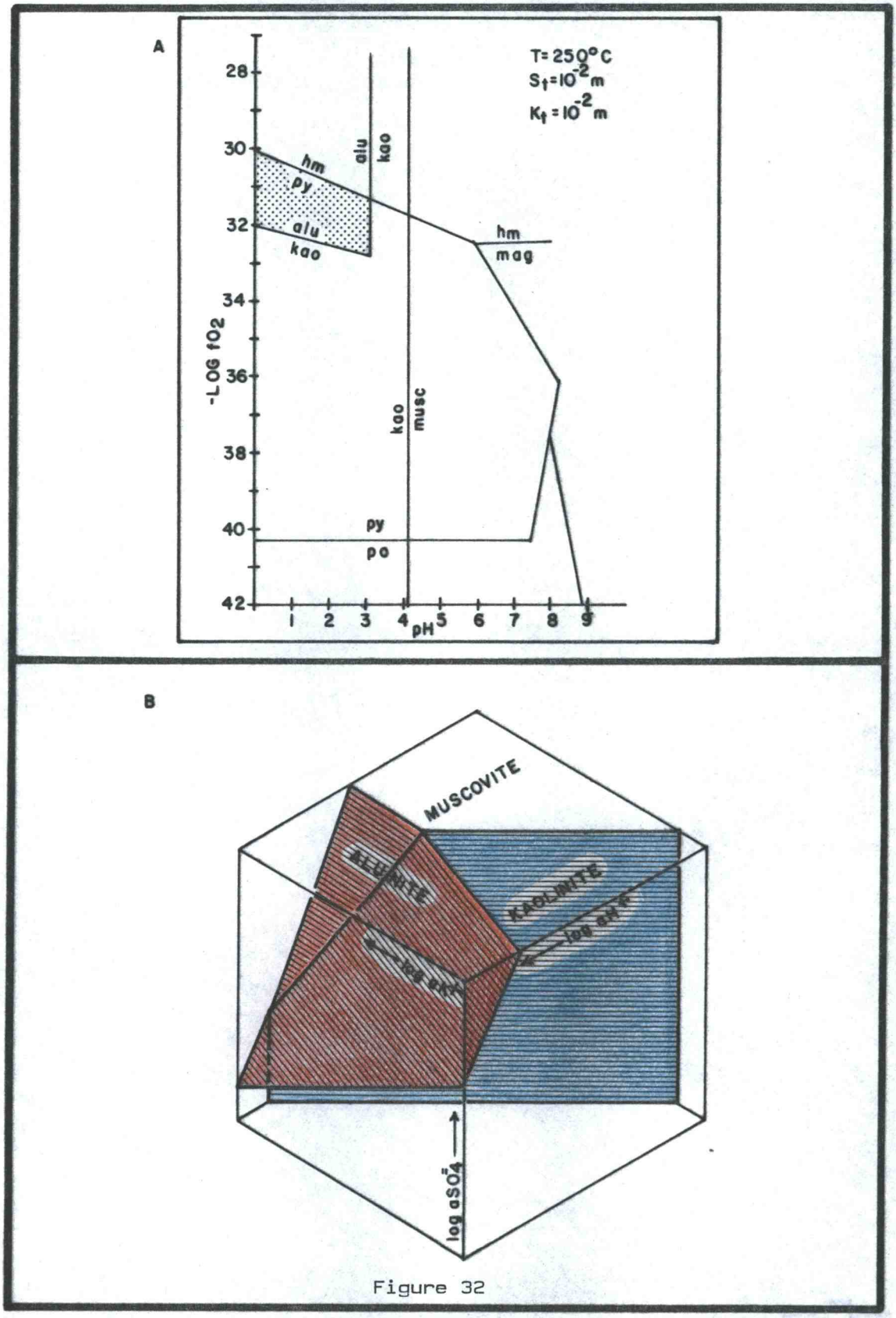
A
T= 250°C
$S_t = 10^{-2}$ m
$K_t = 10^{-2}$ m
hm
py
alu
kao
alu
kao
hm
mag
kao
musc
py
po
-LOG fO_2
28
30
32
34
36
38
40
42
1
2
3
4
pH
5
6
7
8
9
B
MUSCOVITE
ALUNITE
KAOLINITE
log aK+
log aK+
log $aSO_4^=$

Figure 32

a pH of 1 if the sulfur concentration is decreased to 0.001 mole/liter (Hayba and others, 1986). Geologic and mineralogic relationships pertaining to alunite indicate that its origin is primarily hypogene, within the White River basin. Sulfur isotope analysis of one sample of cogenetic alunite-pyrite-enargite also indicate a hypogene origin of the alunite (see Table 6). This sample has $\delta(34)S$ values of +26.2 o/oo in alunite, -2.6 o/oo in pyrite, and -4.8 o/oo in enargite. The large difference in $\delta(34)S$ concentrations between pyrite and alunite listed above is consistent with a large fractionation factor predicted from theory and experiment, and indicates a hypogene origin of both minerals (see Field and Fifarek, 1986; and Hayba and others, 1986). Using the sulfate-pyrite isotopic thermometer equation of Field and Fifarek (1986) the +28.8 o/oo difference in $\delta(34)S$ concentrations of codeposited pyrite and alunite in the West area provide an isotopic temperature of formation of about 190°C. This intermediate temperature is consistent with those suggested by the mineralogy of alteration and vein assemblages present in the West area and is believed to be reasonably accurate. Moreover, such agreement is remarkable because Ohmoto and Rye (1979) have stated that at temperatures less than about 300°C codeposited sulfate and sulfide mineral pairs may not be in isotopic equilibrium.

Kaolinite is present as a minor constituent in pods of alunite near hydrothermal conduits and becomes a dominant mineral in the surrounding envelopes of argillic alteration. Finely crystalline pyrite is disseminated throughout much of the argillic alteration zone as shown in Figure 33. This pyrite formed by replacement of

Table 6. Sulfur isotope analysis of cogenetic alunite-pyrite-enargite (NE1/4, sec. 7, T19N, R8E).

Table 6

Mineral	^{34}S o/oo
Alunite	+26.2
Pyrite	-2.6
Enargite	-4.8
Alunite-Pyrite ^{34}S o/oo	+28.8 = Δ

Isotopic temperature of formation equation for the mineral pair $SO_4^{=}$ - pyrite (after Field and Fifarek, 1986)

$$T^{o}K = \frac{2460}{(\Delta - 0.56)^{1/2}}$$

Comments

The large isotopic fractionation of $\Delta(34)S$ of +28.8 o/oo for the alunite-pyrite mineral pair indicates a probable hypogene origin and provides a reasonable isotopic temperature estimate of about 190°C.

Figure 33. Argillically altered Fifes Peak andesite along East Clay Creek (SE1/4, sec. 28, T20N, R8E). The outcrop consists of 80 - 90 percent clay (mostly kaolinite) and 10 - 20 percent disseminated finely crystalline pyrite. The darker gray material to the right of the rock hammer is finely crystalline pyrite.

ferromagnesian minerals in andesitic volcanics. The presence of coexisting kaolinite and pyrite indicates a low fO2, low to moderate pH, and moderate to high total sulfur content of hydrothrmal fluids (see Fig. 32A).

Mineralogy

Hypogene minerals that are abundant and easy to recognize in the West area include hematite, enargite, quartz and other forms of silica, pyrite, and alunite. Fluorite is present in at least one location (NW1/4, NW1/4, sec. 7, T19N, R8E) and may also have a widespread distribution. Results of geochemical studies indicate that minerals containing Ba, Mo, Cu, As, and Sb are probably present in small amounts, and also possibly those of Ag, Pb, and Zn. Although native gold was not observed during the current investigation, there is indirect evidence for its likely presence. The results of geochemical analyses show that gold is present in minor concentrations (up to 480 ppb) in outcrops. However, historical records indicate the construction of a small stamp mill to process ore coming from the White River adits (Huntting, 1955) and suggest of the presence of native gold at depth.

Hematite (Fe203) is found chiefly as a hypogene matrix mineral within breccia pipes and fractures that cut the silica capping, and is locally interspersed with hypogene alunite. It is commonly associated with gold mineralization as a matrix mineral within explosion breccia pipes, tectonic breccia zones, and veins. Hypogene hematite is also

disseminated in country rocks near hydrothermal conduits, as flat lenses that follow bedding and foliation planes and as dispersed plumes. Oxidation of pyrite within the silica capping such as given by the equation

$$4FeS2 + 4H2O + 17O2 \rightleftharpoons 2Fe2O3 + 8H2SO4 \qquad 1$$

is probably responsible for moderate amounts of earthy hematite stain that is of supergene origin. The majority of hematite in the West area is crystalline and has the morphology of microball-bearings (10 microns to a few millimeters in diameter). Examination of samples by ore microscopy has revealed the existence of two hematite phases, one medium gray and the other light gray in color. It was initially assumed that the light gray oxide phase contained substantial amounts of titanium in solid solution, or was in fact ilmenite ($FeTiO3$). This interpretation was based in part on ore microscopy and partly on the chemical data showing that at least some remobilization of $TiO2$ had taken place within the silica capping, i.e. greater than 100 percent g/cc increase in $TiO2$ in sample 28 (a hematite-cemented silica-breccia), listed in Table 5. A scanning electron microscope KEVEX X-ray spectrum analysis of the two hematite phases has indicated the presence of titanium included in one hematite bearing sample. However, in other samples neither inclusions of ilmenite or other elements could be found to explain the apparently large optical differences between the two phases. The X-ray spectrum of the darker medium gray hematite, shown in Figures 34A and 34B, indicates the presence of an element lighter than iron and heavier than silicon. The approximate atomic weights of Si, Ti, and Fe are 28, 48, and 56,

Figure 34. SEM photomicrographs of two microball-bearing hematite phases. The light gray hematite (H) is a purer phase than the medium gray (H+) variety. See text for additional elaboration of compositional complexities, and note the contrasting euhedral habit of associated quartz (q) crystals (scale given by white bar is 10 microns).

A

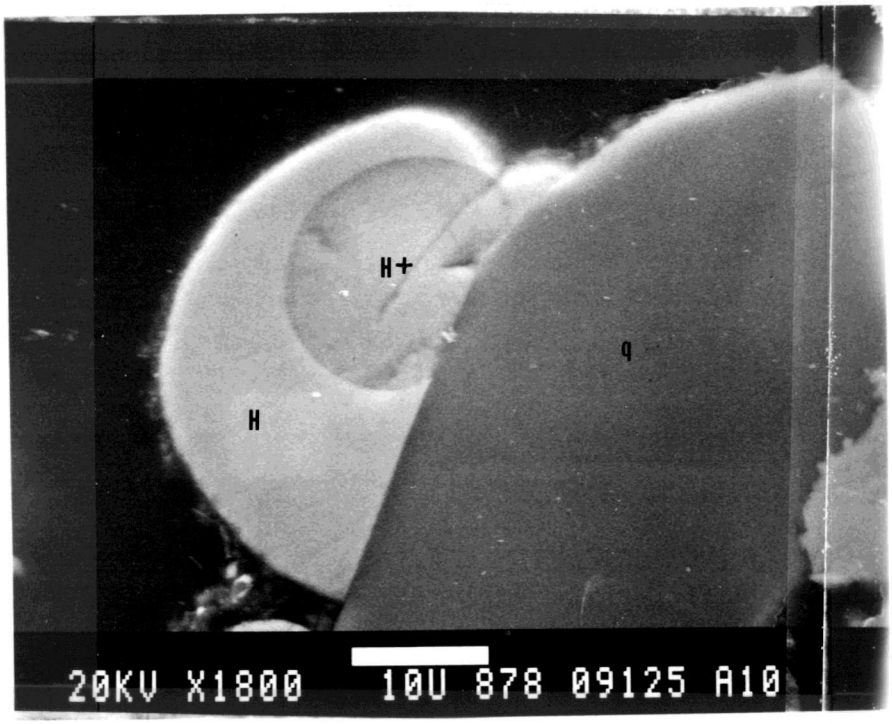
H+
q
H
20KV X1800 10U 878 09125 A10

B

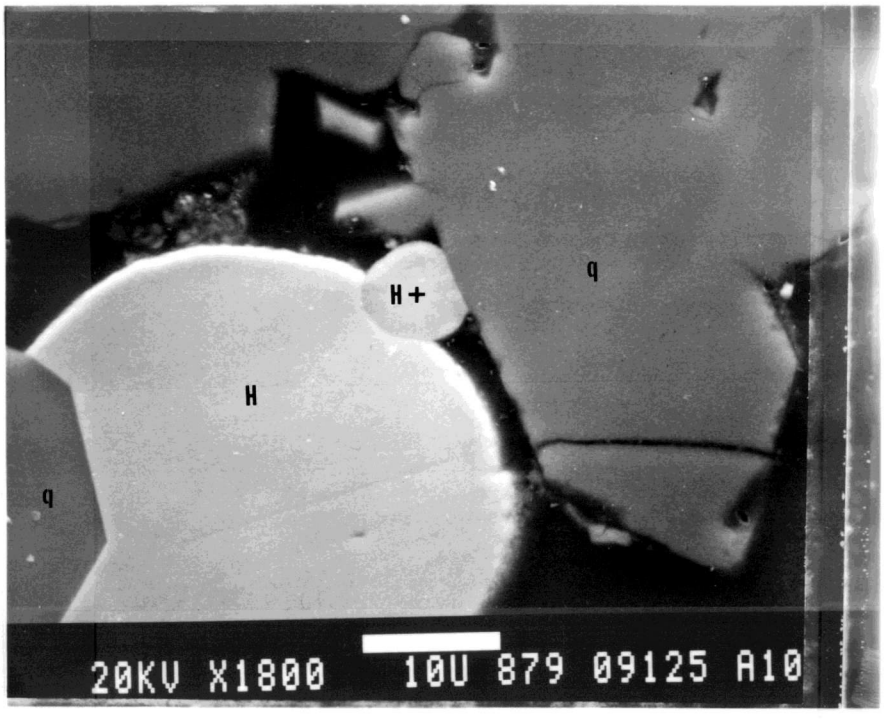
q
H+
H
q
20KV X1800 10U 879 09125 A10

Figure 34

respectively. Based on this data it is concluded that titanium is the probable contaminate of the hematite, although other elements such as sulfur, vanadium, chromium, and manganese with atomic weights between Si and Fe are also other possible impurities.

Enargite (Cu_2AsS_4) has been recognized by Hayba and others (1986) as one of the characteristic minerals of acid-sulfate type volcanic-hosted epithermal precious metal deposits. This mineral has been found at two locations within the West area; in the NE1/4, NE1/4, sec. 7 (sample WR-114) and in the NW1/4, NW1/4, sec. 7 (sample WR-155), both in T19N, R8E. Enargite of sample WR-114 forms discrete crystals that are associated with alunite, pyrite, and silica. Geochemical analysis of this sample also reveals 136 ppm barium, which is probably present as the mineral barite. A scanning electron microscope photomicrograph of enargite from sample WR-114 and its KEVEX X-ray spectrum are shown in Figures 35A and 35B. Data for the KEVEX semi-quantative analysis indicate a As:S ratio of 0.23:1.00 and a Cu:S ratio of 0.56:1.00. This sample was also analyzed for sulfur isotopes and contains $\delta(34)S$ values of -4.83, -2.58, and +26.18 o/oo for cogenetic enargite, pyrite, and alunite, respectively. Enargite is also present at a small silica quarry (NW1/4, NW1/4, sec. 7, T19N, R8E) where it is associated with coexisting pyrite $\pm$ kaolinite and alunite in several small veinlets that cut the silicified volcanic host. Veinlets containing fluorite are also present at this quarry.

Microcrystalline quartz is the most abundant form of silica present in the West and East areas. Aggregates of individual 20 - 500 micron size quartz crystals replace the local volcanic and

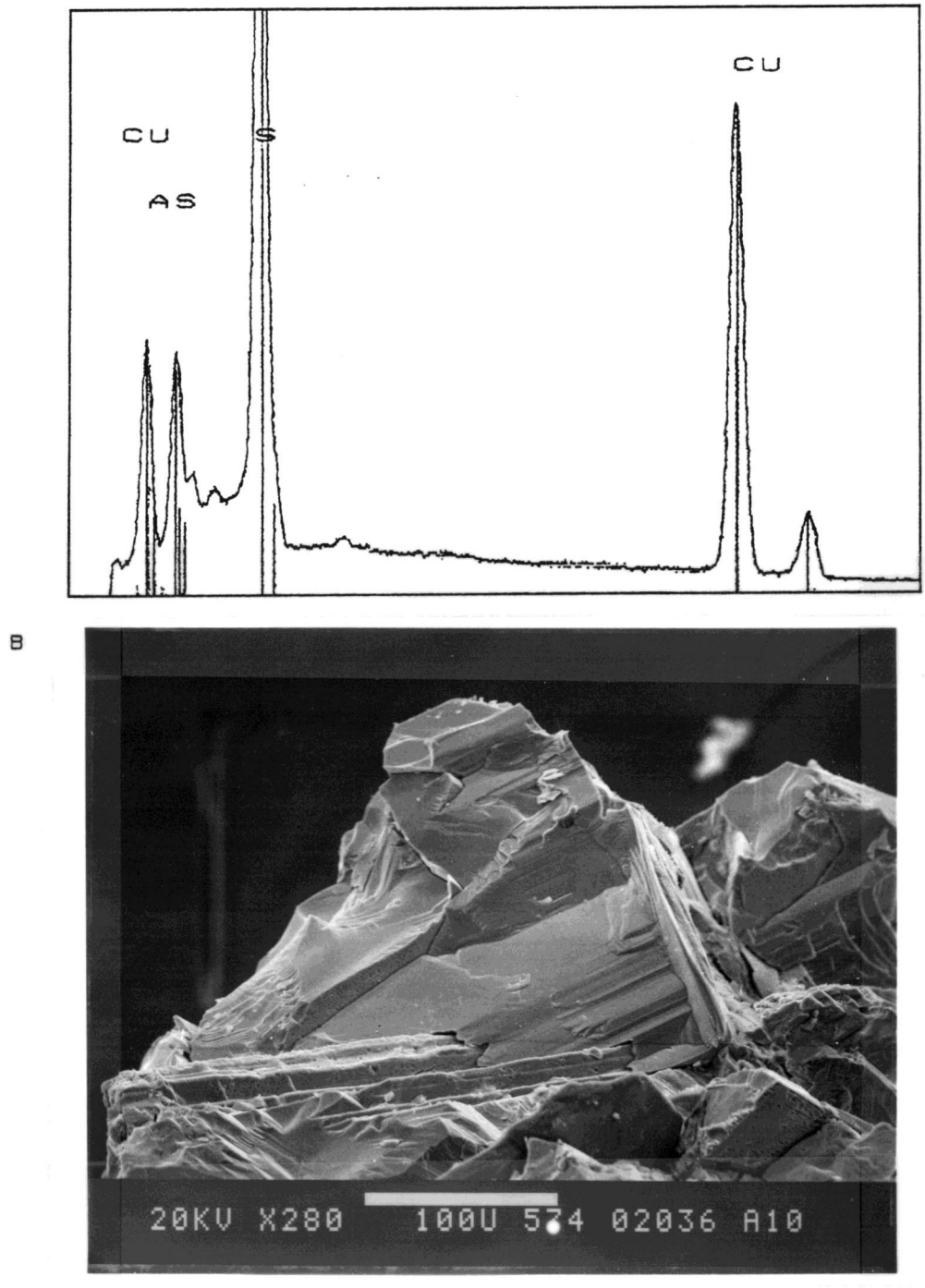

Figure 35. Sample of enargite from the West area (NE1/4, sec. 7, T19N, R8E).

A). Semiquantitative KEVEX X-ray analysis of enargite indicates an As:S ratio of 0.23:1.00 and a Cu:S ratio of 0.56:1.00.

B). SEM photomicrograph of enargite showing its characteristic striations.

intrusive(?) host rocks. The size and morphology of typical quartz crystals that comprise the silica capping are shown in Figure 34B. Each quartz crystal in this figure is about 20 - 40 microns in size and is subhedral to euhedral in shape. Most of the silica capping is composed of a loose network of microcrystalline quartz, which imparts a highly porous and vuggy texture to it. Areas within the porous silica capping are locally composed of massive (dense) silicification and are often located proximal to major veins or breccia zones. Several samples of silica were analyzed by X-ray diffraction and the results of these analyses showed that the silica was in all cases alpha quartz (low temperature), with minor impurities. These samples were representative of quartz veins and veinlets, the porous silica capping, massive (dense) silicification, and an airfall tuff replaced by silica. Quartz veins are abundant within the silica capping, but their presence may be obscured by ground cover. However, a small silica quarry in the center of sec. 1, T19N, R7E (shown in Figs. 36A and 36B) provides excellent exposures of light gray porcelaneous quartz veins cutting the vuggy silica capping. Quartz veins of various colors also cut zones of massive silicification. The most unusual of these types are the dark gray to black quartz veinlets shown in Figure 37A. These dark colored veins appear to be enriched with sulfides or tourmaline. However, examinations with the microscope did not reveal the presence of these minerals. Instead, the dark gray mineral was found to be entirely smokey quartz. Veins of milky quartz are an important type of introduced silica in the West area (see Figure 37B), because they generally host anomalous gold

A

B

Figure 36. Small silica quarry in the center of sec.1, T19N, R7E showing (A) the working face approximately 20 feet in height, and (B) detail of porous silica capping that is cut by porcelaneous quartz veins outlined with magic marker.

Figure 37. Hand specimens showing various types of quartz veining in the West area.
A). Smokey quartz veins (dark gray) cutting massive silicification (SW1/4, SE1/4, section 1, T19N, R7E).
B). Milky quartz vein with hematite, surrounding a core of silicified volcanic tuff (SE1/4, SW1/4, sec. 1, T19N, R7E). For scale, each blue square is one centimeter across.

A

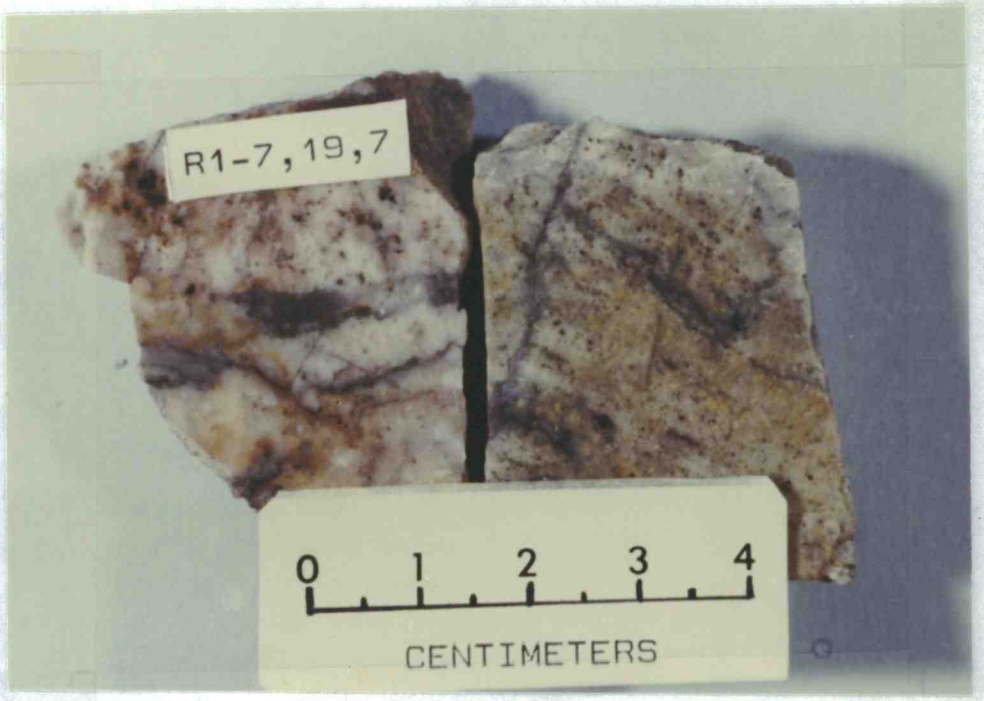

B

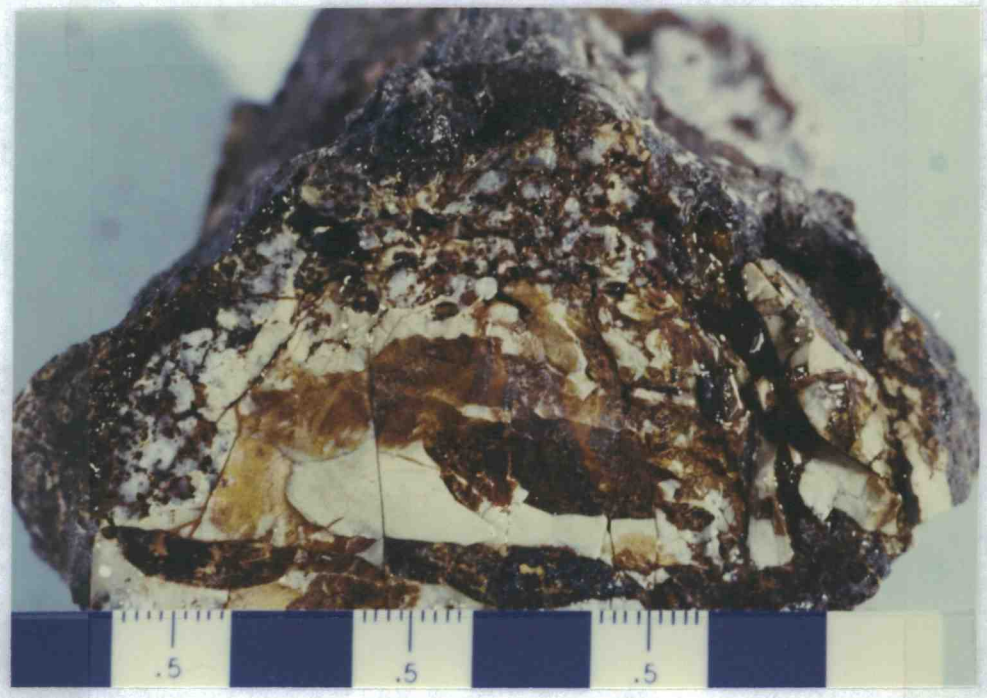

Figure 37

mineralization, and they are discussed in detail in the chapter that follows (Primary Target). All textural varieties of quartz were examined in thin section and none were found to contain fluid inclusions sufficiently large to undertake meaningful thermochemical studies of their types or homogenization and salinity characteristics.

Pyrite (FeS_2) is ubiquitous throughout most of the White River fossil hot-spring systems, with the exception of the areas that have undergone extensive supergene oxidation and leaching. Observations in the field indicate that pyrite was deposited in several different environments and at several different stages throughout the West area. Pyrite is present as fine disseminations in the propylitic, argillic, advanced argillic, and silicic alteration zones, as irregular pods and masses that replace or pervasively flood porous beds of tuff and pumice, and as discrete components in hypogene veins and veinlets. Crystals of pyrite are locally intergrown with alunite, enargite, and silica $\pm$ kaolinite and barite(?) in breccia zones and veins. Much of the silica capping was initially flooded with finely crystalline pyrite. However, supergene oxidation has leached most of the pyrite from this host to depths of over 250 feet in the West area (Weyerhaeuser Company report). Veins and veinlets of pyrite are also common and crosscut all alteration assemblages within this fossil hot-spring system. A specimen from a late-stage (post-gold deposition) pyrite-bearing vein is shown in Figure 38A. It was collected from a vein 3 - 6 feet wide that cuts the silica capping in a N20 - 25°E direction (NW1/4, NE1/4, sec. 12, T19N, R7E) and contains 20 - 40 percent pyrite in association with light green chalcedony.

Figure 38. Hand specimens of various pyrite-bearing rocks from the White River area.
A). Sample from a pyrite-chalcedony vein measuring 3 - 6 feet in width (NW1/4, NE1/4, sec. 12, T19N, R7E).
B). Sample WR-120 is a lapilli tuff partly replaced by pyrite, collected from the East area (NW1/4, sec. 10, T19N, R8E). Sample WR-130 is an example of finely disseminated pyrite in massive quartz, collected from the West area (SE1/4, NW1/4, sec. 36, T20N, R7E).

A

B

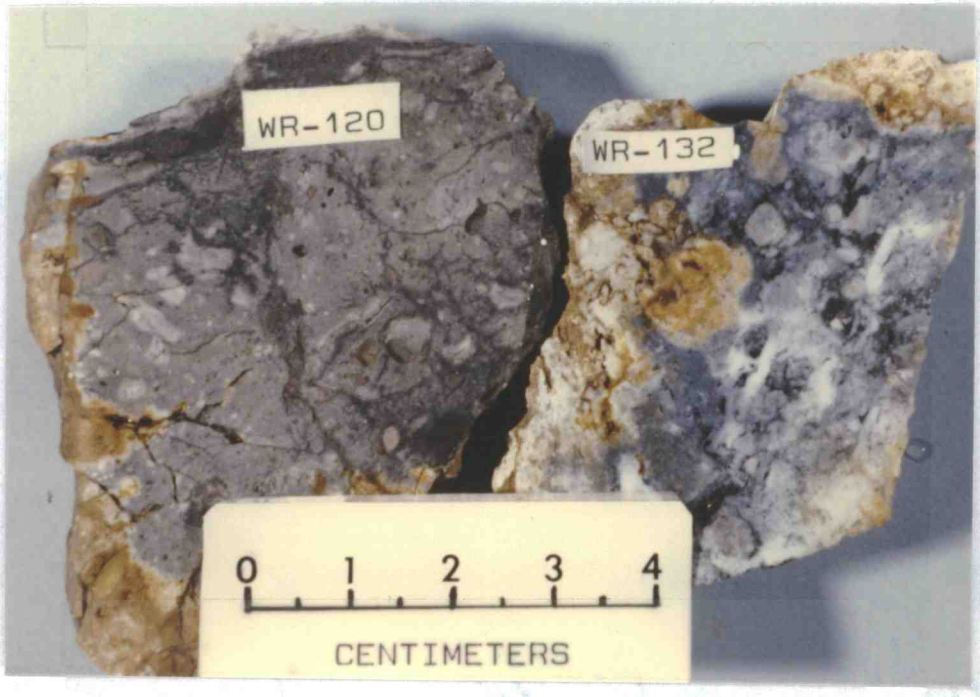

Figure 38

Two other common modes of pyrite occurrence are shown in Figure 38B. Sample WR-120 is a lapilli tuff that is partly flooded with pyrite, whereas sample WR-132 is representative of finely crystalline pyrite disseminated throughout silica that was probably deposited initially as opal. Pyrite is conspicuously absent from breccia pipes and veins that contain hypogene hematite. This is consistent with the separate stability fields of these two minerals, with hematite normally deposited under conditions of increased oxygen fugacity (see Fig. 32A) and thus with restricted availability of sulfide-sulfur.

The presence of alunite $(KAl)3(SO4)2(OH)6$ in the White River area, and its potential as an economic commodity, are reported in detail by Livingston (1971). The local distribution of alunite has been covered in previous sections of this report and the general pH, fO2, potassium, and total sulfur ranges appropriate for its formation have been discussed as shown in Figures 32A and 32B. Field evidence indicates the origin of alunite is primarily as a hypogene mineral, with corroborative evidence from petrographic studies and sulfur isotope fractionation analyses. Alunite forms an isomorphous series with its sodium analogue nautroalunite $(NaAl)3(SO4)2(OH)6$, but pure endmembers are practically nonexistent in nature (Cunningham and Hall, 1976). Using a technique outlined in Cunningham and Hall (1976), results of X-ray diffraction analyses of a sample of alunite from the West area indicate a potassium to sodium ratio of 0.75 : 0.25 in their designated structural sites. This alunite was composed of an aggregate of crystalline, salmon pink, and micaceous-like plates that cements a silica breccia.

Primary Target

The Primary Target is a zone measuring 3,800 by 2,800 feet within the West area that to date exhibits the greatest potential for hosting economic quantities of precious metal mineralization within the White River area (see Fig. 39 for location). Gold mineralization is present in concentrations $\geq$ 20 ppb over an area 2,400 feet in length by 1,000 feet in width, with high gold anomalies in a distinctive central core (the Gold Zone) measuring about 1,600 by 300 - 600 feet (see Fig. 39). The mean values and ranges of Au, Ag, As, Sb, Hg, and Mo for 163 samples collected throughout the entire White River area are listed in Table 7, as are the general ranges of anomalous values for each of these elements. Coincident with, and distributed around, gold mineralization are high geochemical anomalies of silver, arsenic, antimony, mercury, molybdenum, fluorine, and minor to moderate concentrations of barium. This hydrothermal metallization is located in an intensely fractured, brecciated, and veined part of the silica capping and extends downward into the zone of argillic alteration.

Structure

Several periods of fault brecciation, explosive brecciation, and vein formation took place subsequent to development of the silica capping. Four distinct episodes of structural activity have been recognized within the Primary Target area, and each period can be

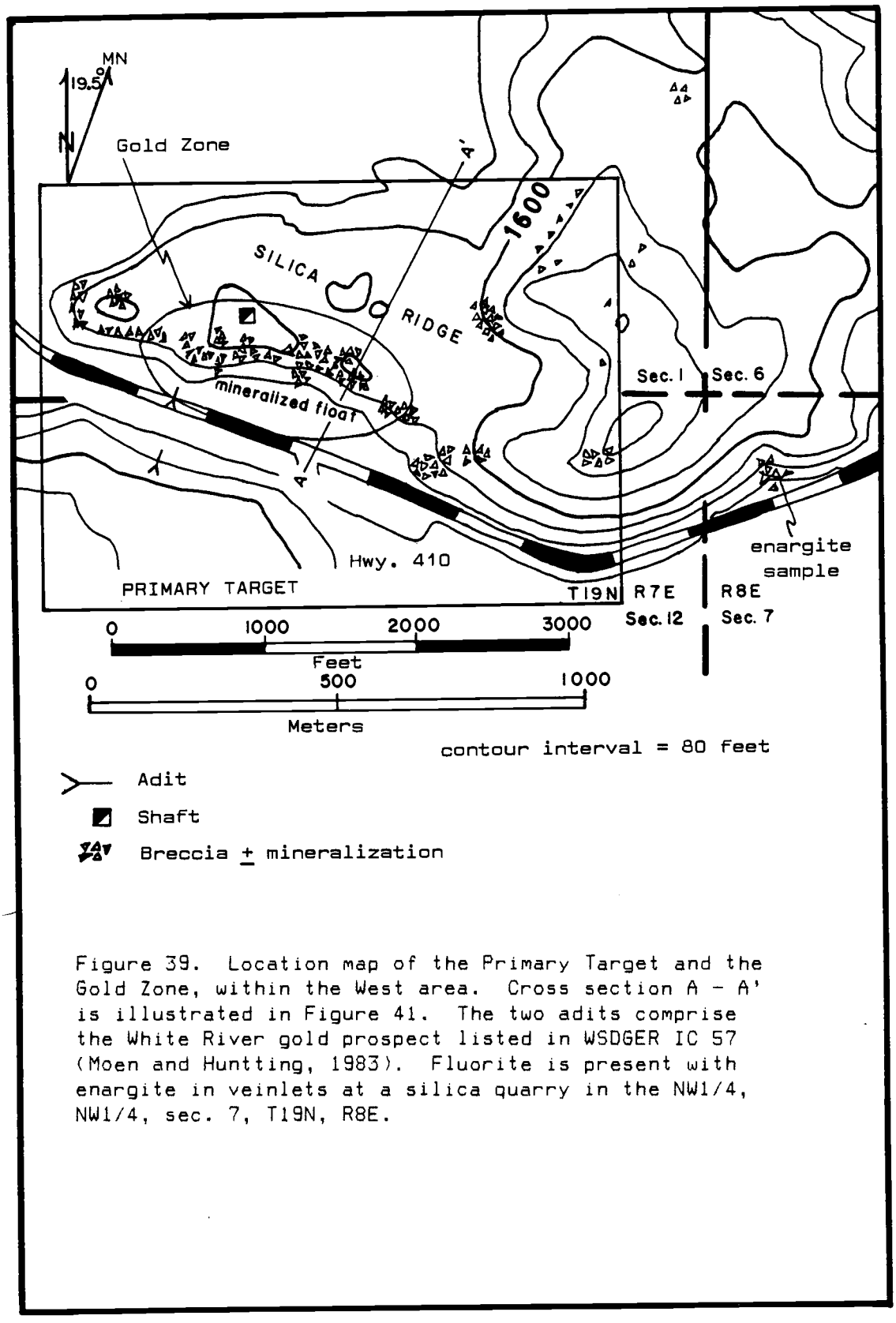

Figure 39. Location map of the Primary Target and the Gold Zone, within the West area. Cross section A - A' is illustrated in Figure 41. The two adits comprise the White River gold prospect listed in WSDGER IC 57 (Moen and Huntting, 1983). Fluorite is present with enargite in veinlets at a silica quarry in the NW1/4, NW1/4, sec. 7, T19N, R8E.

Table 7. The mean and range, and range of anomalous values for Au, Ag, Hg, Mo, As, and Sb in 163 samples collected throughout the White River area. Values listed in brackets are background concentrations of elements in granite, from Rose and others (1979).

Table 7

			RANGE OF ANOMALOUS VALUES		
	Mean	Range	low	medium	high
Gold (2.3 ppb)	18	0.0 - 476	20-49	50-100	100
Silver (0.04 ppm)	0.91	0.0 - 13.7	0.1-0.49	0.5-1.0	1.0
Mercury (0.04 ppm)	0.53	0.005 - 11	0.01-0.49	0.5-1.0	1.0
Molybdenum (1.3 ppm)	10	0.0 - 210	1-10	11-20	20
Arsenic (2.1 ppm)	154	0.0 - 1,900	5-99	100-200	200
Antimony (0.2 ppm)	0.95	0.0 - 213	1-5	6-10	10

Background values for the Western Cascade Mountains of Oregon and Southern Washington (unpublished data from C.W. Field and S.G. Power, 1986).

Gold	2-4 ppb
Silver	0.3-0.5 ppm
Molybdenum	1-3 ppm

identified by a characteristic mineral assemblage that was deposited during or closely following individual structural events. Other less obvious structural episodes undoubtedly have also taken place within and around the area.

The first major event of structural-hydrothermal activity subsequent to formation of the silica capping created widespread and locally numerous fractures throughout the Primary Target area. Hydrothermal fluids migrated along these fractures and deposited veins and veinlets of milky quartz in an anastomosing stockwork pattern. The stockwork veins crop out locally in zones, but do not display a readily apparent large scale structural trend. The presence of numerous fault and explosion breccias record a second major structural event. The clasts within these matrix-supported breccias consist of silicified volcanics, fragments of milky quartz veins up to a few inches in diameter, and volcanics veined by the milky quartz. The brecciation is present in an extensive east-west trending zone, within which several of the individual breccia pipes and conduits strike N10°E - N10°W. These mineralized breccias are abundant on the south side of a west-trending ridge of silica (see Fig. 39), but rarely crop out due to their less resistant nature. Erosion of the breccia zones has resulted in the formation of a west-trending silica cliff face notched periodically by north trending and topographically subdued lows, now largely filled by colluvium. The third episode of structural activity created a fracture system that strikes predominantly N20 - 25°E. Many of these fractures are 0.25 - 6 inches in width and are presently filled with limonite and jarosite. A large

number of the fractures may have contained pyrite, prior to oxidation and supergene leaching, as is corroborated by several locally unoxidized pyrite-rich veins that also strike in the same direction. Most of the pyrite-bearing veins are small, but at least one is several feet in width. The final episode of fault activity noted in the Primary Target is post-mineralization in age. One of these late-stage structures cuts across the west part of the silica ridge in a N10 - 15°E direction (see Plate 1B). This is a high angle normal fault with the west side down-dropped. Although this structure is inferred to be post-mineralization in age, both adits of the White River prospect were driven along its strike. Post-mineralization high angle and west-trending normal faults also cut the south slope of the silica ridge, and downdrop the southern blocks (see Plate 1B).

The four episodes of fault displacement listed above were part of a continuum of local structural-hydrothermal activity which took place throughout the life of the hot-spring system in the West area. Such long-term, periodic, and contemporaneous structural and hydrothermal activity is common to large hot-spring systems and their contemporary geothermal counterparts. They are indicators of a dynamic and long-lived hydrothermal system, which is one of the primary criteria essential to the formation of hot-spring gold deposits.

Metallization

The Primary Target area is best delineated by surface samples containing moderate to high values of gold, arsenic, and antimony.

These anomalous values become progressively larger within the Gold Zone. Out of 24 rock chip samples collected within the Gold Zone 23 contain $\geq$ 20 ppb gold and ranged up to 480 ppb Au. Of these 23 gold-bearing samples, 9 contain $\geq$ 100 ppb Au, 6 range from 50 - 99 ppb Au, and 8 have <50 ppb Au. A few samples of moss were also collected and analyzed for precious metal content. These contain up to 510 ppb gold and up to 28 ppm silver. However, a small follow-up program gave highly erratic and generally nonreproducible results. In contrast, the geochemical assays of rock chip samples were extremely reproducible, even when different analytical laboratories and different analytical methods (fire assay vs atomic absorption) were used. Gold anomalies within the Primary Target are not totally confined to the Gold Zone. Three samples collected from a breccia zone of moderate size, about 800 feet to the northeast, contain up to 75 ppb Au, 160 ppm As, 3.5 ppm Hg, and 48 ppm Sb. The main adit of the White River gold prospect is approximately 300 feet south of the Gold Zone, and about 250 feet lower in altitude. Concentrations of up to 206 ppb Au were detected in outcrops at the portal of the main adit and in float nearby. Samples from the Primary Target contain anomalously high values for several elements and include up to 1,900 ppm As, 213 ppm Sb, and 7.5 ppm Hg, not uncommonly with concentrations ranging from 100 - 500 pm As and 10 - 40 ppm Sb, but <100 ppb Hg. Molybdenum values within the Primary Target are generally low and range up to 10 ppm. However, sporadic high concentations are present elsewhere throughout the West area, i.e. sample WR-164 contains 210 ppm molybdenum and 1,500 ppm arsenic in a hematite-cemented silica

breccia. Distribution patterns of Au, Ag, As, Sb, Hg, and Mo and their interrelationships are covered in detail in the chapter on Statistical Analyses of Geochemical Data.

Mineralization within the White River fossil hot-spring system was primarily introduced after formation of the silica capping. Abundant disseminated pyrite (up to 20 percent by volume) is present throughout most of the silica capping in the West area, especially where near-surface oxidation and supergene leaching has been minor.

The first significant introduction of precious metals took place with formation of the milky quartz veins. Examination of host rocks in the Primary Target area provides evidence of a true stockwork event of vein formation whereby veins of milky quartz cut and locally envelop silicified volcanics as shown in Figure 40A. Ten samples of milky vein quartz were collected specifically to test their precious metal, base metal, and other trace element content within the Primary Target. Of these samples, two contain 90 and 130 ppb gold and the other eight have values between 15 and 50 ppb gold. The abundance of Au, Ag, As, Hg, and Mo in veins of milky quartz are consistently lower than values generally present in samples from zones of breccia, often only a few tens of feet away. However, higher gold contents are known to be present within milky quartz veins. Sample WR-15 contains 480 ppb gold in milky vein quartz that cuts silicified volcanics as is shown in Figure 40A. This initial event of metallization, accompanying the formation of vein stockworks of milky quartz, added only moderately to the overall surface metallization of the hot-spring system, primarily introducing gold and antimony. An increased gold

Figure 40. Specimens of gold-bearing veins and breccias from the Primary Target area.
A). Stockwork of milky quartz veins(q) cutting silicified volcanics (v). This sample, collected from the Gold Zone, contains geochemical anomalies of 480 ppb Au and 9 ppm Mo.
B). Explosion breccia exhibiting multiple hydrothermal events. The clasts are silicified volcanics (v) veined by white milky quartz (q) with abundant clasts of milky quartz. The matrix consists of silica, microball-bearing hematite, and silicified rock flour, and contains 180 ppb Au, 482 ppm As, and 213 ppm Sb.

A

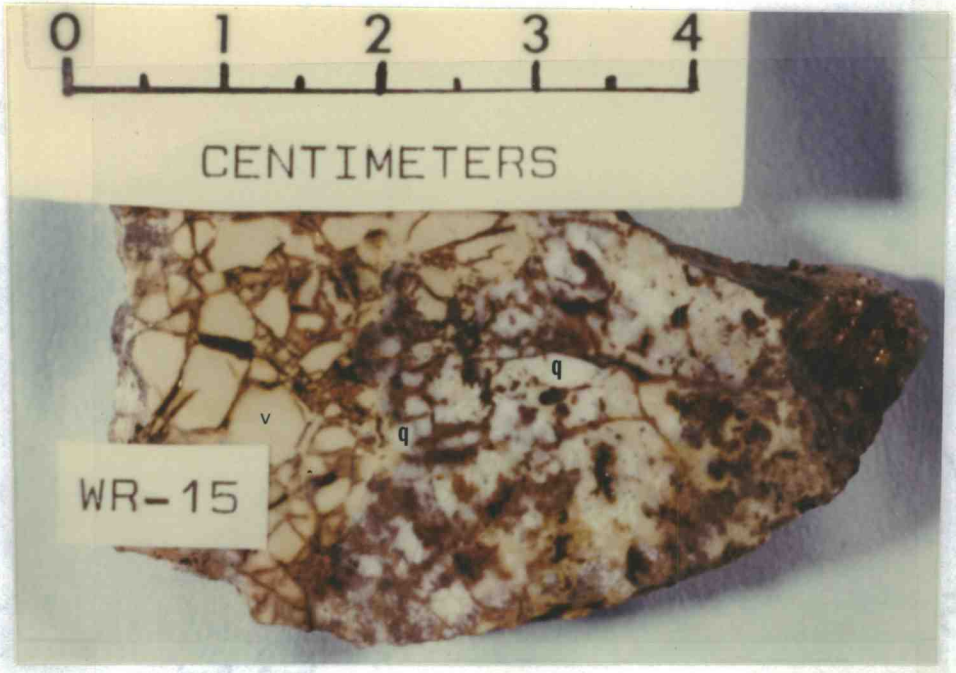

B

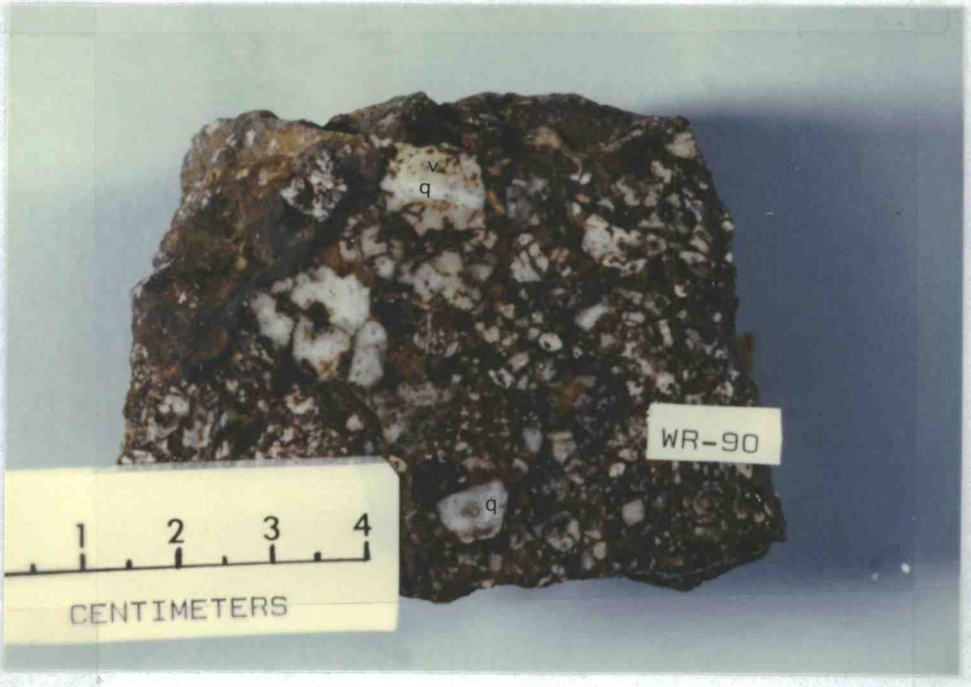

Figure 40

content may be be present in these veins at depth, within or directly below the silica capping.

A second event of gold metallization took place after formation of the milky quartz veins. Evidence for this second event is provided by the presence of matrix-supported breccias in pipes and linear conduits that crop out in abundance on the south cliff face of the Gold Zone, and numerous other locations within the silica capping. Many of these breccias are interpreted as having formed explosively from an overpressured hydrothermal system, and were emplaced selectively along a pre-existing pattern of structural weakness (N10°E - N10°W). Clasts within the breccia pipes are a mixture of fragments of milky quartz veins and silicified volcanics cut by various amounts of milky quartz veins as shown in Figure 40B. Clasts of veins of milky quartz within the breccia pipes document the relative timing of these two metallization events. Matrix material commonly forms 30 - 70 percent by volume of the breccias, and is composed of silica, comminuted fragments of volcanics and vein quartz, abundant microball-bearing hematite, and rock flour. Explosion breccias contain up to 206 ppb Au, 1,200 ppm As, 213 ppm Sb, 3.5 ppm Hg, and 210 Mo, and more importantly, consistently exhibit high values for gold, arsenic, and antimony throughout the Gold Zone. The principal episode of gold deposition in the surface and near-surface environment of the Primary Target appears to have taken place contemporaneously with, or initiated by, the formation of explosion breccia pipes and other conduits. These breccia zones constitute the major exploration targets for gold within the White River area. A diagrammatic cross

section of the Gold Zone, including the mineralized breccia pipes and their possible subsurface continuation into a gold-bearing stockwork vein system at depth is shown in Figure 41, with section A-A' plotted on Figure 39 for reference.

A third event of mineralization in the Primary Target consists of numerous post-breccia veins and veinlets that contain pyrite, chalcedony, and quartz. These veins strike predominantly N20 - 25°E and crop out in abundance on the south cliff face of the silica ridge (see Fig. 39). Oxidation and supergene leaching have removed much of the near-surface pyrite from many of these veins and have left a residue of iron hydroxides (limonite). The veins at several localities exhibit a poorly developed stockwork morphology and contain moderate to high concentrations of As, Sb, Hg, and Mo, but little gold. These pyrite-bearing veins are generally 0.25 - 2 in. in width, but they may range up to at least 3 - 6 feet in width, as at sample location WR-45. There is little direct evidence to indicate the timing of emplacement of the pyrite veins, although they are probably post-main stage gold metallization in age. Only minor amounts of gold were brought to the near-surface environment during this episode of vein formation, but several samples contain significant anomalies of other trace elements, including: 1 ppm Hg in sample WR-45; 1,900 ppm As and 20 ppb Au in sample WR-151; and 7.5 ppm Hg and 25 ppb Au in sample WR-184. Chemical conditions of the hydrothermal fluids were clearly within the stability field of pyrite during this third mineralizing event.

A complex pattern of surface precious and base metal anomalies

Figure 41. Diagrammatic sketch of the surface and possible subsurface alteration and metallization within the Gold Zone. The line of the cross section (A - A') is located on Figure 39 and the approximate vertical dimension is about 500 feet.

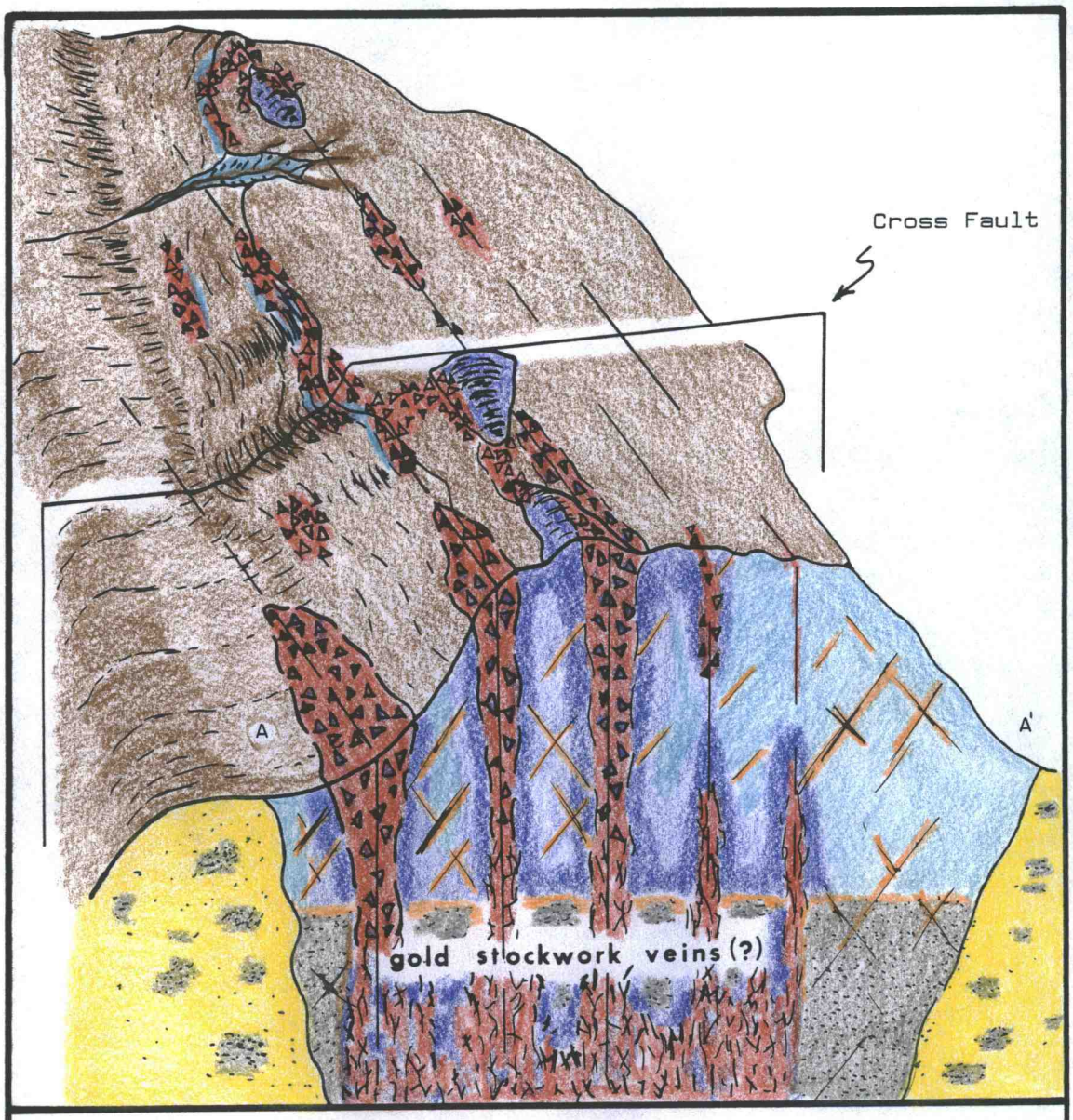

Limonite ± pyrite in veins or fractures

Pyrite

Mineralization (hematite ± gold and anomalous As & Sb)

Brecciation

Stockwork Veins

Faults

Colluvium

Silica Cap, sucrosic/massive

Argillic Alteration

Figure 41

resulted has from the three metallization episodes described above. Other structural-hydrothermal episodes, in part contemporaneous with metalllization events, formed nonmineralized zones of breccia and veins. Precious metals were introduced into the near-surface environment of the Gold Zone in at least one major episode represented by explosion breccias, and two minor episodes represented by veins of milky quartz and veins of pyrite. Mineralized breccia pipes are believed to extend downward into a zone of stockwork veins containing higher concentrations of gold, as illustrated in Figure 41. Miners probably encountered some of this deeper and higher grade gold mineralization during the late 1890's while driving the White River adits. As noted previously, Washington State DGER personnel sampled these adits and reported the presence of up to 0.07 oz gold/ton (Moen and Huntting, 1975). The dump from the upper adit, as shown in Figure 42, is composed of both pyrite-bearing host rock and hematite-cemented siliceous breccias. Part of this dump was removed during construction of U.S. Highway 410 and the portal of the upper adit is caved. The inside of part of the lower adit is shown in Figure 42B. The portal of this adit can be entered, but the working is caved 50 feet from the entrance and no attempt was made to dig through it. Three rock chip samples were collected from the portal face and nearby float of the lower adit, and they contain values of 68, 170, and 206 ppb gold. The dump is composed primarily of sand-size tailings processed by crushing, which is consistent with the former presence of a stamp mill reported by Huntting (1955). This lower adit was diven into a mudflow member of the Fifes Peak Formation that has been pervasively altered

Figure 42. The White River gold prospect consisting of two adits driven in the 1890's (secs. 1 and 12, T19N, R7E).
A). View of the dump from the upper adit (see Figure 39 for location). The portal is caved and part of the dump has been removed during construction of U.S. Highway 410.
B). View from inside the lower adit. A serious blockage is present 50 feet in from the portal. Three samples collected here contain 68, 170, and 206 ppb gold.

A

B

Figure 42

to clays. Kaolinite and pyrite-bearing shears, fractures, and veins cut the mudflow deposit, but gold ore suitable for processing with a stamp mill is not present within the first 50 feet of the portal. Presumably the miners were attempting to intersect high-grade gold ore in veins that may be pesent below the silica capping. Float near the portal indicates that the lower adit extended through the argillically altered mudflow and into hematite-cemented breccias within the silica capping or its root zones.

Geochemistry of Metallization

Knowledge of the chemistry of hydrothermal fluids and the effects of rapid physical and chemical changes on the solubility and transportation of gold is paramount to understanding the genesis of epithermal gold deposits. Several geochemists have combined experimental research on the solubility of gold with thermodynamic studies to achieve this objective (Smith, 1943; Helgeson and Garrels, 1968; and Seward, 1973, among many others). Results from these efforts show that gold is transported primarily as aurous- or auric-chloride and sulfide complexes in hydrothermal solutions, and also may form important, but probably geologically less significant, soluble complexes with I, B, As, Sb, and several other elements.

Research by Helgeson and Garrels (1968) has indicated that gold is highly soluble in chloride-rich solutions at temperatures exceeding 300°C, and that it is probably transported as gold-chloride complexes in hydrothermal fluids that have a high fO2 and a low pH. Conversely,

the precipitation of gold takes place under conditions that tend to destabilize the soluble gold complexes such as with decreasing fluid temperatures and fO2 or increasing pH. These changes might take place as a result of reactions with country rock, boiling, and (or) mixing with cooler and more dilute ground waters. Illustrative of this effect is the formation of alunite from the interaction of acid hydrothermal fluids with aluminum silicate minerals in volcanic host rocks, as indicated by the following reactions.

K-spar → Alunite (2)

$$3KAlSi_3O_8 + 6H^+ + 2SO_4^= \rightleftharpoons KAl_3(SO_4)_2(OH)_6 + 2K^+ + 9SiO_2$$

Albite → Alunite (3)

$$3NaAlSi_3O_8 + 6H^+ + 2SO_4^= + K^+ \rightleftharpoons KAl_3(SO_4)_2(OH)_6 + 3Na^+ + 9SiO_2$$

Muscovite → Alunite (4)

$$KAl_3Si_3O_{10}(OH)_2 + 4H^+ + 2SO_4^= \rightleftharpoons KAl_3(SO_4)_2(OH)_6 + 3SiO_2$$

Kaolinite → Alunite (5)

$$3Al_2Si_2O_5(OH)_4 + 2K^+ + 6H^+ + 4SO_4^= \rightleftharpoons KAl_3(SO_4)_2(OH)_6 + 6SiO_2 + 3H_2O$$

The source of both hydrogen and sulfate ions might be from the oxidation of H2S as given by the following reaction.

$$2H_2S + 4O_2 \rightleftharpoons 3H^+ + HSO_4^- + SO_4^= \quad (6)$$

Hydrogen ions are consumed and the fO2 of hydrothermal solutions is decreased during the process of forming alunite from feldspars, muscovite, or kaolinite, and both of these changes in fluid chemistry serve to destabilize the gold-chloride complexes and thus cause deposition of gold (Helgeson and Garrels, 1968). In this example the rates of fluid flow and hydrogen-ion consumption by wallrock are important in determining the amount and locales of gold deposition. Preferred sites of gold deposition are dilatent zones (i.e. breccia pipes and fractures) where reactions between acid hydrothermal fluids and fresh andesite and rhyolite wallrocks include a high rate of hydrogen-ion metasomatism and reduction of fO2 during formation of the alteration minerals.

At temperatures below 300°C the importance of sulfide complexes as transporting agents of gold generally predominate over gold-chloride complexes in hydrothermal fluids (Seward, 1973). Geochemists and exploration geologists largely agree that gold ions under the proper conditions are highly soluble in sodium-bisulfide complexes. Moreover, these complexes are stable at low to moderate temperature (150 - 350°C) in dilute aqueous fluids at or near neutral pH and moderate ionic concentrations such as characterize hydrothermal fluids of the epithermal type. The paper by F. Gordon Smith (1943) entitled "The Alkali Sulfide Theory of Gold Deposition" contains most of the geochemical principles upon which the modern theory of gold transport in hydrothermal solutions is based, and includes the following relevant considerations.

1. Both chloride and sulfide species are important gold complexing

agents, the former being most important in acid solutions and the latter in neutral to alkaline solutions.

2. Gold is readily soluble in alkali- (sodium or potassium) bisulfide solutions up to at least 300°C.

3. Gold-alkali-bisulfide complexes will remain relatively stable until the chemical system is perturbed by: (a) the loss of sulfide ions from hydrothermal fluids during pyritization of iron-bearing minerals in the country rock; (b) oxidation of sulfide ions to sulfate and concurrent alunitization of aluminum-bearing minerals within the wallrock; (c) volatilization and subsequent loss of H_2S from the hydrothermal fluids; (d) dilution of ascending fluids by an influx of near-surface groundwaters; and (e) temperature reduction.

4. There is a group of elements (gold, silver, arsenic, antimony, mercury, bismuth, and tellurium) that readily complex with, and are transported by, aqueous alkali-bisulfide solutions; the silver complex being important only at increased temperatures. These elements are much more soluble in alkali-bisulfide solutions than most of the base metals and this difference leads to the systematic zonation of metal deposition that commonly is observed in many epithermal gold deposits. and

5. The surficial representation of gold bearing systems is that of hot-springs associated with cooling intrusive activity, and which are often located in areas of young volcanism.

The fossil hot-spring systems present within the White River area are genetically related to intrusive activity near the margin of a resurgent caldera and bordering a structural dome. The possibility

that gold was transported as an alkali-bisulfide complex ((Na,K)Au(HS)2) in the White River hydrothermal system at low temperature is supported by the presence of large quantities of sulfur (as pyrite, alunite, and native sulfur) dispersed throughout host rocks of the Primary Target area. Evidence for the inferred low temperature (less than 300°C) of the hydrothermal fluids is derived from the presence of abundant finely crystalline silica as a product of alteration (silica capping) and vein (milky quartz) deposition, sulfur isotope temperature estimates, and the mineral assemblage alunite-pyrite-enargite ± gold and native sulfur. The stability fields of important minerals present in the White River hydrothermal system and that of gold-bisulfide and metallic gold are plotted on Figure 43 (modified from Kesler and others, 1981; and Lewis, 1982). The geochemical evolution of mineralizing hydrothermal solutions in the Primary Target area is depicted on Figure 43 as a path (1 - 4) that accounts for the presence of various mineral assemblages within the White River area, including: kaolinite-pyrite (at point 1); alunite-pyrite (2); alunite-hematite-gold (3); and hematite-gold (4). The change in chemistry of hydrothermal fluids, as given by the trend defined by points 1 - 4 is probably representative of explosive brecciation and (or) mixing with meteoric waters, which may have rapidly increased the concentration of atmospheric oxygen in the system. The presence of explosion breccia pipes and other conduits throughout the Primary Target area also implies a highly overpressured system and is indicative of widespread boiling. An increase in pH between points 3 and 4 might be the result of vigorous boiling of

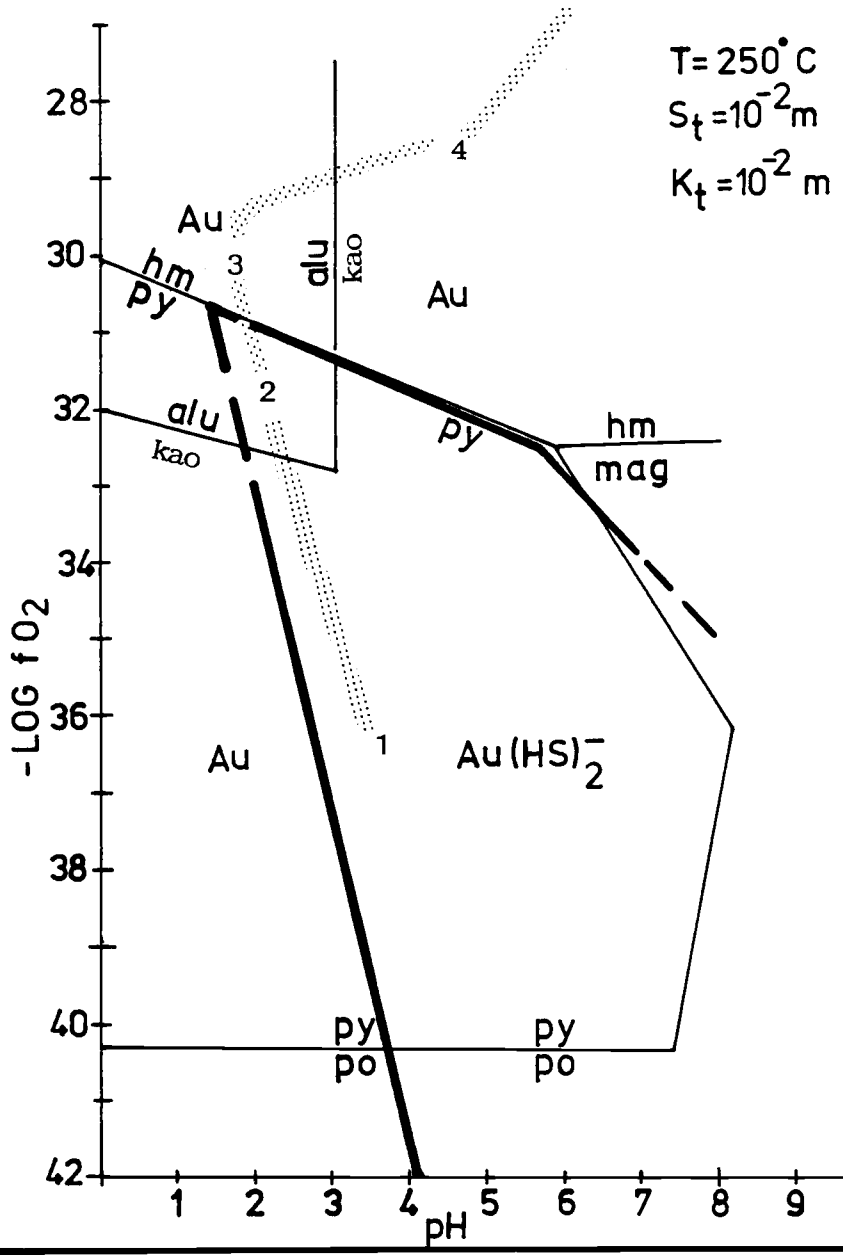

Figure 43. pH verses -Log fO2 diagram showing the stability relations of a gold-bisulfide complex and minerals relevant to the fossil hot-spring systems of the White River area. Possible path of the evolution of hydrothermal solutions (starting at 1 and ending at 4) during at least one episode of metallization within the Gold Zone. The symbols for the minerals are given in Figure 32. Modified after Kesler and others (1981); and Lewis (1982).

hydrothermal fluids with the concurrent partitioning of large quantities of CO2 and H2S into the vapor phase. The partitioning of H2S into a vapor phase would destablize gold-bisulfide, gold-arsenic-sulfide and gold-antimony-sulfide complexes, i.e. $Au(HS)_2^-$; $Au(AsS_2)^\circ$; $Au(AsS_3)^=$; and $Au(Sb_2S_4)^-$, being transported by hydrothermal solutions and cause the deposition of gold, arsenic, and antimony in close spatial proximity; as is a common pattern of their distribution within the Gold Zone.

Breccias

Several types of breccias are present in host rocks of the White River area. Those of the West area are fault breccias, explosion breccias, and intrusion breccias(?). They may be either clast-supported or matrix-supported and some breccias are mineralized. Photographs of a few examples are included to illustrate some of the textural variations of the breccias and also other rock types that may be mistaken for breccias. Both cut and uncut specimens of a matrix-supported explosion breccia are shown in Figure 44A. The light gray clasts are part of the original silica capping whereas the tan material is finely crystalline silica cement and silicified rock flour. The breccias in Figure 44A do not show any evidence of significant mineralization, but a gold-bearing matrix-supported explosion breccia, collected from the same general areas, was shown previously in Figure 40B. The lapilli rich portion of an ash-flow tuff in Figure 44B (sample RA6-2) can be mistaken for a breccia.

Figure 44. Specimens of various types of breccia collected from the Primary Target area.
A). Matrix-supported explosion breccia with gray to white clasts of the silica capping and a matrix of tan microcrystalline quartz and rock flour (S1/2, SE1/4, sec. 1, T19N, R7E).
B). Altered lapilli tuff (sample RA6-2) that is breccia-like in appearance, and silicified intrusion breccia (RA6-12) containing dark gray clasts composed of aggregates of smokey quartz crystals. These clasts were probably originally andesite volcanics prior to replacement.

A

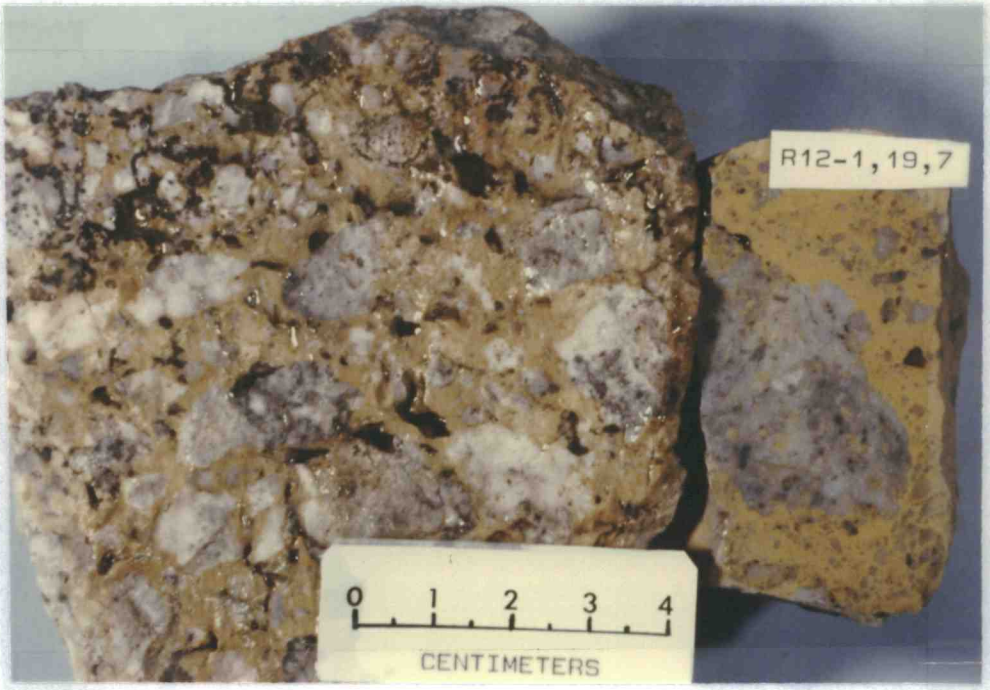
R12-1,19,7
0 1 2 3 4
CENTIMETERS

B

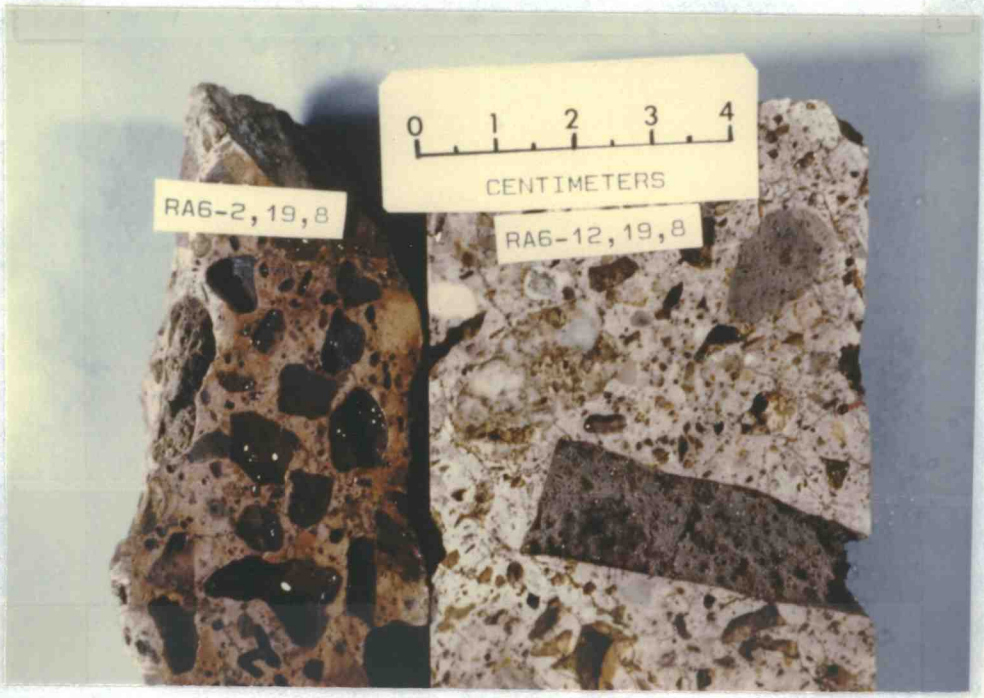
0 1 2 3 4
CENTIMETERS
RA6-2,19,8
RA6-12,19,8

Figure 44

However, voids in this specimen contained pumice prior to hydrothermal alteration, and the matrix is now composed of finely crystalline quartz. Sample RA6-12 (Fig. 44B) is interpreted to be an intrusion breccia. Most clasts are devoid of primary igneous textures because they have been completely replaced by quartz. The dark gray clasts are presumed to be fragments of andesitic volcanics that have been altered to an open framework of sucrosic quartz crystals and are surrounded by a matrix of microcrystalline quartz. Exposures of this intrusion breccia, either as bedrock or large masses of float, exhibit ovoid features up to 30 feet across, in a saddle 750 feet south of VABM Taugow (SW1/4, sec. 6, T19N, R8E). I interpret these rocks to represent intrusion breccias formed by the emplacement of small lobes of highly vesiculated felsic magma that incorporated numerous clasts of the adjacent country rock. The porous texture of these intrusions provided pathways for later hydrothermal fluids that imposed intense base leaching and silicification on the host. A second hypothesis for the origin of these breccias is that they are remnant blocks of vent-facies pyroclastics that have been silicified. A third, but less probable, hypothesis is that these breccias formed with tectonic movement along a west-trending fault that is present within 50 feet of the breccia outcrops.

An example of clast-supported fault breccia and associated veining is shown in Figure 45. This sample (WR-41) is of a limonite-stained clast-supported breccia from the NE1/4, SW1/4, sec. 31, T20N, R8E. It represents a fault breccia formed in tuffaceous country rocks that have been altered to clays, quartz, and alunite.

Figure 45. Specimen WR-41 is a clast-supported fault breccia (NE1/4, SE1/4, sec. 31, T20N, R8E), and WR-136 is part of an extensive area of fault related veining in a felsic tuff and grades upward into breccias such as WR-41 (NE1/4, SE1/4, sec. 31, T20N, R8E).

This sample contains 1.7 ppm Hg and is illustrative of the mobility of mercury as a gas phase and its apparent capacity to concentrate in breccia zones, above the water table. The clast supported breccias (represented by WR-41) may grade downward into veins that formed below the water table and are similar in appearance to the vein fillings in sample WR-136, collected about 500 feet northwest and 250 feet lower than sample WR-41.

Most of the breccia pipes within the Gold Zone are cemented by silica and hematite, indicating they represent channelways through which hydrothermal fluids passed. Some of these fluids transported precious metals and other elements such as arsenic and antimony to the near-surface environment. Only matrix-supported breccias of the type shown in Figure 40B are known to contain high gold values in outcrops of the West area. However, several other hematite-cemented zones of breccia and vein stockworks that are within and proximal to the Primary Target area contain moderate to high concentrations of As, Sb, Hg, and Mo. All of the matrix-supported hematite-bearing breccia zones within the West area that contain Au and Ag and (or) high concentrations of As, Sb, Hg, and Mo represent potential targets that should be evaluated by drilling for their precious metal content at depth.

East Area

The discovery of a second large fossil hot-spring gold target, measuring about 2 by 2.5 miles in size, resulted from geologic mapping

and geochemical sampling south of the White River. Although this target is spatially distinct from the West area, the type of hydrothermal alteration and metallization contained within both areas is similar. The location of the East area, and major zones of silicification cropping out within it, are shown in Figures 28 and 46. Most of this area has been subjected to tree thinning and is largely impassable at present (see Fig. 2 and Plate 3A). For this reason geologic mapping and geochemical sampling were limited primarily to logging roads and a few trails.

Geology

A thick sequence of andesite flows and volcanic breccia with minor volumes of intercalated rhyolitic tuffs and carbonaceous sedimentary rocks of the Fifes Peak Formation, comprise most of the country rocks of the East area. To the south, these volcanics are overlain by extracaldera ash-flow tuffs and are locally cut by rhyolite plugs and dikes of the Clear West Peak complex. Faults, fractures, and shear zones are numerous within the East area and several recent landslides and slumps have taken place locally along the trace of these structures. A large crescent-shaped landslide scarp is present in sec. 10 and exposes abundant near-surface hydrothermal silicification and argillic alteration of the country rocks. The location of this landslide scarp is plotted on Figure 46 and an aerial view is shown in Figure 47A.

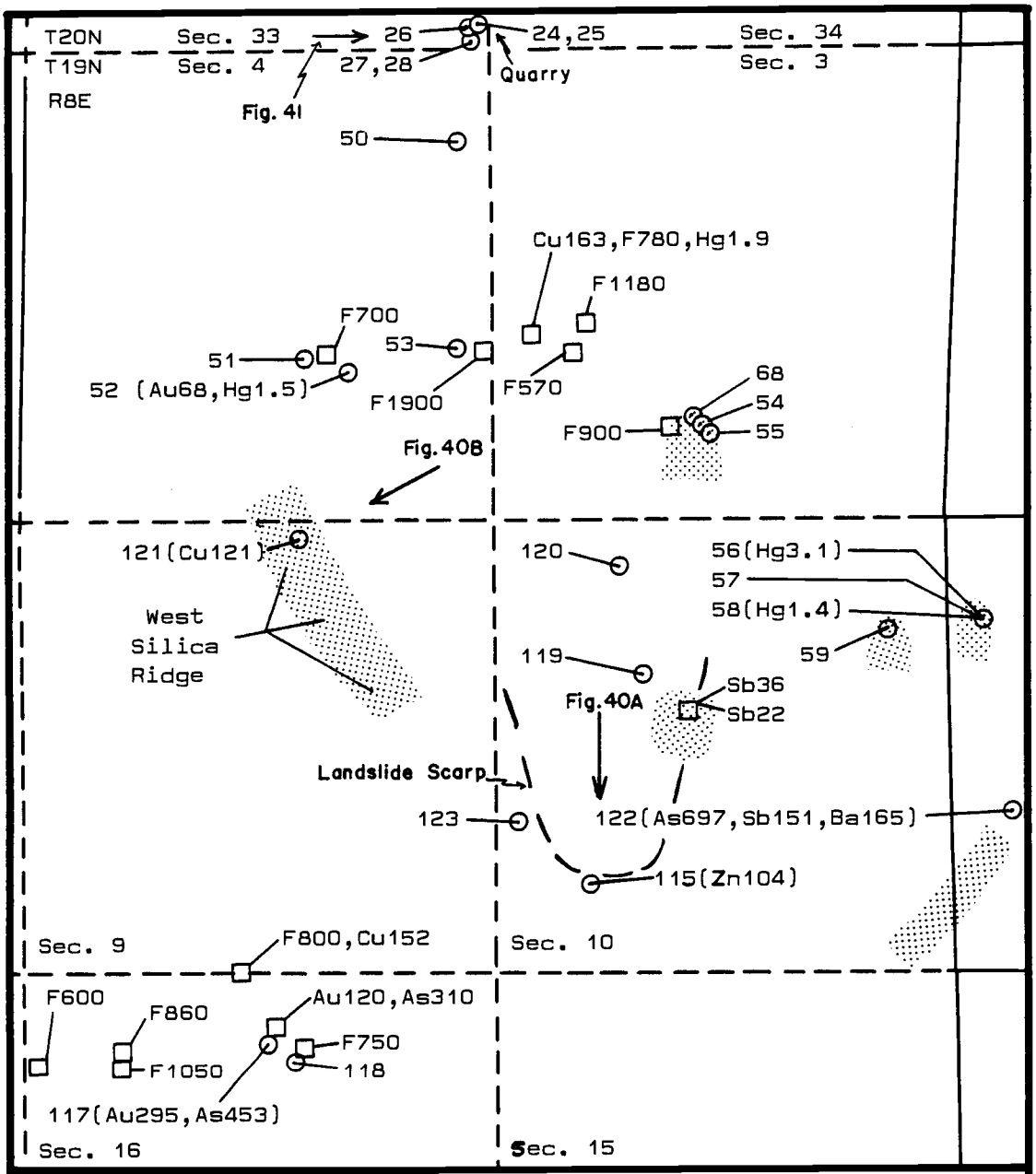

Figure 46. Location map of the East area.

Outcrops of massive silicification that are probably more extensive than represented here.

Geochemical samples with assay results that are reported in ppb for gold, and in ppm for all other elements. Geochemical data from previous studies are depicted by squares and those from the present study are represented by circles.

Figure 47. Aerial views of the East area with sample locations plotted.
A). View south of a major landslide scarp that is coincident with hydrothermal alteration (sec. 10, T19N, R8E).
B). View southwest of the West Silica Ridge showing outcrops of silica (s) that are up to 60 feet high.

A

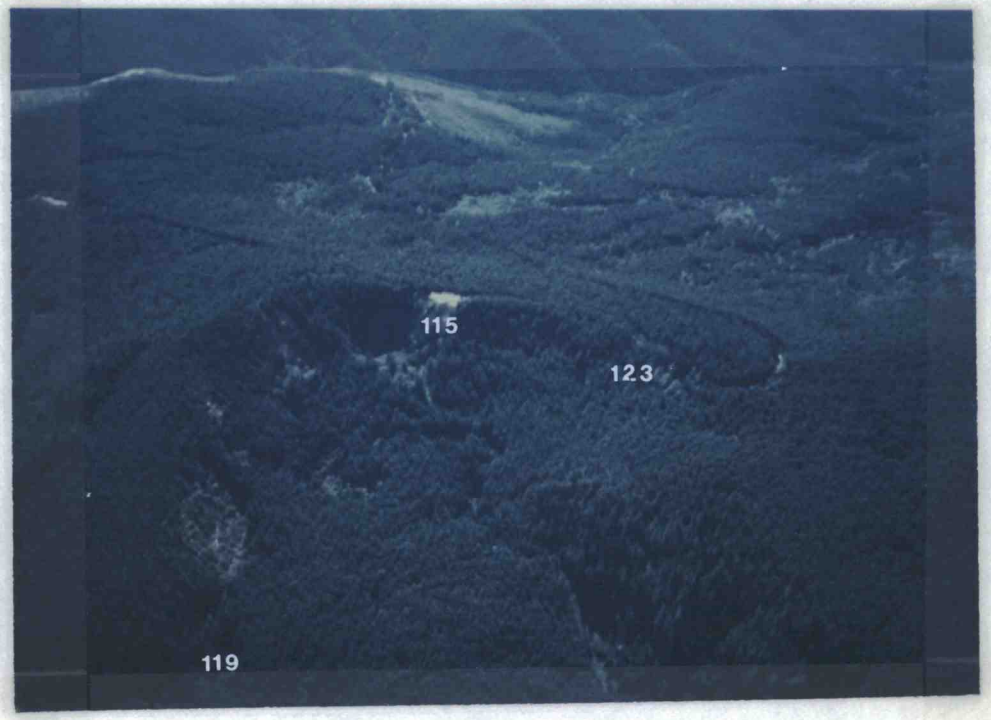

B

Figure 47

Alteration

The andesite volcanics within the East area have been progressively altered from propylitic, through argillic, to advanced argillic mineral assemblages that ultimately merge against central zones of massive silicification. Talc, in addition to the alteration minerals discussed in the section on the West area, is locally abundant in country rocks exposed by a fault scarp, in the SW1/4, sec. 10, T19N, R8E. Petrographic studies show that talc replaces phenocrysts of pyroxene in hydrothermally altered andesites, and is especially abundant along the margins of fractures and veins.

The abundance and distribution of argillic and advanced argillic alteration in this area is similar to that found in the West area. That is, alunite-kaolinite assemblages $\pm$ pyrite and quartz border zones of silicification and are also present as matrix minerals in breccias and as vein fillings. The presence of alunite is commonly accompanied by high concentrations of fluorine (in excess of 500 ppm). An assemblage of kaolinite-quartz $\pm$ pyrite is generally present adjacent to zones of alunite, and is locally abundant along faults.

Massive and pervasive replacement of andesites by silica is present in several outcrops throughout the area. Most of the western border of the landslide scarp shown in Figure 47A is composed of massive silica that crops out locally for over 100 feet in height and forms a prominent ridge. An aerial view of some silicified outcrops that comprise the northern part of this ridge is shown in Figure 47B. The pervasive silicification at the southern end of the landslide

scarp gives way to sporadic quartz veining ± talc, pyrite, and calcite in andesites. Although major zones of silicification are distributed throughout the East area, most appear to be limited in extent. The localization of the silica capping in this area, as in the West area, is controlled primarily by the distribution of rhyolitic host rocks. Had a larger rhyolitic unit been capping the East area at the time of intense hydrothermal activity, more extensive replacement by silica would undoubtedly have taken place. The massive silicification that is present exhibits a close spatial proximity to hydrothermal vents, unlike parts of the more flat lying silica capping in the West area. The types and distributions of alteration assemblages present within the East area are indicative of an epithermal acid-sulfate system. Moreover, the broad areal extent and distribution patterns of the zones of argillic and advanced argillic alteration are suggestive of a large hydrothermal system (approximately 1.5 miles in diameter) with many of its major vents now marked by outcrops of massive silica.

Metallization

A suite of precious and base metals with other trace elements is located in the East area that is similar in type and occurrence as those of the West area. The maximum geochemical anomalies detected for these elements include: 295 ppb Au; 6.8 ppm Ag; 697 ppm As; 151 ppm Sb; 165 ppm Ba; 3.1 ppm Hg; 1,900 ppm F; 25 ppm Mo; 163 ppm Cu; and 115 ppm Zn. All sample locations from the present study and significant geochemical anomalies from both the present and past

studies are plotted on Figure 46. The most anomalous sample from the East area (WR-117) contains 295 ppb gold, 453 ppm arsenic, and 13 ppm molybdenum and was collected from a pyrite-bearing quartz vein in a silicified and brecciated rhyolite intrusion. This vein was preferentially emplaced along a major fault that cuts the rhyolite plug and is exposed sporadically along the local stream drainage. Moreover, a sample collected prior to the present study (near WR-117) contained 120 ppb gold and 310 ppm arsenic (Weyerhaeuser Company reports). This sample was presumably taken from the same fault zone, and suggests the potential for additional structurally controlled gold mineralization along and adjacent to the fault. A gold-bearing vein is also present in the northern part of the East area. Here, sample WR-52, representing a quartz-pyrite vein hosted by an airfall tuff contains 68 ppb Au and 1.5 ppm Hg. The tuff is pervasively altered to an alunite-silica mineral assemblage and locally contains minor amounts of native sulfur. This sample location marks the approximate northern limit of intense hydrothermal alteration and metallization in the East area. This boundary is also geochemically defined by anomalously high values for mercury (up to 3.1 ppm) and fluorine (up to 1,900 ppm) from samples representing a zone that trends in a northwest-southeast direction. Elsewhere, anomalous values for base metals and (or) fluorine and mercury are present in veins and veinlets that are widely distributed throughout the area. Although only a few anomalous gold concentrations were located by the present sampling program, their occurrence in veins along the outer borders of the fossil hot-spring system indicates the potential for economically

significant mineralization within the central core of the system.

The apparent lack of outcrops and restricted access to the East area has greatly hindered mineral resource evaluation and geologic mapping of this terrane. Although it lacks extensive zones having consistently anomalous gold values, such as those found within the Primary Target area, their apparent absence may simply be a function of limited exposures. The wallrock alteration and metallization present within the East area indicate that the local hydrothermal system was geochemically similar to that of the West area. Whether or not these two areas were formed by geographically separate hydrothermal systems or by a single large one, is unclear. Regardless, similarities in their mineralogy, geochemistry, and close spatial proximity suggests a genetic tie to one main intrusion at depth. It is speculated that this intrusion is a shallowly emplaced, yet largely unexposed, stock or pluton having a composition similar to that of the Carbon River stock (granodiorite). A ring fracture system, visible from satellite imagery as seen in Figure 25, may be the structural expression of this unexposed intrusion. Through local apophyses, this intrusion may be the progenitor of rhyolitic domes(?) in the West area and rhyolite dikes and plugs in the East area, as well as of the subsequent hydrothermal activity (single or dual?) imposed on each.

STATISTICAL ANALYSES OF GEOCHEMICAL DATA

Statistical analyses of the geochemical data obtained for samples of the White River area were undertaken to better understand the distribution of precious metals and other trace elements, their interrelationships, and to help select pathfinder elements that might delineate the subsurface distribution of gold mineralization. The data set consists of 163 geochemical samples collected throughout the White River area, and with 76 of these samples from the West area. An additional 16 rock chip samples were collected and analyzed subsequent to the statistical analysis presented here. All samples were analyzed for gold, silver, arsenic, antimony, mercury, and molybdenum. The data from these analyses show that the West area in particular, exhibits an anomalous suite of hydrothermally introduced elements that could be indicative of subsurface gold mineralization.

Statistical methods applied to the White River data set consisted of basic statistics, R-mode factor analysis, and Q-mode factor analysis. The data set of 163 samples was divided into three groups. The first includes 17 samples collected from the Gold Zone (central zone) of the fossil hot-spring system. The second consists of 17 samples from an area extending 2,000 feet outward from the Gold Zone. The outer group contains 129 samples from the remainder of the White River area. Samples were not collected on a grid system and are geologically biased, with most being selected to test the precious metal content of various types of veins, vein-stockworks, breccias,

and assemblages of pyrite and hematite.

Basic Statistics

Mean concentrations of Au, Ag, As, Sb, Hg, and Mo are plotted on a logarithmic scale with respect to the central, middle, and outer zones of the White River area hydrothermal system in Figure 48. A diagrammatic sketch of this fossil hot-spring system is also shown. The plotted distributions of the geochemical data are symmetrically mirrored for simplicity of representation, and not because of identical values for these elements outward in all directions from the central zone.

The mean values, ranges, and standard deviations of the data are presented in Table 8 and the variances of the six elements for each of the three zones are listed in Table 9. An F-statistical analysis as listed in Table 10 has been applied to the data set to determine if the variances among these three zones are statistically different. Four elements (Au, Hg, Sb, and Mo) exhibit significant statistical differences in the variances between the central and outer zones. These results indicate a change in the intensity of mineralization outside the inner two zones, and to a lesser degree between the central and middle zones. The reason high variances are exhibited within individual areas is the presence of discrete accumulations of elements deposited in widely dispersed fractures or veinlets (the nugget effect). Random sampling of these areas generally indicates a wide variation in the geochemical abundances of the elements present,

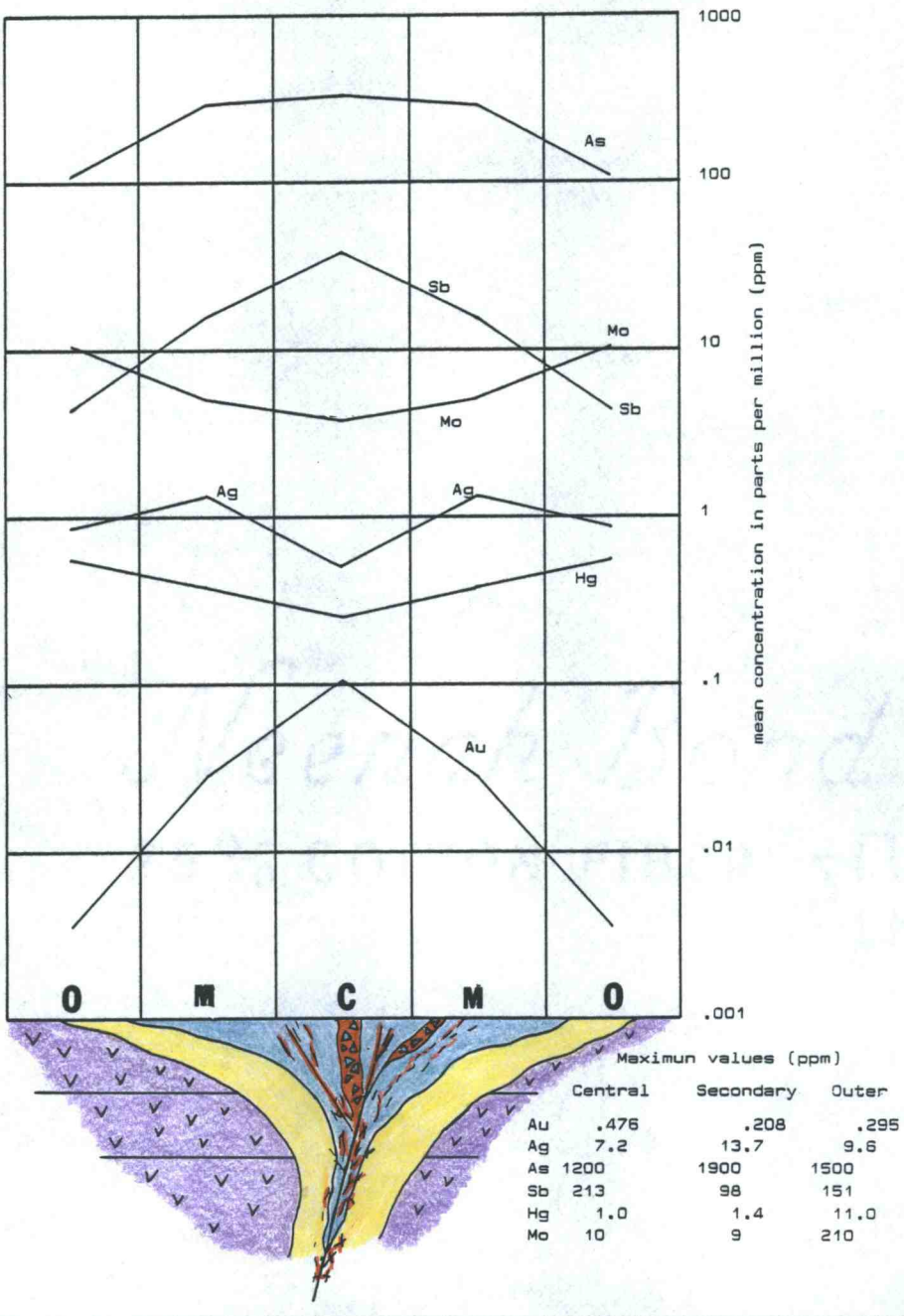

Figure 48. Mean concentrations of Au, Ag, As, Sb, Hg, and Mo versus the central (C), middle (M), and outer (O) zones of the fossil hot-spring system. At the bottom right are maximum geochemical abundances for each element in each zone.

Table 8. Mean values, standard deviations, and ranges of Au, Ag, Hg, Mo, As, and Sb of the White River data set (183 samples) for the central, middle, and outer zones.

Table 8

		Mean	Standard Deviation	Range
Central Zone	Au	0.116	0.118	0.0 - 0.476
	Ag	0.512	1.73	0.0 - 7.2
	Hg	0.253	0.31	0.005 - 1.0
	Mo	4	2.5	1 - 10
	As	342	347	34 - 1,200
	Sb	39	52	0 - 213
Middle Zone	Au	0.029	0.063	0 - 0.208
	Ag	1.47	3.4	0 - 13.7
	Hg	0.399	0.414	0.005 - 1.4
	Mo	5	2.8	1 - 9
	As	279	439	18 - 1,900
	Sb	17	26	0 - 98
Outer Zone	Au	0.004	0.028	0 - 0.295
	Ag	0.9	2.2	0 - 9.6
	Hg	0.50	1.27	0.005 - 11.0
	Mo	12	27	0 - 210
	As	114	195	- - 1,500
	Sb	5	17	0 - 151

Table 9. The variances of six elements in the central, middle, and outer zones with data sets of 17, 17, and 129 samples, respectively.

Table 9

ELEMENT	CENTRAL ZONE	SECONDARY ZONE	OUTER ZONE
Gold	0.0138	0.00398	0.00076
Silver	2.2986	11.42	4.817
Arsenic	$1.2X10^3$	$1.9X10^5$	$3.8X10^4$
Mercury	9.645	0.1716	1.616
Antimony	$2.7X10^3$	659	286
Molybdenum	6.360	7.809	717

Table 10. The F statistics of variances between the three geochemical zones. The data sets are the same as those in Table 9.

Table 10

F-Test

ELEMENT	CENTRAL VS SECONDARY		CENTRAL VS OUTER		SECONDARY VS OUTER	
		F(5%)		F(5%)		F(5%)
Gold	3.47	2.34	18.23	1.74	5.25	1.74
Silver	3.82	"	1.61	2.05	2.37	"
Arsenic	1.60	"	3.16	1.74	5.05	"
Mercury	1.78	"	16.75	2.05	9.42	2.06
Antimony	4.12	"	9.50	1.74	2.31	1.74
Molybdenum	1.23	"	112.66	2.05	91.75	2.06

i.e. high variances.

R-mode Factor Analysis

R-mode factor analysis is a statistical method of partitioning variables, which in this case is each of the six elements, into groups that contain or exhibit similar or related characteristics or behaviors. Each group of similar variables is represented in M-dimensional space as one of a set of orthonormal axes. This statistical technique commonly reduces the number of variables by combining those with similar characteristics (i.e. if Cu, Pb, and Zn all behaved geochemically similarly, then R-mode factor analysis would place them in a single group, defined by a single axis). The usefulness of R-mode factor analysis to the present study is not restricted to the grouping of variables. These groups represent spatially and temporally similar patterns of element dispersion and mineral deposition and provide a method whereby the potential importance of pathfinder elements may be evaluated. R-mode factor analysis is a useful method of defining the natural groupings of Au, Ag, As, Hg, Sb, and Mo in the White River area and provides a more effective way of understanding the interrelationships between these variables than does basic statistics. Histograms of the normalized results of R-mode factor analyses of the White River data set (163 samples) with one varimax rotation are shown in Figure 49. Three axes (factors) have been chosen to represent the six original geochemical variables and they show a distinct clustering of elements irrespective

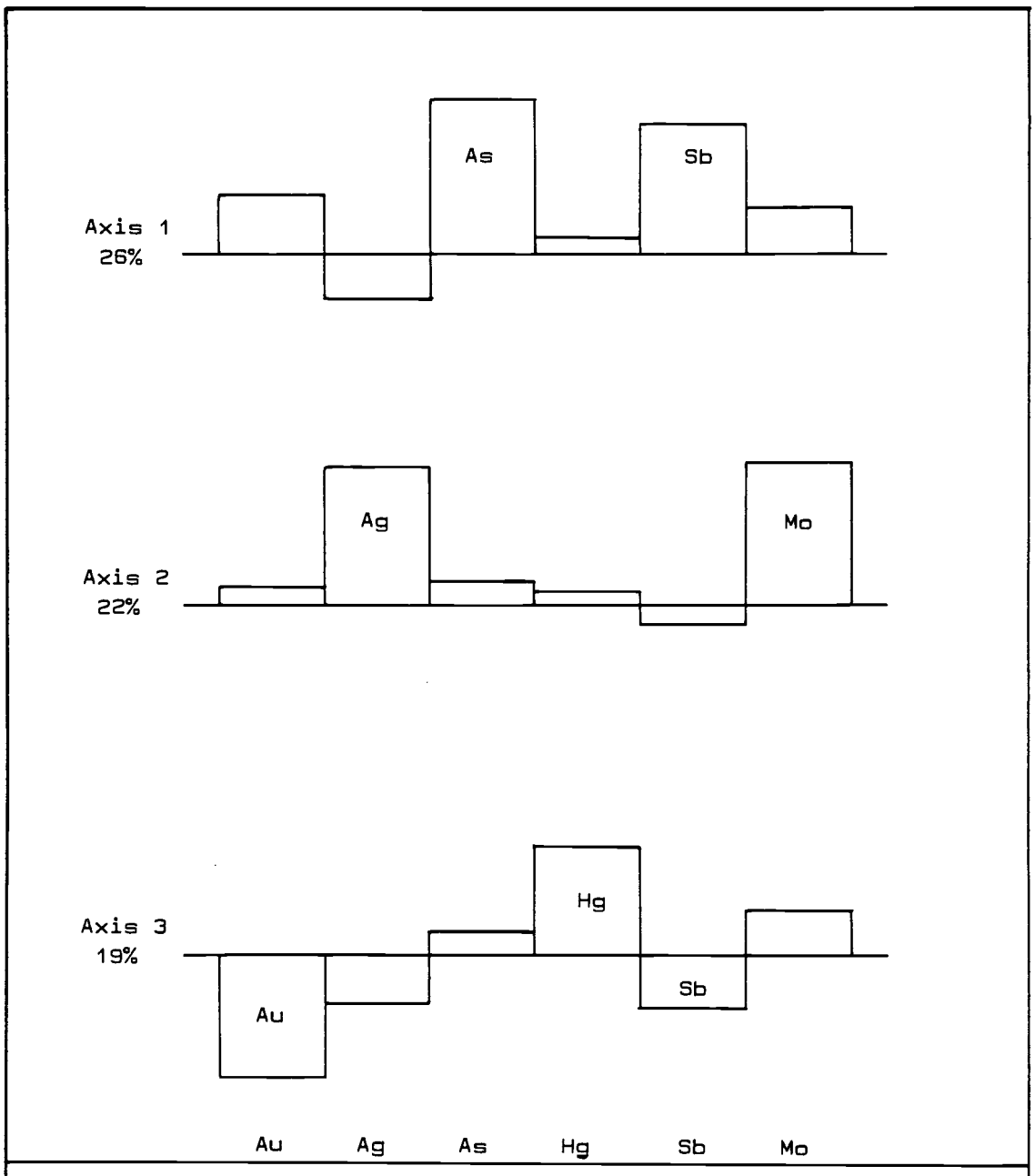

Figure 49. Histogram of unitized R-mode factor analyses of 163 samples. A distinct grouping of As-Sb and Ag-Mo and an antipathetic association of Au and Hg are implied.

of whether or not the raw geochemical data are subdivided into individual zones or analyzed collectively. The data illustrated depict covariant associations for As-Sb (axis 1, 26%) and Ag-Mo (axis 2, 22%) whereas an antipathetic association is implied for Au-Hg (axis 3, 19%). Also given is the percentage of data explained by each axis. A trigram representation of these trends is illustrated in Figure 50 and was constructed by plotting the same data used to construct the histograms on three orthonormal axes of positive and negative unit lengths. The trigram plot affords a better visual representation of the interrelationships between elements than do the histograms in Figure 49. Based solely on this trigram plot, elements that are associated with gold and could be used as pathfinders, should surface gold abundances be minor or below detection, are antimony and to a lesser extent arsenic. A trigram of the central and middle zones combined (34 samples) has groupings of elements similar to those of the entire data set (163 samples).

Q-mode Factor Analysis

Q-mode factor analyses compare the variables or traits of samples and then groups together the samples containing similar characteristics. This method of analysis was applied to the data set from the West area (76 samples) and compared element abundances of samples, and then grouped those with similar concentrations of Au, Ag, As, Sb, Hg, and Mo together. The results of these analyses indicate that samples containing gold may commonly host anomalously high

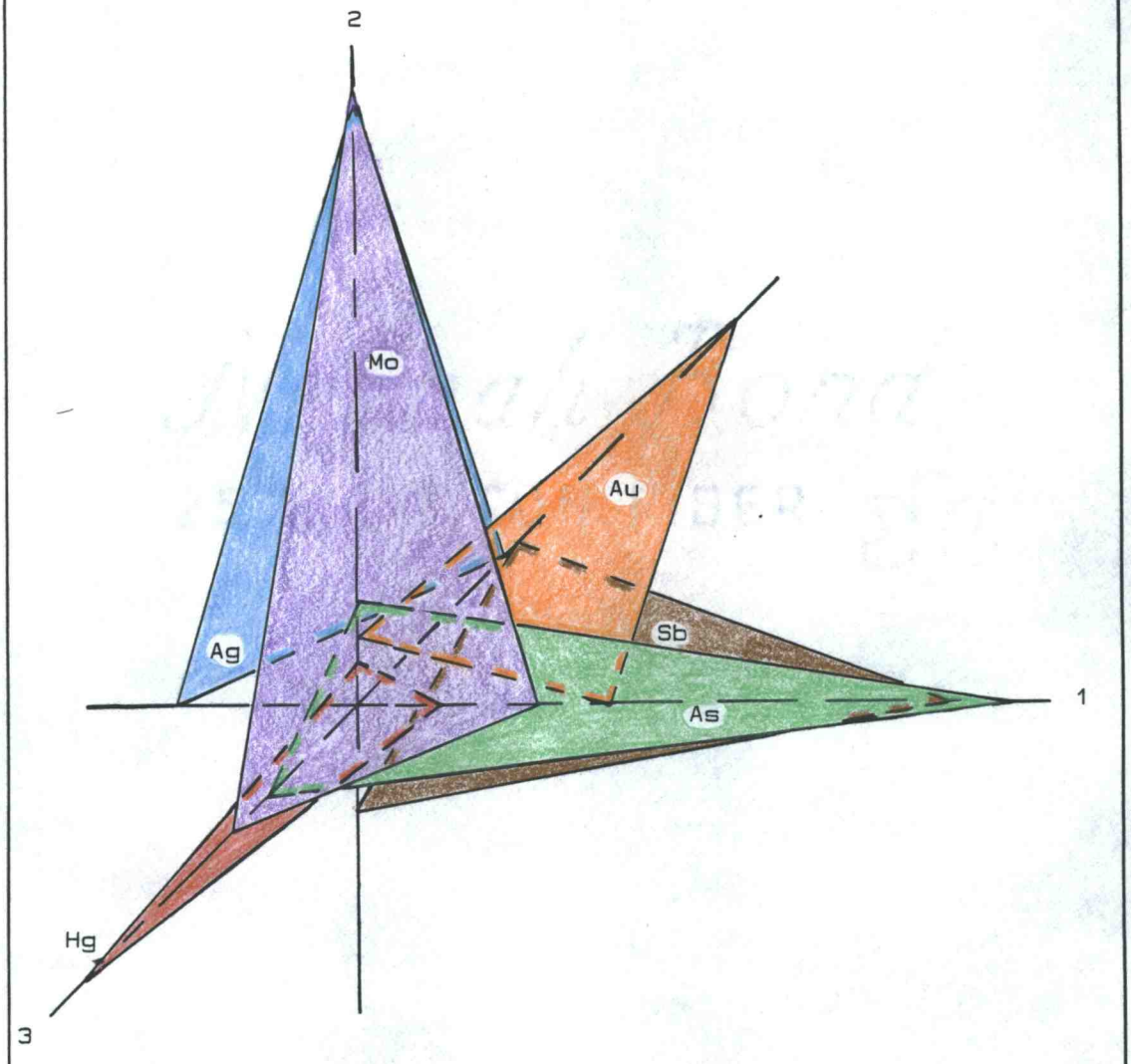

Figure 50. Trigram representation of the unitized results of R-mode factor analysis of 163 that illustrates the interrelationships between Au, Ag, As, Sb, Hg, and Mo.

concentrations of antimony. This positive interrelationship between gold and antimony, that has been determined independently by both R-mode and Q-mode factor analysis, was then used to group samples and plot the locations of areas that exhibit high potential for hosting gold and antimony mineralization as shown in Figure 51. A contour of the raw geochemical values of mercury is also plotted on this figure and areas of high concentrations of mercury are seen to border highs of gold and antimony. Although contour plots of the raw geochemical data indicate that surface occurrences of gold are mostly restricted to the Primary Target area (area 1 Fig. 51), both R-mode and Q-mode factor analyses imply the potential for a subsurface gold occurrence at another location (area 2, Fig. 51) in the West area (NW1/4, sec. 33, and the NE1/4, sec. 32, T20N, R8E). This inference is based on positive geochemical interrelationship between the values of gold and antimony, as well as for the close spatial relationship of anomalously high concentrations of mercury (see Fig. 51).

Basic statistics have provided useful information about geochemical zonations within and surrounding the fossil hot-spring system in the West area. However, the use of R-mode factor analysis has been indispensable in defining several interrelationships among Au, Ag, As, Sb, Hg, and Mo. Additional useful information was obtained from contoured plots of Q-mode and R-mode factor analyses, combined with the results of contoured plots of the raw geochemical data for mercury. These plots have led to the delineation of a previously unrecognized zone of potential subsurface gold mineralization in area 2. A summary diagram of the spatial

Figure 51. Plan map of the West area showing major alteration patterns. Computer generated contours of Au-Sb highs, as determined by R-mode and Q-mode factor analysis, and the 2 ppm contour for mercury are plotted.

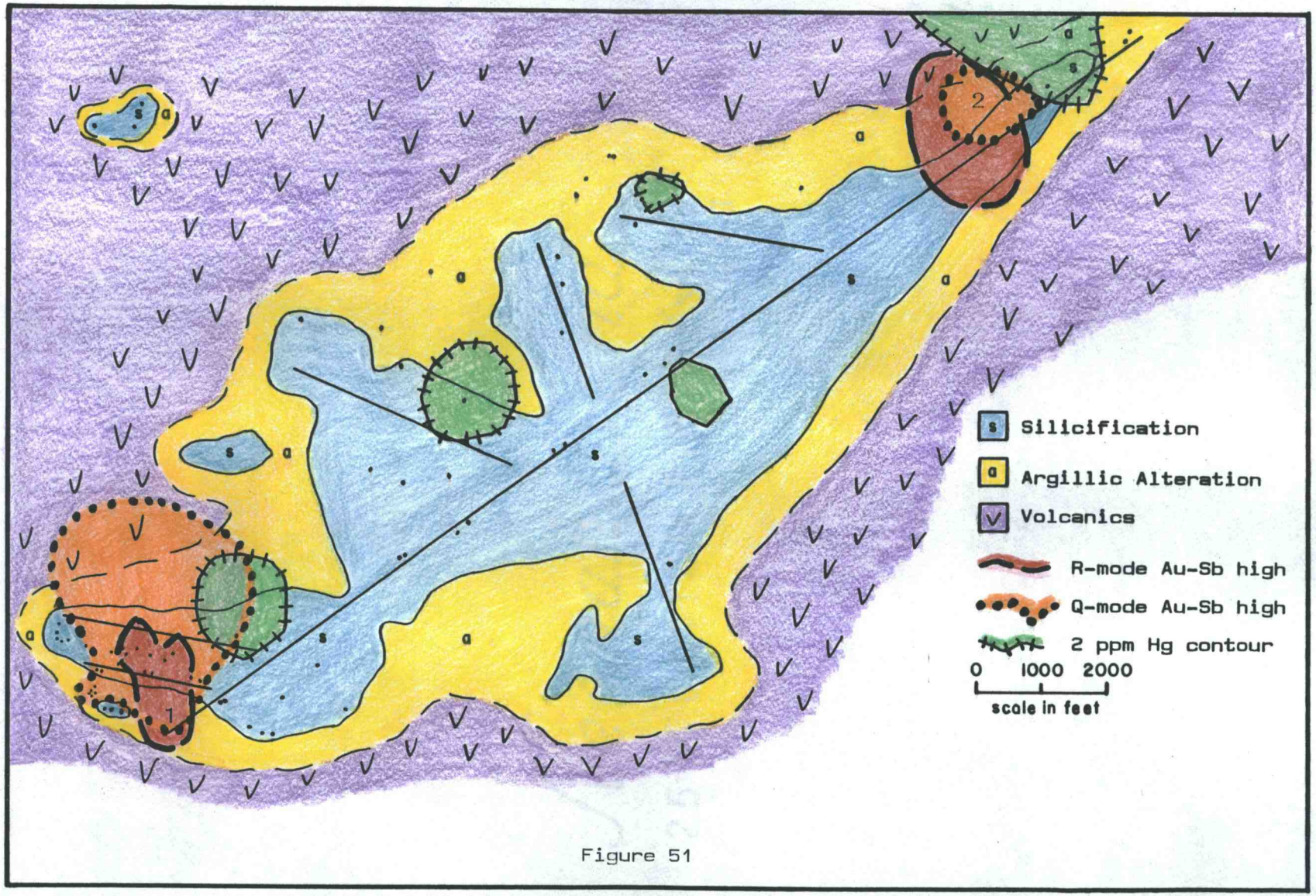
s
a
V
Silicification
Argillic Alteration
Volcanics
R-mode Au-Sb high
Q-mode Au-Sb high
2 ppm Hg contour
0 1000 2000
scale in feet
1
2

Figure 51

distributions of Au, Ag, As, Sb, Hg, and Mo and the alteration mineral assemblages present in the White River area are illustrated in Figure 52. These patterns of mineral and element distributions are based on data from samples derived from surface outcrops and the results of basic statistical analyses and combined with those of R-mode and Q-mode factor analyses.

Figure 52. Summary diagram of hypogene metallization and alteration patterns in the White River fossil hot-spring systems (presentation modified from Berger and Eimon, 1983).

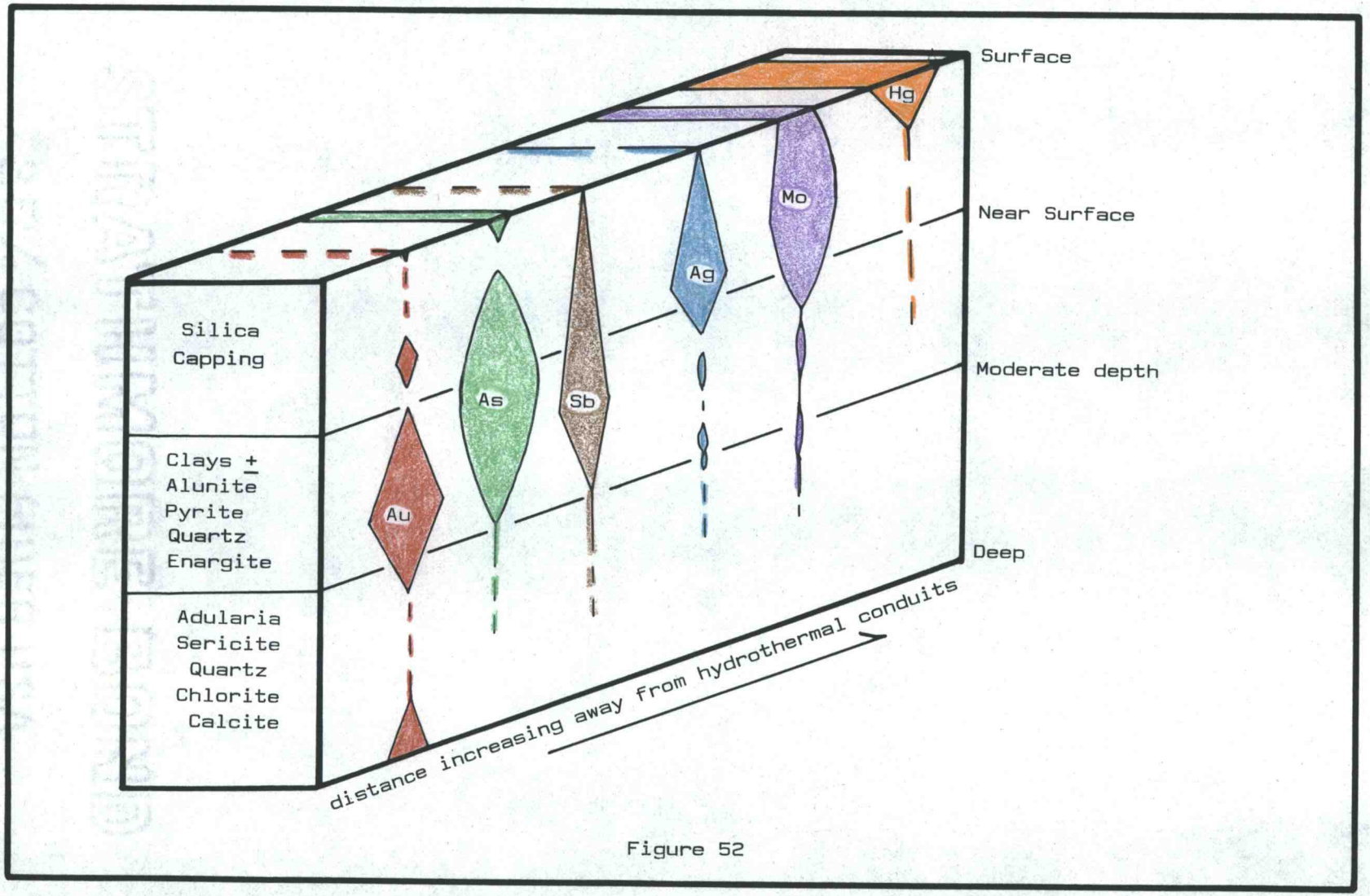
Surface
Near Surface
Moderate depth
Deep
Hg
Mo
Ag
As
Sb
Au
Silica
Capping
Clays ±
Alunite
Pyrite
Quartz
Enargite
Adularia
Sericite
Quartz
Chlorite
Calcite
distance increasing away from hydrothermal conduits

Figure 52

SUMMARY AND CONCLUSIONS

The Pacific Northwest region has been the site of several major Tertiary age geologic events that include: (a) interaction of the North American craton with the Yellowstone Hot Spot, which initiated intracontinental megashearing and a possible continental rifting event; (b) development of the two spatially separate and temporally distinct Challis and Cascade volcanic arcs; and (c) accretion of a large block of oceanic crust (the Willamette plate) to the continent and its clockwise rotation. The Cascade volcanic arc has been differentially uplifted and eroded, exposing numerous batholithic intrusions of intermediate composition in the central and northern Cascades of Washington. A few of these intrusions host porphyry copper-type mineralization and others host polymetallic base metal veins ± gold and silver. The volcanic cover of the Cascade arc to the south of this batholithic core is moderately well preserved in Washington. These volcanic rocks host ore deposits that formed under shallower and lower temperature conditions than the batholithic-hosted ore deposits to the north. The White River area is at the boundary of these metallogenic provinces, and mining districts around it contain both copper-gold veins hosted by intrusive stocks, and gold-silver veins ± base metals hosted by generally coeval volcanic country rocks.

The White River and Greenwater River valleys are both structurally controlled drainages formed by the White River and Twin Creek faults, and they represent the southern boundary of the

Olympic-Wallowa lineament. These faults border two large structural domes, each about 10 - 12 miles in diameter and each hosting precious and base metal mineralization. The westernmost of these domes is adjacent to the White River area and cuts across the Clear West Peak caldera and the Carbon River stock. All three geologic features are probably genetically related to the emplacement of a large subsurface pluton. Important structural preparation for the localization of hydrothermal fluids was provided by the White River fault and structures related to local intrusive activity.

A diverse group of industrial minerals, including abundant silica, alunite, high-alumina clays, and minor amounts of native sulfur is present within the White River area. Individually, these minerals could have several diverse origins, but collectively they represent a hydrothermal alteration assemblage commonly present in acid-sulfate type hot-spring systems. Surface mapping of the White River area has defined the West and East areas that contain massive silicification and extensive argillic and advanced argillic alteration over several square miles. The intensity and extent of this hydrothermal activity is best represented by outcrops of silica. In the West area, extremely intense and pervasive base leaching has removed nearly all major-element oxides except SiO2 and TiO2 from several hundreds of millions of tons of andesitic and rhyolitic country rock. The base leaching by acid hydrothermal solutions was probably aided by the presence of moderate to high concentrations of fluoride that promoted the dissolution and mobilization of alumina. The presence of alunite as a hypogene mineral is evident in veins and

breccias containing intergrown mineral assemblages of alunite and unoxidized sulfides, and its hypogene origin has been corroborated by sulfur isotope data. A sample containing the cogenetic mineral assemblage alunite-pyrite-enargite provided $\delta(34)S$ o/oo values of +26.2, -2.6, and -4.8 for these sulfate and sulfide phases, respectively. The large isotopic fractionation of +28.8 o/oo $(34)S$ between pyrite and alunite indicates a temperature of formation of about 190°C. This isotopic temperature estimate is consistent with field and mineralogic relationships observed for this hot-spring system and with the results for similar deposits elsewhere. However, hydrothermal solutions at higher temperature were probably present in other parts of this large hot-spring system, especially near major veins and areas that host abundant explosion breccias.

Two epithermal targets of potential gold mineralization were located within the White River basin as a result of this study and they are designated the West and East areas, respectively. Both areas manifest important features of alteration and metallization that are regarded to be characteristic of acid-sulfate type hot-spring gold deposits. The close spatial proximity to a Miocene caldera complex, as well as the presence(?) of an unexposed intrusion, and local faults associated with both events were paramount to the generation and localization of two surface-venting acid-sulfate type hydrothermal cells. One of these cells was focused on and along the East Clay Creek fault and its subsidiary faults and fractures, and these hydrothermal fluids caused extensive base leaching of local volcanic country rocks and deposited quartz, alunite, kaolinite and other

clays, pyrite, native sulfur, fluorite, enargite, hematite, and trace amounts of Au, Ag, As, Sb, Hg, Mo, and Ba. A schematic cross section of this pattern of alteration and metallization within the White River area is illustrated in Figure 53. At the center of alteration in the West area is a silica capping that extends for 3.5 miles in length, up to 1 mile in width, and contains siliceous root zones that extend downward along hydrothermal conduits for at least 400 feet. This capping is composed primarily of aggregates of microcrystalline quartz crystals (30 - 500 microns in size) that form outcrops of either porous silica-sponge or massive (dense) silica replacements. A zone of advanced argillic alteration (alunite and quartz $\pm$ kaolinite, pyrite, fluorite, enargite, and barite) extends outward and downward from the silicification. This zone grades into widespread argillic alteration (kaolinite with other clays, quartz, and pyrite) that in turn is surrounded by propylitic alteration (chlorite, epidote, calcite, and pyrite) and fresh volcanic country rocks. Quartz veins, explosion breccias, and pyrite-rich veins are present in several places within the hot-spring system of the West area and are abundant locally.

The Primary Target is a zone, measuring 2,800 by 3,800 feet, that exhibits the greatest potential for hosting significant quantities of precious metals, within the West area. Detectable gold (greater than 20 ppb) is present in several samples collected from an area of about 2,400 by 1,000 feet in surface dimensions, with higher gold values forming a distinctive central core (the Gold Zone) about 1,600 feet in length by 300 - 600 feet in width. From this area, herein called the

Figure 53. Diagramatic sketch of hypogene metallization and alteration patterns in the White River fossil hot-spring systems. Method of presentation is modified from Berger (1983).

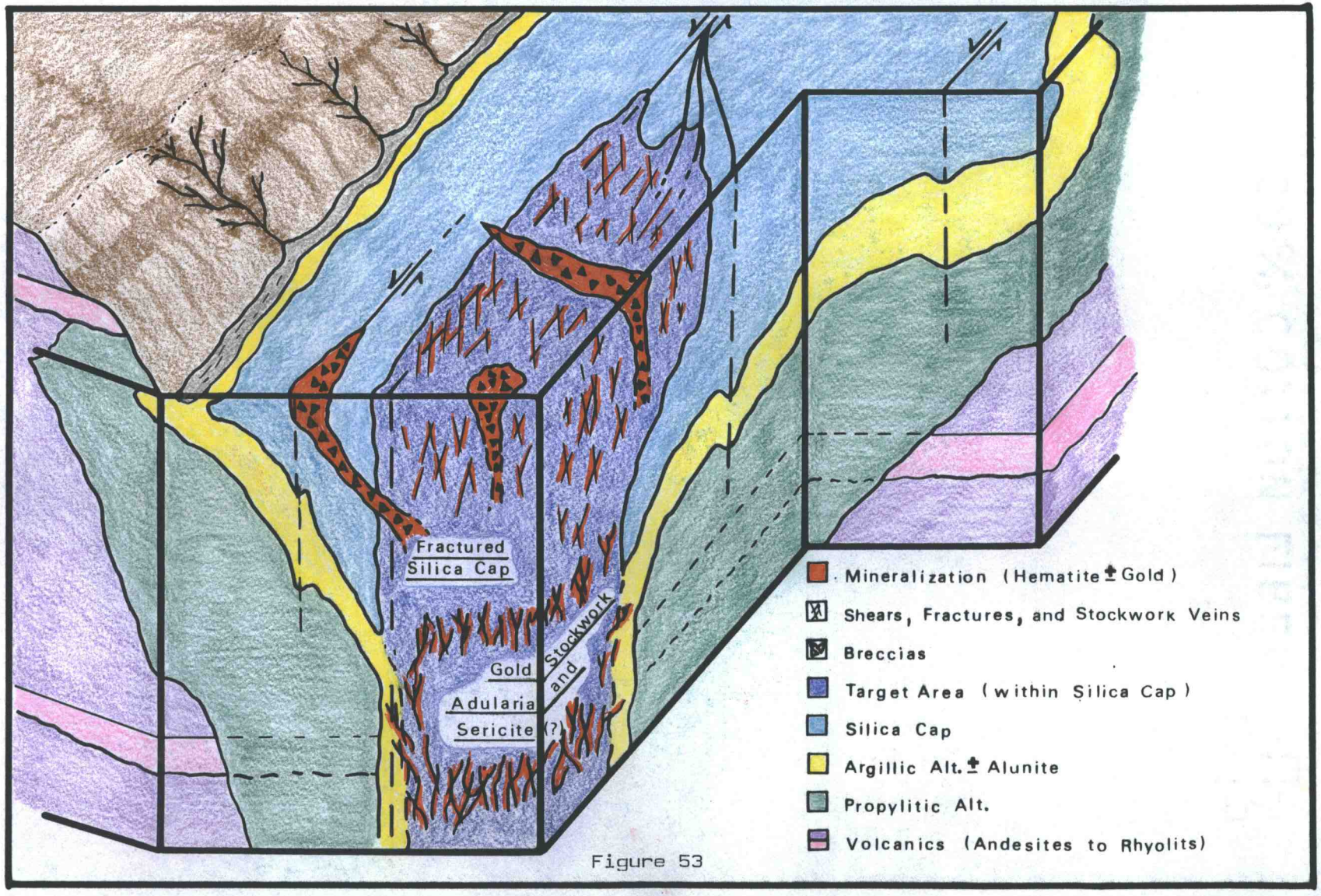
Fractured
Silica Cap
Gold
Adularia
Sericite (?)
Stockwork
and
Mineralization (Hematite ± Gold)
Shears, Fractures, and Stockwork Veins
Breccias
Target Area (within Silica Cap)
Silica Cap
Argillic Alt. ± Alunite
Propylitic Alt.
Volcanics (Andesites to Rhyolits)

Figure 53

Gold Zone, 23 out of 24 rock chip samples contain gold ranging from 20 - 480 ppb, with geobotanical samples (moss) containing up to 510 ppb gold. Associated with this gold metallization and distributed around it are high geochemical anomalies of various elements, with maximum detected values of 28 ppm Ag, 1,900 ppm As, 213 ppm Sb, 7.5 ppm Hg, 6,000 ppm F, and minor to moderate amounts of Cu, Pb, Zn, Mo, and Ba. This mineralization is confined to a highly fractured, brecciated, and veined portion of the silica capping that exhibits several paragenetically distinct periods of brecciation and metallization. The introduction of gold appears to have taken place in three episodes. The first discernible introduction of gold was in a stockwork vein system composed of milky quartz that crops out locally over a large area within the Primary Target. A second episode of gold deposition represents the major period of gold introduction and took place concurrent with the formation of explosion breccia pipes. These matrix-supported explosion breccias are abundant throughout the Gold Zone and contain clasts of the earlier formed milky vein quartz and silicified volcanics that are suspended in a matrix of silica, rock flour, and microball-bearing hematite. Explosion breccia pipes within this area host concentrations of up to 206 ppb Au, 13.7 ppm Ag, 1,200 ppm As, 213 ppm Sb, 3.5 ppm Hg and form an east to west-trending zone, with individual pipes and conduits preferentially emplaced along a cross-cutting N10°E - N10°W direction. A third mineralizing event took place with the introduction of gold-bearing pyrite veins that cut the silica capping predominantly in a N20 - N25°E direction. Minor amounts of gold and locally high concentrations of mercury and arsenic

have been detected in these veins. Gold is also present in veinlets and breccias that contain pyrite and enargite ± alunite, kaolinite, and quartz and cross cut the silica capping, but whether or not this represents a separate metallization event is unclear. The White River gold prospect (consisting of two adits) is located within the Primary Target area. Assays from these adits were reported by the Washington State Department of Geology and Earth Resources to contain values of 0.02 to 0.07 oz Au/ton. However, these results could not be checked because the upper adit is caved and the lower adit is blocked 50 feet from the portal.

The East area measures about 2 by 2.5 miles in size and was also the site of a surface-venting acid-sulfate hydrothermal system. The type and distribution of alteration around hydrothermal vents in this area is similar to that of the West area, with zones of massive silica enclosed by advanced argillic, argillic, and propylitic alteration mineral assemblages. Of 23 samples collected within the East area only 2 contained significantly anomalous gold values (68 and 295 ppb). The higher value was for a sample collected from a fault zone, and from which a previous study reported the presence of 120 ppb gold. These anomalous gold values are for samples collected from faults or veins on the outer fringe of this hot-spring alteration zone, and they indicate the possibility of additional mineralization within the central core of the system. Moderate to high geochemical values of other elements are present in the East area and range up to 151 ppm Sb, 3.1 ppm Hg, 1,900 ppm F, 25 ppm Mo, 697 ppm As, 165 ppm Ba, 163 ppm Cu, and 104 ppm Zn, and these anomalous samples are generally

representative of veins or breccias. Most of the East area has been subjected to tree thinning and is largely impassible at present. For this reason geologic mapping and geochemical sampling were limited primarily to logging roads and a few trails. However, those portions that could be investigated suggest the potential for precious metal mineralization, but at a lower level of certainity than was obtained for the West area.

A statistical analysis of the White River geochemical data for Au, Ag, As, Sb, Hg, and Mo from 163 samples has provided a better understanding of the distributions and zonations of precious metal, base metal, and trace elements within and around the Gold Zone. Results of simple statistics combined with R-mode and Q-mode factor analyses also show the depositional interrelationships between these trace elements. Statistical analyses of the data indicate a strong geochemical grouping (covariance) of arsenic with antimony, silver with molybdenum, and relatively independent behaviors of gold and mercury. However, R-mode factor analysis of the data indicate that antimony, and to a lesser extent arsenic, could be useful as pathfinder elements for gold. On the basis of the Au-Sb association both R-mode and Q-mode factor analyses have independently defined a previously unrecognized zone of potential subsurface gold mineralization.

This study of the White River acid-sulfate epithermal gold system has provided geologic, geochemical, and mineralogical criteria for developing a model of precious metal mineralization on a local scale, and those factors may be incorporated into regional exploration

programs elsewhere in the Pacific Northwest. Structure has played a key role in the focusing of mineralized hydrothermal cells in both the West and East areas. Satellite imagery appears to be useful in locating regional lineaments, major local structures and structural domes associated with unexposed intrusions and should be employed in the initial stages of regional mineral exploration programs. The White River hydrothermal system exhibits a close genetic tie to the formation of the Clear West Peak caldera (with age determinations of 19.1, 21.8, and 22.6 m.y.), its probable resurgence, and the contemporaneous local emplacement of intrusive stocks and apophyses from an underlying pluton of the Tatoosh batholith. An age determination of crystalline alunite (20.4 $\pm$ 0.1 m.y.) by the 40Ar/39Ar method indicates that hydrothermal activity took place during the formation of the Clear West Peak caldera, or subsequent resurgent activity. Wallrock alteration patterns such of the White River basin are similar to those of acid-sulfate type hot-spring gold systems elsewhere, and may be useful as guides to regional exploration. However, exploration should not be restricted to the use of this hot-spring model alone, because other genetic types of gold mineralization are likely to be present throughout the Pacific Northwest.

REFERENCES

Ampian, S.G. and Polk, D.W., 1980, Clays: U.S. Bureau of Mines, Minerals Yearbook, v.1, p.201-236.

Anderson, N.R., 1954, Glacial geology of the Mud Mountain district, King County, Washington: Seattle, University of Washington, M.S. thesis, 48p.

Berger, B.R., 1985, Geologic-Geochemical features of hot-spring precious-metal deposits: U.S. Geological Survey Bulletin 1646, p.47-53.

Berger, B.R., and Eimon, P.L., 1982, Comparative models of epithermal precious metal deposits: American Institute of Mining Engineers Preprint 82-13, 36p.

Berger, B.R., and Silberman, M.L., 1986, Relationships of trace-element patterns to geology in hot-spring-type precious-metal deposits: Reviews in Economic Geology, v.2, p.233-247.

Bingler, E.C., Trexler, D.T., Kemp, W.R., and Bonham, H.F., Jr., 1976, PETCAL a BASIC language computer program for petrologic calculations: Nevada Bureau of Mines and Geology, Report 28, 27p.

Bonham, H.F., Jr., 1985, Characteristics of bulk-minable gold-silver deposits in cordilleran and island-arc settings: U.S. Geological Survey Bulletin 1646, p.71-77.

Bretz, JH., 1913, Glaciation of the Puget Sound region: Washington Geological Survey, Bulletin 8, 244p.

Coney, P.J., Jones, D.L., and Monger, J.W.H., 1980, Cordilleran suspect terranes: Nature, v.288, p.329-333.

Crandell, D.R., and Miller, R.D., 1974, Quaternary stratigraphy and extent of glaciation in the Mount Rainier region, Washington: U.S. Geological Survey Professional Paper 847, 59p.

Crandell, D.R., and Waldron, H.H., 1956, A Recent volcanic mudflow of exceptional dimensions from Mt. Rainier, Washington: American Journal of Science, v.254, p.349-362.

Cunningham, C.G., 1985, Characteristics of boiling-water-table and carbon dioxide models for epithermal gold deposition: U.S. Geological Survey Bulletin 1646, p.43-46.

Cunningham, C.G., and Hall, R.B., 1976, Field and laboratory tests for the detection of alunite and determination of atomic percent potassium: Economic Geology, v.71, p.1596-1598.

Cunningham,C.G., Rye, R.O., Steven, T.A., and Mehnert, H.H., 1984, Origins and exploration significance of replacement and vein-type alunite deposits in the Marysvale Volcanic Field, West Central Utah: Economic Geology, v.79, no.1, p.50-71.

Duncan, R.A., 1981, A captured island chain in the Coast Range, Oregon and Washington: EOS, v.62, no.45, p.1028.

Ewing, T.E., 1980, Paleogene tectonic evolution of the Pacific Northwest: The Journal of Geology, v.88, no.6, p.619-638.

Field, C.W., and Fifarek, R.O., 1986, Light stable-isotope systematics in the epithermal environment: Reviews in Ecoomic Geology, v.2, p.99-128.

Fischer, J.F., 1970, The geology of the White River-Carbon Ridge area, Cedar Lake quadrangle, Cascade Mountains, Washington: Santa Barbara, University of California, Ph. D. thesis, 200p.

Fiske, R.S., Hopson, C.A., and Waters, C.A., 1963, Geology of Mount Rainier National Park, Washington: U.S. Geological Survey Professional Paper 444., 93p.

Frizzell, V.A., Jr., Tabor, R.W., Booth, D.B., Ort, K.M., and Waitt, R.B., Jr., 1984, Preliminary geologic map of the Snoqualmie Pass 1:100,000 Quadrangle, Washington: U.S. Geological Survey Open-File Map OF-84-693, 42p.

Frizzell, V.A., Jr., and Vance, J.A., 1983, Cenozoic volcanism of the Cascades of Washington: EOS, v.64, no.45, p.886.

Giles, D.L., and Nelson, E.E., 1982, Principal features of epithermal lode gold deposits of the Circum-Pacific rim: Circum-Pacific Energy and Minerals Resource Conference, Honolulu, Hawaii, 17p.

Hammond, P.E., 1963, Structure and stratigraphy of the Keechelus Volcanic Group and associated Tertiary rocks in the west-central Cascade Range, Washington: Seattle, University of Washington, Ph. D. thesis, 264p.

Hammond, P.E., 1980, Reconnaissance geologic map and cross sections of southern Washington Cascade Range: Publication of the Department of Earth Sciences, Portland State University, Portland, Oregon, 31p.

Hartman, D.A., 1973, Geology and low grade metamorphism of the Greenwater River area, central Cascade Range, Washington: Seattle, University of Washington, Ph. D. thesis, 99p.

Hayba, D.O., Bethke, P.M., Heald, P., and Foley, N.K., 1986, Geologic, mineralogic, and geochemical characteristics of volcanic-hosted epithermal precious-metal deposits: Reviews in Economic Geology, v.2, p.129-167.

Helgeson H.C., and Garrels, R.M., 1968, Hydrothermal transport and deposition of gold: Economic Geology, v.63, p.622-635.

Hem, J.D., 1978, Solubilities of mineral species which may control aluminum concentrations in natural water; adsorption processes: Handbook of Geochemistry, v.II/1, p.13H1-13H5.

Hemley, J.J., Hostetler, P.B., Gude, A.J., and Mountjoy, W.T., 1969, Some stability relations of alunite: Economic Geology, v.61, no.6, p599-612.

Henley, R.W., 1973, Solubility of gold in hydrothermal chloride solutions: Chemical Geology, v.11, p.73-87.

Henley, R.W., and Elis, A.J., 1984, Geothermal systems ancient and modern: A geochemical review: Cordilleran Section, Geological Association of Canada, Short Course No. 3, 50p.

Howell, D.G., and McDougall, K.A., 1978, Mesozoic Paleogeography of the Western United States: Pacific Coast Paleogeography Symposium 2, Pacific Section of the Society of Economic Paleontologists and Mineralogists, 573p.

Huntting, M.T., 1955, Gold in Washington: Washington State Division of Mines and Geology, Bulletin no.42, 158p.

Kesler, S.E., Russell, N., Seaward, M., Rivera, J. McCurdy, K., Cumming, G.L., and Sutter, J.F., 1981, Geology and geochemistry of sulfide mineralization underlying the Pueblo Viejo gold-silver

oxide deposit, Dominican Republic: Economic Geology, v.76, p.1096-1117.

Knight, J.E., 1977, A thermochemical study of alunite, enargite, luzonite, and tennantite deposits: Economic Geology, v.72, p.1321-1336.

Lewis, A., 1982, Gold geochemistry: Engineering and Mining Journal, December 1982, p.56-60.

Livingston, V.E., Jr., 1971, Geology and Mineral Resources of King County, Washington: Washington State Division of Mines and Geology, Bulletin no.63, 200p.

Magill, J.R., Wells, R.E., Simpson, R.W., and Cox, A.V., 1982, Post 12 m.y. rotation of southwest Washington: Journal of Geophysical Research, v.87, no.B5, p.3761-3776.

Mattinson, J.M., 1977, Emplacement history of the Tatoosh volcanic-plutonic complex, Washington: Ages of zircons: Geological Society of America Bulletin, v.88, p.1509-1514.

Meyer, C., and Hemley, J.J., 1967, Wall Rock Alteration: Geochemistry of hydrothermal ore deposits, H.L. Barnes, editor, Holt, Reinhart, and Winston, New York, p.166-235.

Moen, S.W., and Huntting, M.T., 1975, Handbook for gold prospectors in Washington: Washington State Division of Geology and Earth Resources, Information Circular 57, 90p.

Ohmoto, H., and Rye, R.O., 1979, Isotopes of sulfur and carbon: Geochemistry of hydrothermal ore deposits, H.L. Barnes, editor, Wiley Interscience Publication, p.509-567.

Raisz, E., 1945, The Olympic-Wallowa lineament: American Journal of Science, v.243-A, p.479-485.

Rose, A.W., Hawkes, H.E., and Webb, J.S., 1979 Geochemical characteristics of the elements: Geochemistry in Mineral Exploration, Academic Press, 657p.

Schoen, R., White, D.W., and Hemley, J.J., 1974, Argillization by descending acid at Steamboat Springs, Nevada: Clays and Clay Minerals, v.22, p.1-22.

Seward, T.M., 1973, Thio complexes of gold and the transport of gold in hydrothermal ore solutions: Geochimica et Cosmochimica Acta, v.37, p.379-399.

Smith, F.G., 1943, The alkali sulphide theory of gold deposition: Economic Geology, v.38, no.7, p561-590.

Stewart, J.H., Stevens, C.H., Fritsche, A.E., 1977, Paleozoic Paleogeography of the Western United States: Pacific Coast Paleogeography Symposium 1, Pacific Section of the Society of Economic Paleontologists and Mineralogists, 502p.

Strachan, D.G., 1985, Geologic discussion of the Borealis gold deposit, Mineral County, Nevada: U.S. Geological Survey Bulletin 1646, p.89-94.

Tabor, R.W., and Frizzell, V.A., Jr., 1979, Tertiary movement along the southern segment of the Straight Creek fault and its relation to the Olympic Wallowa lineament in the central Cascades, Washington: The Geological Society of America, Cordilleran Section, 75th Annual Meeting, abstracts with programs, v.11, no.2, p.131.

Tabor, R.W., Frizzell, V.A., Jr., Vance, J.A., and Naeser, C.W., 1984,

Ages and stratigraphy of lower and middle Tertiary sedimentary and volcanic rocks of the central Cascades, Washington: Application to the tectonic history of the Straight Creek fault: Geological Society of America Bulletin, v.95, p.26-44.

Taylor, E.M., 1978, Field geology of S.W. Broken Top quadrangle, Oregon: Oregon Department of Geology and Mineral Industries, Special Paper 2, 50p.

Vance, J.A., 1982, Cenozoic stratigraphy and tectonics of the Washington Cascades: The Geologicl Society of America, Cordilleran Section, 78th Annual Meeting, abstracts with programs, v.14, no.4, p.241.

Weaver, C.E., 1916, The Tertiary formations of western Washington: Washington Geological Survey Bulletin 13, 327p.

Wells, R.E., Engebretson, D.C., Snavley, P.D., Jr., and Coe, R.S., 1984, Cenozoic plate motions and the volcano-tectonic evolution of western Oregon and Washington: Tectonics, v.3, no.2, p.275-294.

White, D.E., 1985a, Vein and disseminated gold-silver deposits of the Great Basin through space and time: U.S. Geological Survey Bulletin 1646, p.5-14.

_____ 1985b, Summary of the Steamboat Springs Geothermal area, Nevada, with; attached road-log commentary: U.S. Geological Survey Bulletin 1646, p.79-87.

Wilcox, R.E., Harding, T.P., and Seely, D.R., 1984, Basic wrench tectonics: The American Association of Petroleum Geologists Bulletin, v.57, no.1, p.74-96.

APPENDICES

Appendix 1. Age determination of alunite by the 40Ar/39Ar method. The analysis was performed by L.W. Snee of the U.S. Geological Survey in Denver, Colorado, from a sample irradiated in January 1986.

Incremental Heating

T°C	Percent Argon Released
300	0.1
450	61.2
500	20.9
600	14.3
700	3.0
800	0.4
Fuse	0.2

Steps 2 through 4 account for 96.4 percent of argon gas released, and an apparent age of 20.4 ± 0.1 m.y. is indicated.

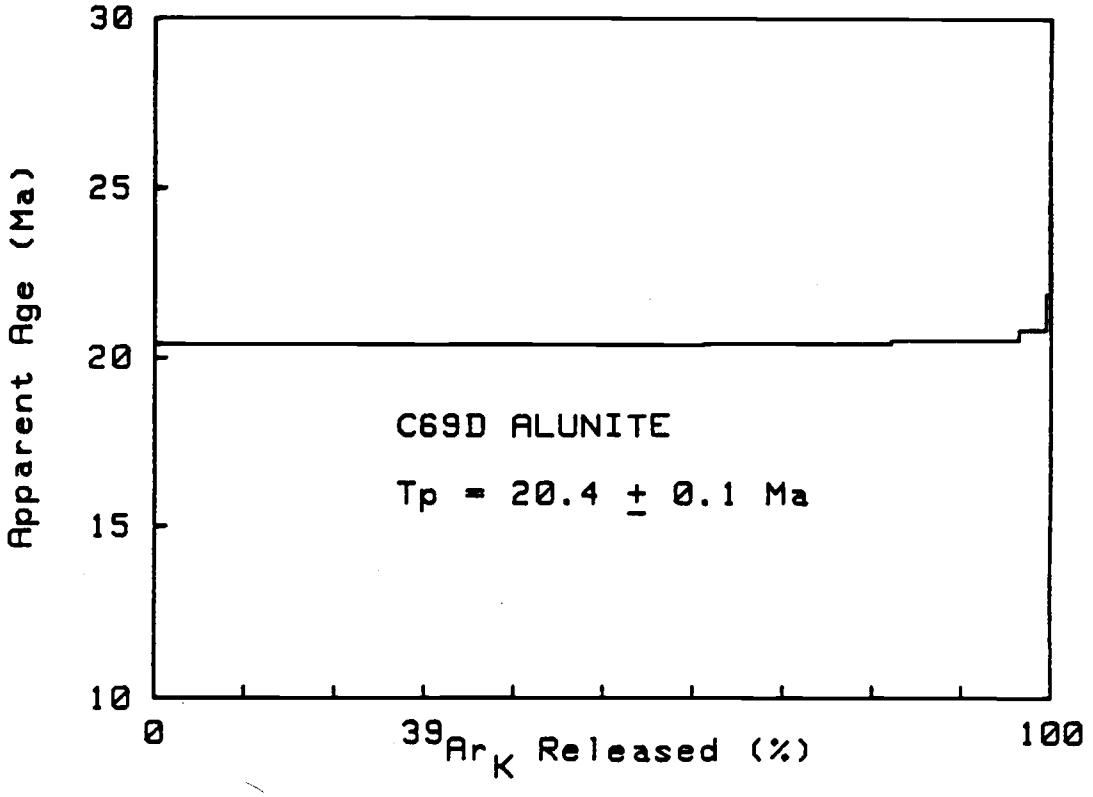

Appendix 2. Assay results of rock chip samples.

APPENDIX 2

Sample	Au (ppm)	Ag (ppm)	As (ppm)	Sb (ppm)	Hg (ppb)	Mo (ppm)
WR- 1F*	0.068	3.4	-		380	
2F*	0.343	3.8	-		50	
3F*	0.034	5.5	-		70	
4F*	0.068	2.4	-		30	
5F*	-	10.6	-		-	
6F*	-	6.8	-		-	
7	-	-	120	2	120	7
8	-	-	240	-	140	-
9	-	0.1	170	-	270	5
10	-	-	190	-	390	3
11	-	-	200	-	85	2
12	-	-	100	-	190	4
13	-	6.8	160	5	480	4
14	0.030	10.3	170	7	750	10
15F	0.480	7.2	-	3	70	9
16F	-	-	220	50	590	6
17F	-	13.7	14	-	20	4
18	-	-	130	6	610	5
19	-	-	52	-	670	1
20	-	-	57	-	890	4
21	-	-	62	-	1200	6
22	-	-	54	-	1100	3
23	-	-	52	-	800	4
24	-	3.4	89	-	100	5
25	-	-	49	-	60	6
26	-	3.4	37	-	90	5
27	-	-	37	-	60	5
28	-	-	50	1	40	5
29	-	-	52	1	150	4
30	-	-	160	-	140	3
31	-	-	69	-	470	4
32	-	-	44	-	840	4
33	-	-	47	-	1200	10
34	-	-	20	-	70	4
35	-	-	30	3	20	4
36	-	3.4	460	-	140	4
37	-	-	42	-	100	5
38	-	-	53	-	70	5
39	-	-	29	2	2800	4
40	-	-	21	-	2500	10
41	-	-	220	-	1700	6
42	-	-	12	-	140	2
43	-	-	50	-	470	5
44	-	3.4	55	-	70	5
45	-	-	120	-	1000	4
46F	-	-	14	-	20	4

Appendix 2 (continued)

Sample	Au	AG	As	Sb	Hg	Mo
47F	-	-	110	-	3700	2
48F	0.206	-	83	1	40	6
49F	-	-	11	-	500	2
50F	-	-	10	-	15	4
51F	-	5.5	14	-	30	1
52F	0.068	6.2	73	4	1500	2
53F	-	-	32	12	390	2
54F	-	-	390	-	130	2
55F	-	-	9	1	410	3
56F	-	-	230	6	3100	9
57F	-	3.4	23	-	170	-
58F	-	6.8	130	5	1400	5
59F	-	-	88	9	740	13
60F	-	2.7	-	-	20	2
61F	-	-	12	-	60	1
62F	0.068	0.7	91	-	570	4
63F	0.206	3.1	46	-	220	4
64F	-	4.1	18	-	80	1
65F	-	2.1	22	-	30	1
66F	-	-	58	2	220	2
67F	-	-	150	4	1400	2
68F	-	0.7	19	-	220	10
69F	-	2.1	-	-	50	66
70F	-	3.4	27	-	80	5
71F	-	2.1	13	-	380	6
72F	-	4.1	-	-	40	10
73F	-	2.7	-	-	400	10
74F	-	3.4	-	-	50	15
75F	-	-	-	-	1100	53
76F	-	5.5	-	-	1600	39
77F	-	8.9	13	-	180	13
78F	-	7.5	-	-	40	11
79F	-	9.6	-	-	490	5
80F	-	5.5	10	-	40	65
81F	-	6.9	-	-	20	90
82F	-	6.9	110	-	40	70
83F	0.068	9.6	220	4	3000	160
84F	-	6.9	53	1	90	25
85I	-	0.1	9	2	5	1
86I	-	0.1	39	2	20	6
87I	0.180	0.1	34	58	5	1
88I	0.170	0.1	60	39	5	3
89I	0.042	0.4	1012	13	10	3
90I	0.180	0.1	482	213	5	3
91I	-	0.2	168	2	11000	2
92I	-	0.1	112	11	10	2
93I	-	0.1	19	2	30	1
94I	-	0.1	493	2	240	7
95I	-	0.1	76	3	30	3
96I	-	0.1	53	2	240	7

Appendix 2 (continued)

Sample	Au	Ag	As	Sb	Hg	Mo
97I	-	0.1	248	10	5	4
98I	-	0.1	739	2	80	2
99I	-	0.1	42	6	20	4
100I	-	0.1	9	2	5	3
101I	-	0.1	4	2	20	1
102I	-	0.1	93	2	30	3
103I	-	0.1	5	2	5	1
104I	-	0.1	2	2	5	1
105I	-	0.1	221	3	1900	18
106I	-	0.1	291	2	2000	22
107I	-	0.2	86	2	50	3
108I	-	0.1	35	2	20	4
109I	-	0.3	117	2	10	17
110I	0.035	0.6	89	2	240	9
111I	-	0.1	12	2	10	3
112I	-	0.1	47	2	5	3
113I	-	0.1	3	2	5	1
114I	-	0.1	12	2	30	66
115I	-	0.1	4	2	200	1
116I	-	0.1	38	2	30	1
117I	0.295	0.6	453	5	270	13
118I	-	0.1	97	8	20	1
119I	-	0.1	39	2	120	2
120I	-	0.1	38	2	600	9
121I	-	0.3	21	2	270	5
122I	-	0.3	697	151	210	25
123I	-	0.1	86	2	200	2
124I	-	0.1	6	2	30	1
125I	-	0.3	27	2	5	12
126I	-	0.1	8	2	350	3
127I	-	0.1	148	2	50	2
128I	-	0.1	19	2	70	1
129I	-	0.1	13	2	80	1
130I	-	0.3	30	2	10	2
131I	-	0.1	5	2	5	3
132I	-	0.1	7	2	1700	1
133I	-	0.1	53	2	20	3
134I	-	o.1	60	2	5	7
135I	-	0.1	175	27	10	8
136	-	-	45	-	440	-
137	-	-	36	-	170	-
138	-	-	210	-	15	1
139	-	-	230	10	910	10
140	-	-	210	11	170	9
141	0.020	-	1000	28	210	32
142	0.080	0.1	120	38	210	1
143	-	-	330	110	1300	3
144	-	-	62	25	3800	-
145	-	-	80	-	670	-
146	-	-	90	6	80	3

Appendix 2 (continued)

Sample	Au	Ag	As	Sb	Hg	Mo
147	-	-	350	14	110	4
148	-	-	20	-	10	9
149	-	-	41	2	10	11
150	0.020	0.5	320	13	700	9
151	0.020	0.3	1900	98	870	8
152	-	0.3	400	13	970	6
153	-	0.1	430	40	670	7
154	0.170	0.1	140	7	20	7
155	-	-	200	3	50	5
156	-	-	96	-	240	4
157	-	-	160	-	350	2
158	0.060	-	690	5	120	5
159	0.020	0.2	200	16	220	3
160	0.025	-	490	18	780	4
161	0.195	-	500	74	50	4
162	0.060	-	1200	29	220	3
163	0.150	0.1	240	57	240	2
164	-	-	1500	-	20	210
165	-	-	490	9	50	33
166	-	-	170	36	80	35
167	-	-	89	-	4500	2
168	0.075	-	150	21	3500	3
169	0.105	0.2	250	83	100	3
170M*	0.514	0.5				
171M*	-	3.5				
172M*	-	28.0				
173M*	-	4.8				
174M*	-	5.4				
175*	0.020	-	160	33	30	5
176*	-	-	160	48	60	4
177*	0.025	-	120	47	210	4
178*	0.050	0.1	160	41	70	1
179*	0.035	-	43	6	-	2
180*	0.040	-	140	28	70	5
181*	0.130	-	110	14	30	3
182*	0.050	-	56	10	30	3
183*	0.090	0.2	84	13	400	2
WR-184*	0.025	0.2	420	14	7500	2
		DETECTION LIMITS				
AA	0.020	0.1	5	1	10	1
F	0.68	0.02	5	1	10	1
I	0.020	0.1	2	2	5	1

Numbers followed by an F indicate samples that were analyzed by fire assay for Au and Ag and by atomic absorption for As, Sb, Hg, and Mo. Those followed by an I indicate samples that were analyzed by the ICP

(inductively coupled argon plasma) method, with gold content being determined by AA. All others were analyzed by the atomic absorption method (AA). Sample numbers followed by an M are geobotanical samples of moss, all others are of rock chips. Samples with an * were not included in the 163 samples of the White River data set used for statistical analyses. Of those samples not included, 10 were collected after statistical analyses were performed and 11 were not analyzed for all six elements (Au, Ag, As, Sb, Hg, and Mo). Hunter Mining Laboratory, Inc., Sparks, Nevada performed all AA and fire assays, and Acme Analytical Laboratories Ltd., Vancouver, B.C. performed all ICP analyses.

Locations of Samples Not Plotted on Plates 3A and 3B

WR- 60	SW1/4, SW1/4, sec. 21, T20N, R8E -- Along Weyerhaeuser road 5700.
98	NE1/4, NE1/4, sec. 30, T19N, R9E -- At the intersection of the east fork of Camp Creek with Weyerhaeuser road 6111.
99	Central, N1/2, sec. 30, T19N, R9E -- Along Weyerhaeuser road 6111, approximately 1500 feet west of sample WR-98.
101	NW1/4, NW1/4, sec. 30, T19N, R9E -- At the intersection of the west fork of Camp Creek with Weyerhaeuser road 6111.
109	SW1/4, sec. 28, T19N, R8E -- Along the south side of Lyle Creek on Weyerhaeuser road 6020.
WR-170M	A combination of 4 samples of moss collected throughout the West area.

Appendix 3. Weight percent of major-element oxides, as determined by XRF analysis (P.R. Hooper, Washington State University, 1984) with: Clear West Peak (CWP) intracaldera (i) and extracaldera (e) ash-flows; Stevens Ridge formation (SR); Fifes Peak formation (FP); Eagle Gorge formation (EG); intrusive diorite porphyry (DP); propylitic (p) and argillic (a) alteration; tourmaline (t) and alunite (alu) minerals; and samples plotted on Figures 8 and 9 (*).

		SiO2	TiO2	Al2O3	Fe2O3	FeO	MgO
1*	intrusion	59.26	0.82	16.31	3.81	4.37	3.59
2*	CWPi	74.70	0.39	13.46	1.06	1.22	0.24
3	FP breccia	82.51	1.19	0.09	7.45	8.54	0.00
4*	FP	62.36	0.80	16.45	3.00	3.44	3.08
5*	FP	61.53	0.97	16.30	3.37	3.86	3.45
6*	intrusion	70.61	0.88	13.86	2.78	3.19	0.46
7*	FP	61.23	0.96	16.70	2.87	3.29	3.10
8*	FP p	58.92	0.86	16.73	3.58	4.10	4.50
9*	SR	74.26	0.38	13.03	1.31	1.50	0.52
10	FP p-a	56.28	1.09	19.19	3.79	4.34	3.27
11*	FP	64.61	0.97	16.09	3.60	4.12	2.75
12	FP	63.47	0.89	15.73	2.95	3.38	2.42
13*	FP	60.02	0.87	17.43	3.22	3.69	3.11
14*	FP	62.99	0.78	15.90	2.75	3.15	3.35
15*	FP p	61.53	0.77	16.19	3.36	3.84	3.27
16*	CWPe	76.96	0.35	13.73	0.34	0.39	0.00
17*	FP p	61.61	0.78	16.52	3.48	3.99	4.16
18*	FP	63.44	0.81	16.43	2.96	3.39	2.24
19*	DP	59.33	0.94	16.92	3.57	4.09	3.59
20	FP p	61.24	0.92	18.88	2.94	3.37	2.68
21*	FP	61.68	0.88	16.86	2.94	3.37	2.76
22	breccia	86.3	0.94	0.00	5.70	6.52	0.00
23	silica cap	98.96	1.01	0.00	0.00	0.00	0.00
24*	FP	62.22	0.78	16.36	3.10	3.55	3.07
25	FP p-a-t	68.22	0.84	16.87	2.50	2.87	1.39
26	silica cap	98.82	1.07	0.00	0.00	0.00	0.00
27	silica cap	98.20	0.65	0.73	0.00	0.00	0.00
28	silica cap	97.08	2.84	0.00	0.00	0.00	0.00
29	silica cap	98.88	0.97	0.00	0.00	0.00	0.00
30	breccia	91.51	1.03	0.04	3.37	3.86	0.00
31	breccia	87.58	0.73	1.70	4.49	5.14	0.00
32	intrusion	66.23	0.75	15.44	2.49	2.85	2.42
33*	DP	59.24	1.00	17.50	3.94	4.51	3.24
34	clay-pyrite	43.90	1.68	26.85	5.59	6.40	3.69
35*	FP	59.85	0.91	16.52	3.47	3.97	4.04
36	clay	66.19	1.30	30.97	0.34	0.39	0.17
37	clay	70.98	1.59	21.80	0.18	0.21	0.34
38*	FP	58.27	1.07	16.82	3.52	4.04	3.46
39*	EG	60.43	1.20	15.63	3.99	4.57	2.76
40	alu-silica	77.28	0.78	17.21	0.00	0.00	0.00
41*	FP	58.55	1.13	16.99	3.31	3.79	3.54

Appendix 3 (continued).

	CaO	Na2O	K2O	P2O5	MnO
1	7.64	2.85	1.04	0.14	0.16
2	0.96	3.16	4.73	0.05	0.03
3	0.00	0.20	0.00	0.02	0.00
4	5.51	3.23	1.87	0.16	0.09
5	5.40	3.16	1.69	0.18	0.10
6	1.86	3.05	2.96	0.22	0.12
7	7.00	2.80	1.73	0.20	0.12
8	7.50	2.62	0.89	0.16	0.12
9	2.11	2.88	3.89	0.09	0.03
10	6.61	3.66	1.42	0.21	0.14
11	3.48	2.68	1.45	0.17	0.08
12	5.51	3.30	2.06	0.18	0.10
13	6.80	3.09	1.46	0.16	0.15
14	5.94	3.30	1.58	0.17	0.09
15	6.18	2.93	1.65	0.14	0.13
16	0.43	2.79	4.98	0.03	0.00
17	5.62	2.54	0.94	0.14	0.21
18	5.47	3.31	1.71	0.16	0.08
19	6.88	3.26	1.11	0.17	0.13
20	4.33	2.95	2.40	0.18	0.11
21	6.27	3.42	1.56	0.16	0.11
22	0.00	0.19	0.00	0.03	0.00
23	0.00	0.01	0.00	0.02	0.00
24	6.27	2.83	1.53	0.15	0.13
25	2.78	2.62	1.75	0.11	0.05
26	0.00	0.10	0.00	0.02	0.00
27	0.00	0.33	0.08	0.02	0.00
28	0.00	0.05	0.00	0.03	0.00
29	0.00	0.13	0.00	0.02	0.00
30	0.00	0.17	0.00	0.03	0.00
31	0.01	0.32	0.02	0.02	0.00
32	4.86	2.81	1.91	0.15	0.09
33	5.93	3.22	1.10	0.18	0.14
34	7.48	1.05	3.04	0.21	0.11
35	6.47	3.04	1.44	0.16	0.13
36	0.12	0.15	0.33	0.04	0.00
37	0.35	2.79	1.70	0.07	0.00
38	7.52	2.95	1.98	0.22	0.16
39	6.36	3.15	1.57	0.21	0.14
40	0.06	0.63	3.91	0.13	0.00
41	7.61	2.86	1.90	0.20	0.17